Photonic Emissions of Living and Non-Living Matter

by

Justin N. Costa

A thesis submitted in partial fulfillment
of the requirements for the degree of
Master of Science (MSc) in Biology

The Faculty of Graduate Studies
Laurentian University
Sudbury, Ontario, Canada

© Justin N. Costa, 2016

THESIS DEFENCE COMMITTEE/COMITÉ DE SOUTENANCE DE THÈSE
Laurentian Université/Université Laurentienne
Faculty of Graduate Studies/Faculté des études supérieures

Title of Thesis Titre de la thèse	Photonic Emissions of Living and Non-Living Matter
Name of Candidate Nom du candidat	Costa, Justin
Degree Diplôme	Master of Science
Department/Program Département/Programme	Biology
Date of Defence Date de la soutenance	January 27, 2017

APPROVED/APPROUVÉ

Thesis Examiners/Examinateurs de thèse:

Dr. Michael Persinger
(Supervisor/Directeur(trice) de thèse)

Dr. Rob Lafrenie
(Committee member/Membre du comité)

Dr. Mazen Saleh
(Committee member/Membre du comité)

Dr. Rod O'Connor
(External Examiner/Examinateur externe)

Approved for the Faculty of Graduate Studies
Approuvé pour la Faculté des études supérieures
Dr. David Lesbarrères
Monsieur David Lesbarrères
Dean, Faculty of Graduate Studies
Doyen, Faculté des études supérieures

ACCESSIBILITY CLAUSE AND PERMISSION TO USE

I, **Justin Costa**, hereby grant to Laurentian University and/or its agents the non-exclusive license to archive and make accessible my thesis, dissertation, or project report in whole or in part in all forms of media, now or for the duration of my copyright ownership. I retain all other ownership rights to the copyright of the thesis, dissertation or project report. I also reserve the right to use in future works (such as articles or books) all or part of this thesis, dissertation, or project report. I further agree that permission for copying of this thesis in any manner, in whole or in part, for scholarly purposes may be granted by the professor or professors who supervised my thesis work or, in their absence, by the Head of the Department in which my thesis work was done. It is understood that any copying or publication or use of this thesis or parts thereof for financial gain shall not be allowed without my written permission. It is also understood that this copy is being made available in this form by the authority of the copyright owner solely for the purpose of private study and research and may not be copied or reproduced except as permitted by the copyright laws without written authority from the copyright owner.

Abstract

Photons are known to be the product of electrochemical states of excitability. The interaction of photons between chemical and biological systems allows statistical methods to be employed to discern frequency- and time-dependent data. The present document demonstrates photon emissions sources attributed to chemical, biomolecular, and living and non-living tissues through theoretical and empirical photon counting measures. The results suggest that photon count intensity is statistically significant when measuring variance in volumes of matter. In addition, photon count measures when lagged between the cerebral hemisphere of human subject, display significant correlations. Spectral analyses revealed significant peak frequencies from living biological sources when exposed to incident photons and/or magnetic fields. The photon emissions from differing levels of discourse may exist to be used as energy sources responsible for the mechanisms that interact within open systems and their environments. Photons may reflect a form of communication within more complex aggregates of matter.

Keywords

Periodic Elements, Fixed Human Brain; Spontaneous Photon Emissions; 10^{-12} $W \cdot m^{-2}$; Flux Density; Hameroff-Penrose “Orch-OR Theory”; Mach; Kant; Spinoza, Biophotons, Interhemispheric Correlations, Imagination, Human Brain, Quantitative EEG (QEEG) Visualization, Corpus Callosum, Aharanov-Bohm Effect, Weak Magnetic Fields, Cellular Aggregates

Acknowledgments

I would like to acknowledge my colleagues of the Neuroscience Research Group (NRG) that I have had the honour of meeting and working alongside with throughout my years at this institution. I have enjoyed teaching alongside the very same colleagues about the unique anatomy and function of the brain. You have all taught me that there are many ways to view the world, to challenge my beliefs, and to aim for exceptional heights to become the researcher I have worked so hard to be. I would like to thank Dr. Blake Dotta, whom had introduced me to the studies of photons deriving from biological systems. Without his inspiration and curiosity of the unknown; the complex mechanisms behind consciousness, I would probably have not have studied the physical applications among biological systems. Thank you for all my committee members for their support and guidance, as well as their patience from all my proposed ideas that may have seemed to grandiose at the time. Lastly, I am indebted to my Supervisor and Professor; Dr. Persinger. He has been a tremendous influence in my post-secondary life, both in and out of the laboratory. He has taught me a variety of subjects and ideas spanning from the smallest particles to the astronomical, and their implications toward the human brain. Dr. Persinger, you have been an inspiration for me to teach, question, test, and apply my knowledge towards greater discoveries and shaping other individuals to become creative thinkers.

I feel privileged to have been introduced to subjects that leave me asking more questions than when I had first started as a graduate level researcher. My only regret is that I do not have enough time in my lifetime to read every work, test every hypothesis, and solve the unexplainable to satisfy my curiosities. Thank you for this chapter in my life.

Table of Contents

List of Figures

List of Tables

Chapter 1 – Sources of Photon Emission

Chemical Photon Sources

Einstein had proposed that light consists of finite amounts of quanta and can only be emitted or absorbed as complete units (Einstein, 1905). This quanta has now become to be known as photons, the elementary particles of light. The proposed idea that light consists of individual units or particles of discrete energy, confirmed the experimental data of the photoelectric effect between photons and electron dynamics. The Planck- Einstein equation explains the wave-particle duality of the photon by the equation:

$$E = hf = \frac{hc}{\lambda} \quad (1),$$

where E is energy in Joules, h is Planck's constant ($6.62607004 \times 10^{-34}$ m^2 kg/s), f is the frequency of the photon, c is the speed of light (~3×10^8 m/s), and λ is the photon wavelength. As h remains constant, the energy of a photon is proportional to its frequency, rather than its intensity.

Photons with shorter wavelengths have higher frequencies, which have higher energy. Longer wavelengths along the electromagnetic spectrum have lower frequencies and lower energies per unit quanta. Visible light for example includes photons of wavelengths of approximately 400 (violet) to 700 (red) nanometers, with ranging energies of 4.97×10^{-19} J to 2.84×10^{-19} J respectively. Energies greater than this range include photons of the ultraviolet spectra and X-rays. Energies below this range include the infrared spectra, which is prevalent in heat energy observed in living organisms, and in thermodynamics of chemical reactions.

In his later works, Einstein proposed that atoms can absorb and emit photic energy by use of Planck's radiation law (Einstein, 1917). Simply stated, radiation was demonstrated to act between atoms and photons. They were conserved and dictated by the laws of thermodynamics and momentum. Momentum exchange can be ignored because of its minute effect on the atom. When an atom is stimulated by an incident photon, the energy exchange remains constant. A photon is absorbed when the atom transitions from low energy to high energy state. This is attributed to its electron excitability. Conversely, when an atom transitions from a high energy to low energy state a photon is emitted. The amount of energy is conserved during these reactions as an elastic scattering of photons if a threshold of required energy is reached. Because the photon energy is dependent on the frequency, an atom may not release a photon from an exchange of photic energy if the incident photon energy is not great enough. This pattern of an all-or-nothing release of photons can be seen in the firing of an action potential where a threshold of net change in voltage is required in neurons to fire.

If one were to imagine the size of a photon and its interaction with matter, it would be most probable to be very small. On a large scale, a single photon would not have much influence on a biological system directly. At the atomic level, the energy attributed to the wavelength of a single photon would affect the electric properties of the atomic configurations respective to the elements that make up matter in such systems. Due to the many different configurations of protons and electrons of each individual element, how the photon interacts is unique for each of the known elements. Of the many elements that compose the periodic table of elements, each individual element emits and absorbs visible range photons uniquely based on their observable emission spectra. By taking the energies associated with the visible wavelength photons (2.84×10^{-19} J to 4.97×10^{-19} J) and applying it to the chemical constant for particles per mole units,

Avogadro's constant, the energy ranges per mole of photons would be that of 171 kJ/mol (red) to 299 kJ/mol (violet). Any direct chemical analysis that pertains to energy is used in kiloJoules per unit mole, and may include thermodynamic results within this energy range. Although chemical elements make up matter in the simplest models, complexities arise as bonds begin to form allowing molecules to exist. These larger and more diverse structures dictate biological function.

Biological Photon Sources

Photons emissions have been studied from biological systems as well. Most markedly, thorough and inclusive work on biological sourced photon emissions have been studied by Popp (1979). He concluded that the photon emissions termed 'biophotons' were between the near infrared and near ultraviolet range that can be detected around various biological systems such as plants and cells (Popp, 1979). This range within the electromagnetic spectrum would be exclusive to photons of approximately 300-1400nm in wavelength. The visible light range fits well within this definition. Energy values of photons within this extended range for biophotons stated by Popp would have energy values of 6.62×10^{-19} J (300nm) to 1.42×10^{-19} J (1400nm). Calculated further, the mole energy units of these value for chemical application would be between the range of 85kJ/mol and 399kJ/mol. These 'biophotons' are thought to be a product of chemical processes within cells from various organelles. The most common source for biophoton emissions are hypothesized to be from reactive oxygen species (ROS) and reactive nitrogen species (RNS), and by the biochemical processes involved with metabolism.

A study that injected hydroperoxides into rat livers *in situ* and perfused livers, resulted in increased photon counts of chemiluminescence (Boveris, Cadenas, Reiter, Filipkowski, Nakase & Chance, 1980). The term chemiluminescence is similar, if not the same as biophotons. The

semantic meaning behind biophotons proposed by Popp is simply any photonic emission measured from a biological system. The chemiluminescense presented in the research by Boveris *et al.* (1980) applies to the reaction of oxidative species within and onto biological organs. Terminologies aside, the findings support the idea that photon emissions can be simulated from biological tissue when reactive oxygen species are present. This was reliably tested based on the positive relationship noted between the concentration dependence of peroxides added and with the increases in photon emission from the rat livers in the study. Boveris *et al.* (1980) had noted that the perfused liver emitted red light (approximately 600nm) predominantly after performing a partial spectral analysis on the collected data. They had concluded that the sources of emissions, which are oxygen dependent, are most likely due to high energy, excitable free radicals that are short lived during reactions within the biological system.

Cohen & Popp (1997) had provided details on the emission patterns of the human body from Popp's previous work on biophotons (visible range). Their extensive work measured the emission patterns from the surface area of human subjects' head, chest, and hands. Photons that are emitted from the human body vary in intensity throughout different times of the 24-hour day, and a calculated average value of 10^6 photons per m^2 are emitted from the surface area. It is interesting to note that this research shows varying levels of intensity based on the area being measured on the human body. Areas of high metabolic activity may emit larger amounts of biophoton emission as predicted in Popp's earlier works, and may exclude cases of oxidative stress. However, differences due to high activity organs within the human body may have not been considered initially.

Similar methods of photon counting measures have been used to study the significance of such energy exchange within the neurological domain. Hippocampal slices of rats have been

studied using ultra-weak photon counting measures and had found biological source photon emissions (Isojima *et al.,* 1995). Later research using rat models had found photon count increases from rat brains *in vivo* that were correlated to oxidative stress and metabolism (Kobayashi *et al.*, 1999). The results found *in vivo* strengthen the findings that photon emissions in real-time can be observed both temporally (time) and spatially (through computerized imaging). If biological systems are reduced to cells, as the simplest functioning unit, then observations made at the microscopic level provide greater insight into the role of biophoton emissions in life systems. Neurons (cells of the nervous system) do not differ greatly between other cells such as skin cells in terms of organelle make up. Neurons do have a higher rate of metabolism and overall activity compared to other cells based on their function (Mink, Blumenschine & Adams, 1981). Biophoton sources from the heads of human and other animal models may be attributed to the nervous system. Because photons could mediate information between cells and have been implied in non-locality phenomena, a separate communication system might exist.

More recent studies have found that there is indication that the human brain, during cognition, can emit light at increased quantities (Dotta & Persinger, 2011). More specifically, these increases of photon emissions coupled to cognition have shown hemisphere favourability towards the right hemisphere of live human subjects. The increases in power density found in the same study was that of ~10^{-11} W/m^2. If photon storage is possible in biological systems such as in nervous tissue, the physical matter correlated to cognition and memory, then the possibility of photon communication within brain matter becomes an important area of research. The present thesis will relate some of these previous findings to similar values found in the proceeding chapters.

Living biological systems are unique however, in that they do not follow the laws of thermodynamics compared to that of simple chemical elements and molecules. Schrödinger argued that Life exists by opposing the second law of thermodynamics; life exists by negative entropy (Schrödinger, 1967). Schrödinger noted that living organisms must retain net energy in order to prolong their existence as a functioning living unit. Biology may constitute many subunits of cellular aggregates and proteins that are made up of chemical molecules. They also have more complex interactions with photon radiation. If life exists by retaining energy from photons of the electromagnetic spectrum, then their photon emission profiles would be much different than tissues or matter that are not distinctly labelled, clinically, as living. Photon measures from non-living tissue have not, to current knowledge, been researched. It may be assumed to be of no importance to study a collection of preserved matter because there are no clear indications that biological processes still exist within matter that was once considered living. The distinction of photon count differences between living and non-living matter will be examined in proceeding chapters.

If a living biological system is open (by which it may gain or lose heat/energy from or towards its environment) it must retain energy in order for death to not occur for each cell that makes up the entirety of the system. It is then optimal for biological systems to conserve energy rather than expend it toward the surrounding environment that it resides in. Thus, net energy must be favourably endothermic by nature, rather than exothermic. It must be noted that if biological systems need to follow this assumption then it is not optimal for such net increases in photonic emissions to be present. This assumption may not be valid if emissions are a reflection of an underlying process of communication (Sun, Wang & Dai, 2010). If increases of photonic emissions from neurological tissues are coupled to cognition (Dotta & Persinger, 2011), then

such increases that have been found may serve as a form of communication between the functioning units of the brain: the neurons. Popp (1979) had studied the storage of photons within biological systems as well comparative to just the release of photons. Photons and their energy are dependent on their own frequency. If the storage of specific photon frequencies, and by proxy, wavelengths within biological systems occur then the possibility of information exchange can by hypothesized. Persinger (2010) postulated that the source of photons coming from the neuronal plasma membrane is due to the energy dynamics during action potentials. As neurons communicate with surrounding cells through chemical and electrical potentials, the possibility for photon emissions would be consistent with what occurs within basic cell constituents: atoms. This hypothesis would provide a non-chemical, non-voltage related pathway commonly seen in cellular processes. Speculation must be met with rigorous testing of this hypothesis by measuring and analyzing biological sourced photons.

Photon Detection

Photons can be measured by the use of photomultiplier tubes (PMTs) that can readily detect photons at extremely low intensities (Inaba, 1988). The photomultiplier tubes used in the subsequent chapters to detect low intensity photons were designed to measure photons within the 300-800nm range inclusively. This range includes all wavelengths of photons within the visible spectra. The methods used in human trials within this document are similar in design to previous works (Dotta & Persinger, 2011; Dotta, Saroka & Persinger, 2012) to confirm retest reliability. Due to the sensitivity of the equipment, all photon recordings take place within very dark, enclosed areas where minimal external influences can be affected on matter being recorded. Temporal photon count measures provide other statistical methods to be used in analyzing that

retrieved data. This document will display methods of spectral analyses and time- and phase-lagged coherence to explore the possibilities of photon based communications in matter.

By measuring the dynamics of photonic emissions from various tissues and matter, we may examine complex distribution of energy that is underestimated or previously not studied thoroughly amongst sample cell populations and nervous tissue. The complexities within the framework of neural organization allows inferences to be made about such emissions such as the dispersion of photic energy and its contribution to the correlates of consciousness. Although consciousness is not the primary topic of debate, the differences in living and non-living matter and their respective photonic emission profiles allows us to hypothesize that photons may contribute towards higher functioning systems.

References

Boveris, A., Cadenas, E., Reiter, R., Filipkowski, M., Nakase, Y., Chance, B. (1980). Organ chemiluminescence: Noninvasive assay for oxidative radical reactions. *Biophysics*, *77*(1), 347-351.

Cohen, S., & Popp, F. A. (1997). Biophoton emission of the human. *Journal of Photochemistry and Photobiology*, 40, 187-189.

Dotta, B. T., & Persinger, M. A. (2011). Increased Photon Emissions from the Right But Not the Left Hemisphere While Imagining White Light in the Dark: The Potential Connection Between Consciousness and Cerebral Light. *Journal of Consciousness Exploration & Research*, *2*(10), 1463-1473.

Dotta, B.T., Saroka, K.S. & Persinger, M.A. (2012). Increased Photon Emissions from the Head While Imagining Light in the Dark Is Correlated with Changes in Electroencephalographic Power: Support for Bokkon's Biophoton Hypothesis. *Neuroscience Letters*, 513, 151-154.

Einstein, A. (1905). Concerning an Heuristic Point of View Toward the Emission and Transformation of Light. *Ann. Phys.*, 17, 132.

Einstein, A. (1917). The Quantum Theory of Radiation. *Physikalische Zeitschrift*, 18, 121.

Inaba, J. (1988). Super-high sensitivity systems for detection and spectral analysis of ultraweak photon emission from biological cells and tissues. *Experentia*, 44: 530-559.

Isojima, Y., Isoshima, T., Nagai, K., Kikuchi, K., Nakagawa, H. (1995). Ultraweak biochemiluminescence detected from rat hippocampal slices. *NeuroReport*, 6, 658-660.

Kobayashi, M., Takeda, M., Sato, T., Yamazaki, Y., Kaneko, K., Ito, K.I., Kato, H., Inaba, H. (1999). In vivo imaging of spontaneous ultraweak photon emission from a rat's brain correlated with cerebral energy metabolism and oxidative stress, *Neuroscience Research* 34, 103-113.

Mink, J.W., Blumenschine, R.J., Adams, D.B. (1981). Ratio of central nervous system to body metabolism in vertebrates: its constancy and functional basis. *American Journal of Physiology*, 241 (3): 203–212.

Persinger, M. A. (2010). 10^-20 Joules as a Neuromolecular Quantum in Medicinal Chemistry: An Alternative Approach to Myriad Molecular Pathways? *Current Medicinal Chemistry*, 17, 3094-3098.

Popp, F. A. 1979. Photon storage in biological systems. *Electromagnetic bioinformation*. Urban and Schwarzenberg: N.Y. 123-149.

Schrödinger, E. (1967). What is life?: The physical aspect of the living cell & Mind and matter. *Cambridge: University Press*.

Sun, Y., Wang, C. & Dai, J. (2010) Biophotons as Neural Communication Signals Demonstrated by *in Situ* Biophoton Autography. *Photochemical and Photobiological Sciences*, 9, 315-322.

Chapter 2 – The Periodic Elements and their Implications toward Photonic Emissions in Biology

Introduction

The periodic table of elements is a well-known tool used to categorize and group the chemical elements based on observable characteristics found within the laboratory. The nature of each element is unique and is noted in the past by scientists such as Mendeleev and Moseley. The observable patterns of the elements sorted into periods and groups of the periodic table may provide insight in the roles that the chemical elements partake in biological processes in living organisms such as that of the nervous system. The current study is a compilation of the known data of the chemical elements and applying the patterns toward photonic emissions found in biological systems similar to the works of Popp (1979).

Methods

Online (Dayah, 1997; webelements.com, n.d.) and paperback (CRC Press, 2006) references were used to create a dataset for each periodic element and their physical traits. All thermodynamic data retrieved were obtained, or converted, into variables measured in unit Kelvin. All data were imported into IBM SPSS Statistics v20 and run through various statistical analyses to observe the periodic trends presented in the current table of periodic elements. The elements of the periodic table are listed in numerical order of their respective atomic number (Table 1).

Table 1. List of the periodic elements with accompanying abbreviated notation and respective atomic number.

Element	Symbol	Atomic Number
Hydrogen	H	1
Helium	He	2
Lithium	Li	3
Beryllium	Be	4
Boron	B	5
Carbon	C	6
Nitrogen	N	7
Oxygen	O	8
Fluorine	F	9
Neon	Ne	10
Sodium	Na	11
Magnesium	Mg	12
Aluminum	Al	13
Silicon	Si	14
Phosphorus	P	15
Sulfur	S	16
Chlorine	Cl	17
Argon	Ar	18
Potassium	K	19
Calcium	Ca	20
Scandium	Sc	21
Titanium	Ti	22
Vanadium	V	23
Chromium	Cr	24
Manganese	Mn	25
Iron	Fe	26
Cobalt	Co	27
Nickel	Ni	28
Copper	Cu	29
Zinc	Zn	30
Gallium	Ga	31
Germanium	Ge	32
Arsenic	As	33
Selenium	Se	34
Bromine	Br	35
Krypton	Kr	36
Rubidium	Rb	37
Strontium	Sr	38
Yttrium	Y	39
Zirconium	Zr	40
Niobium	Nb	41
Molybdenum	Mo	42
Technetium	Tc	43
Ruthenium	Ru	44
Rhodium	Rh	45
Palladium	Pd	46
Silver	Ag	47
Cadmium	Cd	48
Indium	In	49
Tin	Sn	50
Antimony	Sb	51
Tellurium	Te	52
Iodine	I	53
Xenon	Xe	54
Caesium	Cs	55
Barium	Ba	56
Lanthanum	La	57
Cerium	Ce	58
Praseodymium	Pr	59
Neodymium	Nd	60
Promethium	Pm	61
Samarium	Sm	62
Europium	Eu	63
Gadolinium	Gd	64
Terbium	Tb	65
Dysprosium	Dy	66
Holmium	Ho	67
Erbium	Er	68
Thulium	Tm	69
Ytterbium	Yb	70
Lutetium	Lu	71
Hafnium	Hf	72
Tantalum	Ta	73
Tungsten	W	74
Rhenium	Re	75
Osmium	Os	76
Iridium	Ir	77
Platinum	Pt	78
Gold	Au	79
Mercury	Hg	80
Thallium	Tl	81

Lead	Pb	82
Bismuth	Bi	83
Polonium	Po	84
Astatine	At	85
Radon	Rn	86
Francium	Fr	87
Radium	Ra	88
Actinium	Ac	89
Thorium	Th	90
Protactinium	Pa	91
Uranium	U	92
Neptunium	Np	93
Plutonium	Pu	94
Americium	Am	95
Curium	Cm	96
Berkelium	Bk	97
Californium	Cf	98
Einsteinium	Es	99
Fermium	Fm	100
Mendelvium	Md	101
Nobelium	No	102
Lawrencium	Lr	103
Rutherfordium	Rf	104
Dubnium	Db	105
Seaborgium	Sg	106
Bohrium	Bh	107
Hassium	Hs	108
Meitnerium	Mt	109
Darmstadtium	Ds	110
Roentgenium	Rg	111
Copernicium	Cn	112
Ununtrium	Uut	113
Flerovium	Fl	114
Ununpentium	Uup	115
Livermorium	Lv	116
Ununseptium	Uus	117
Ununoctium	Uuo	118

Results

Non-Periodic Trends

The strongest correlation found between the periodic elements' atomic number (number of protons in atom) and their respective atomic masses ($r = 0.999$, $p<.001$) are displayed on Figure 1. A linear equation provides an average trend of approximately a 2.5 atomic mass unit increase as the number of atomic protons increase in the periodic table of elements.

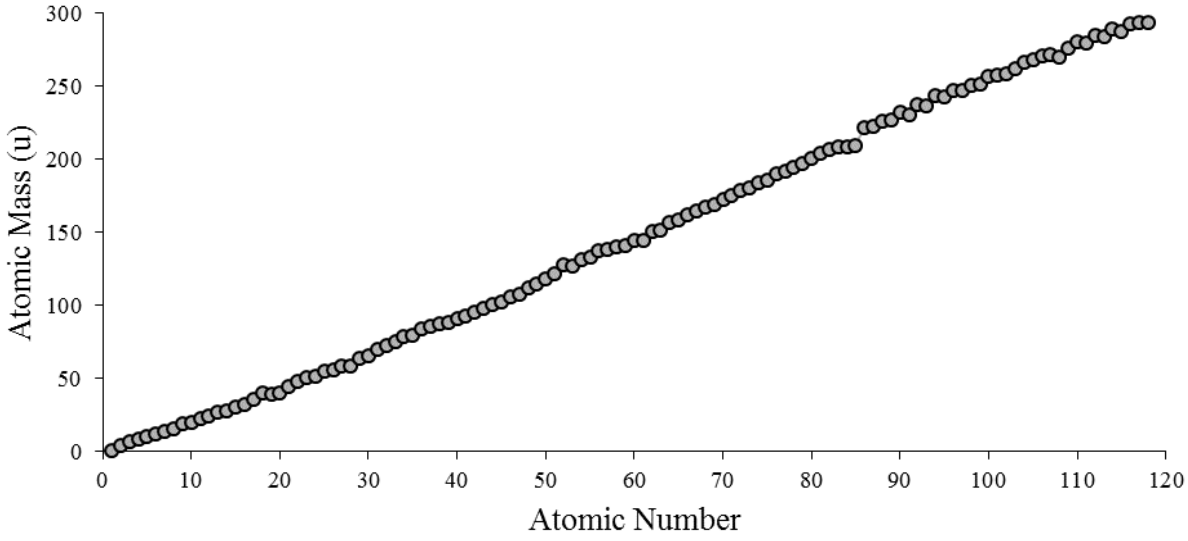

Figure 1. Correlation of atomic mass of each periodic element in relation to the number of protons in the atomic nucleus.

Periodic Trends

The visual representation of the elements on the periodic table are organized into Periods (horizontal rows of the periodic table of elements) and Groups (vertical columns of the periodic table of elements) as represented in Figure 2. As the atomic number increases, the amount of elements in the elemental Periods increase; two elements in Period 1, eight elements in Period 2 and Period 3, eighteen elements in Period 4 and Period 5, and 32 elements in Periods 6 and 7.

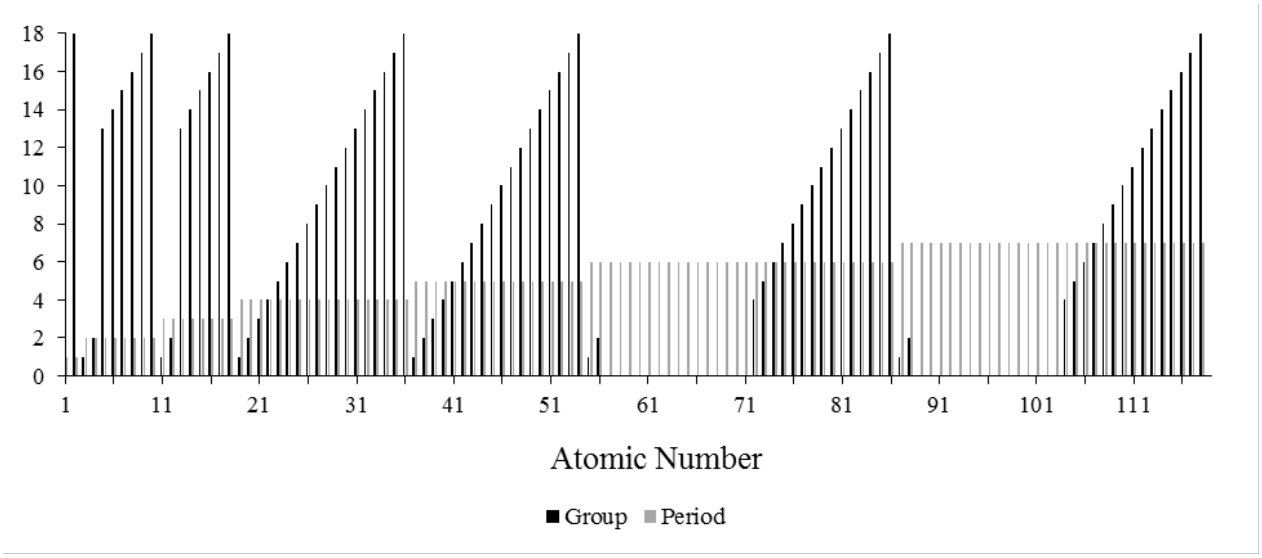

Figure 2. Representation of the Groups and Periods of the atomic elements. The Lanthanide (Elements 57-71) and Actinide (Elements 89-103) Groups are represented as a value of zero.

Figure 3 displays the valence of the periodic elements from which the basis of the organization of the periodic table derived. The valence of the elements allow the sorting of elements into Groups as presented in Figure 2. Valence electron number is determined on the amount of electrons in the last orbital (s, p, d, f) left to be filled.

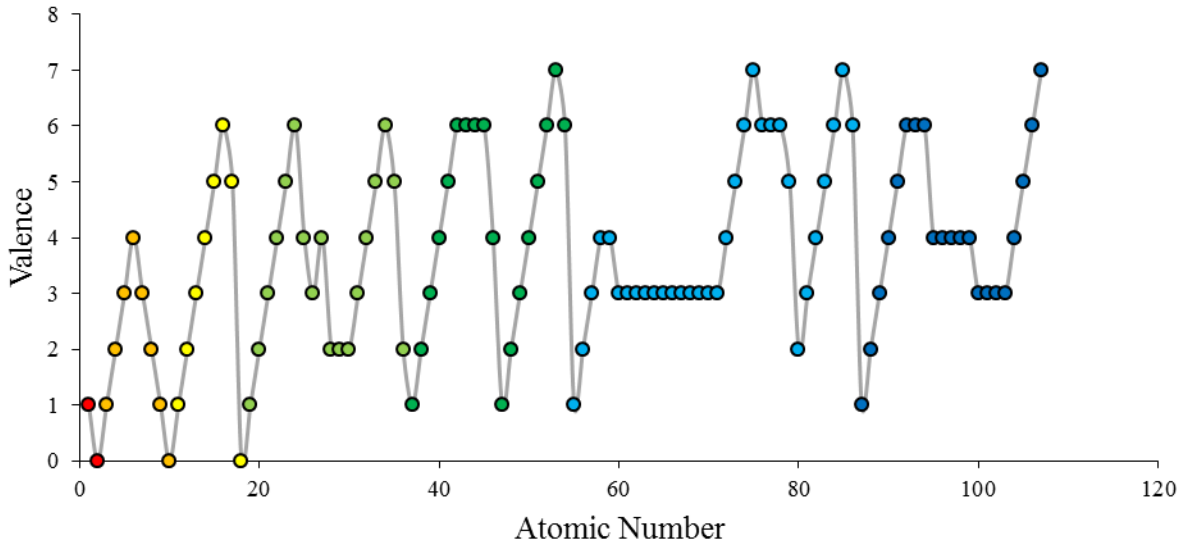

Figure 3. The valence of the atomic elements. The first three noble gas (Group 18) elements (Helium, Neon, Argon) have full electron orbitals and have a valence of zero.

The quantity of protons of an element within the periodic table reveal periodic trends in relation to the density of the elements. Figure 4 displays such relations. The densest element recorded is Iridium with a density of 22.65g/ml. Of the periodic elements, the elements that occur as a gas in nature are the least dense, where the most dense elements are most commonly solid.

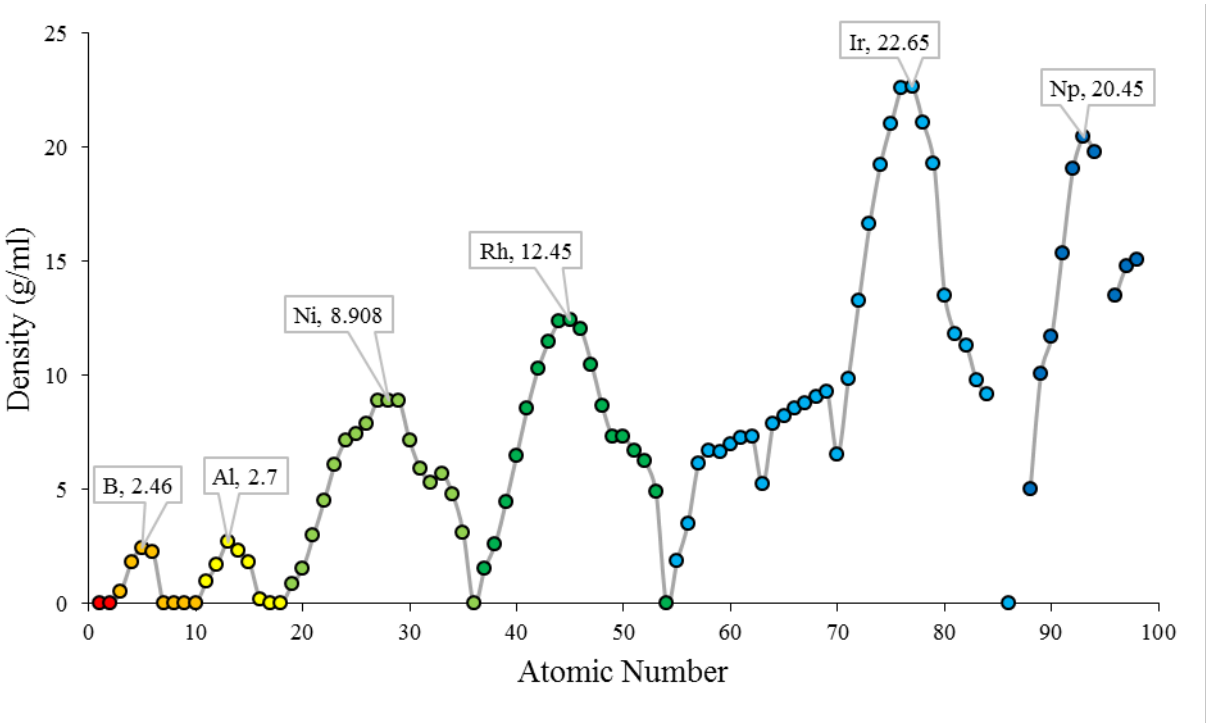

Figure 4. The atomic densities of the periodic elements. The elements of greatest densities of each period are labelled, excluding the first period.

The thermodynamic properties of the periodic elements vary in relationship with the number of protons in the atom of each element. The elements with the highest melting and boiling points are found within most of the solid phase elements of the periodic table. The lowest

melting and boiling points are shared amongst the gas phase elements of the periodic table. Refer to Figure 5. There were insufficient data on obtaining the boiling points of elements 97-118.

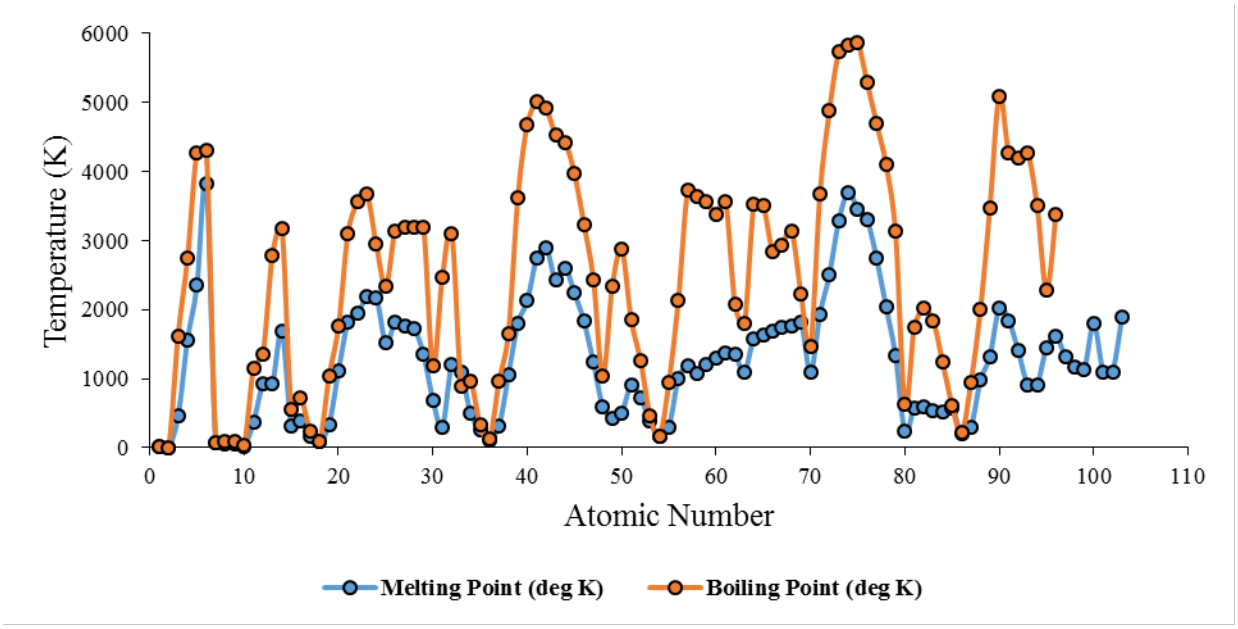

Figure 5. The comparative melting points and boiling points of the periodic elements in degrees Kelvin.

Thermodynamic data including the heat of fusion of the periodic elements can present the amount of enthalpy change during the transition of solid to liquid phase. The latent heat of fusion is measured in kilojoules per mole of element resulting in how much energy is required per mole to convert an element from its solid phase to liquid phase (Figure 6). Carbon (105 kJ/mol), silicon (50.2 kJ/mol), and boron (50 kJ/mol) have the highest latent heat of fusion.

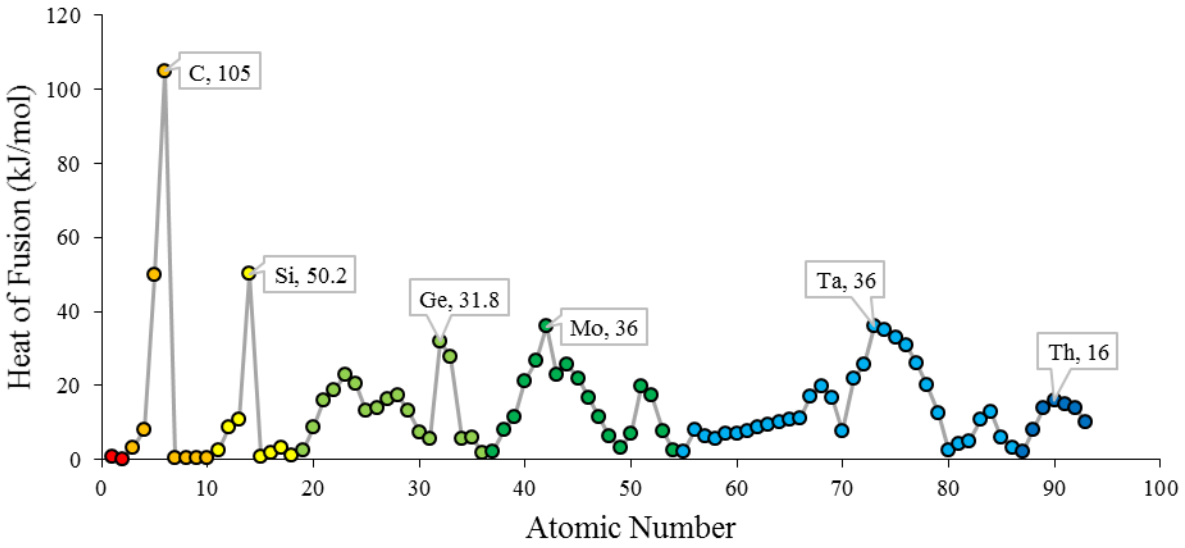

Figure 6. The latent heat of fusion of the periodic elements. Elements with the greatest values per period are labelled, with the first period as the only exception.

The enthalpy change during the liquid to gas phase of the atomic elements also known as the latent heat of vaporization measures the amount of energy per mole of element required to convert one mole of an element from liquid to gaseous phase (Figure 7).

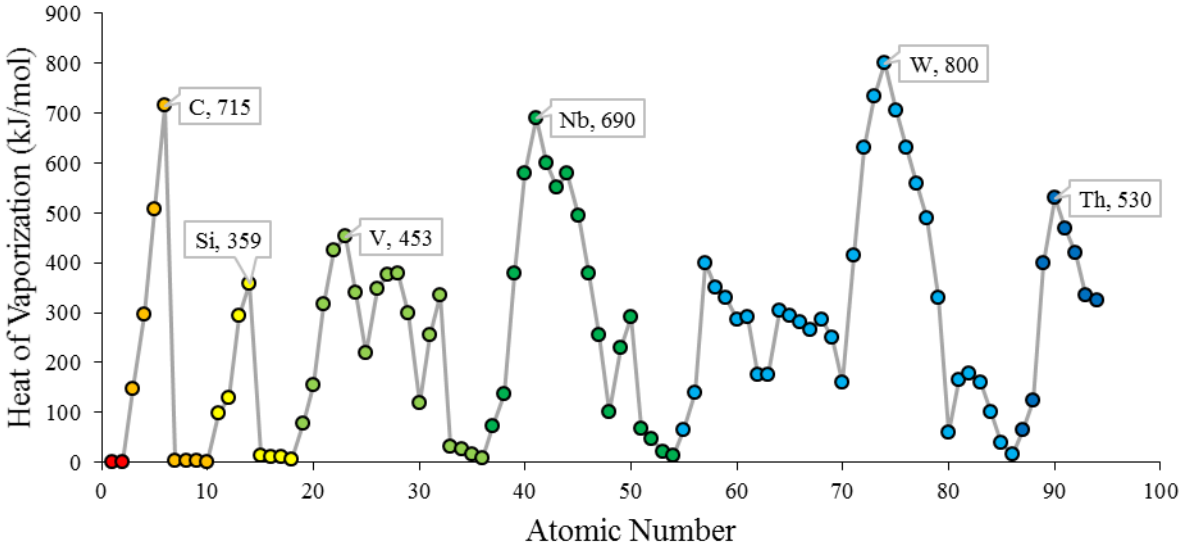

Figure 7. The latent heat of vaporization of the periodic elements. Elements with the greatest heat of vaporization constants of each period are labelled, with the exception of the first period.

The molar heat capacity is the measure of how much energy (Joules) is required to increase one mole of an element by one degree Kelvin, assuming there is no phase change (Figure 8). The molar heat capacity is the product of the specific heat capacity of a pure element multiplied by its molar mass.

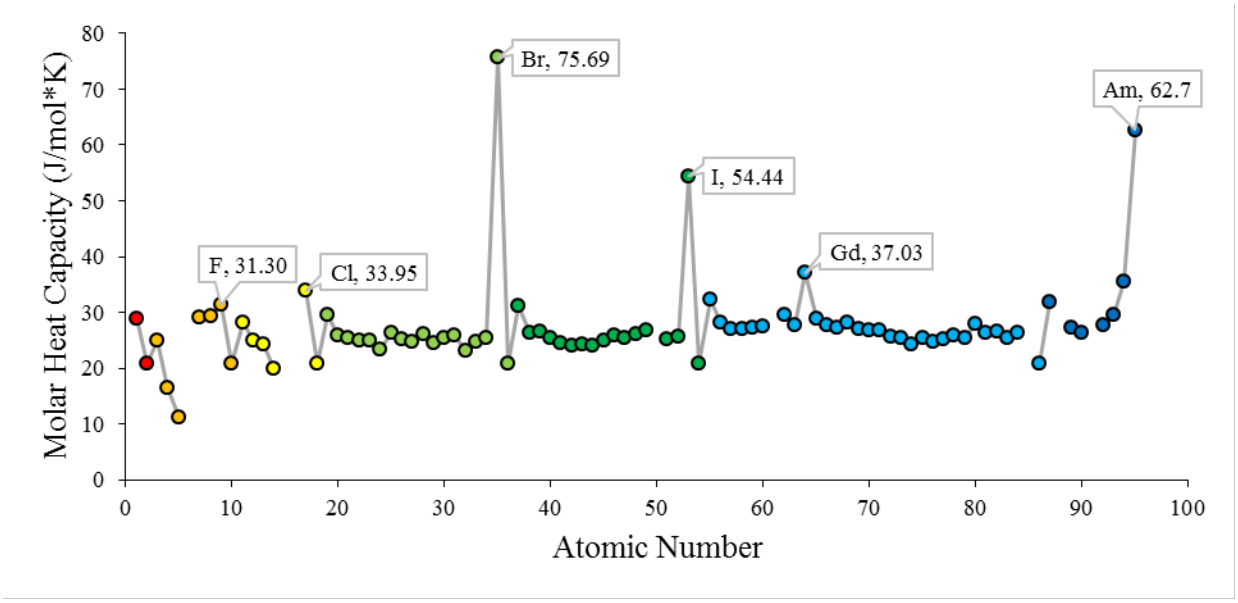

Figure 8. The molar heat capacity of the periodic elements. Elements with the greatest values of each period are labelled, with the exception of the first period.

The electrodynamic properties of the periodic elements display unique periodicities based on electron interactions. The amount of electrons are equal to that of the atomic number. Figure 9 displays the electronegativity of the periodic elements using the Pauling scale; the measure of how likely an atom will attract electrons. Fluorine has the highest electronegativity of all the elements, followed by the remaining halogen elements (Group 17) inclusive up to Iodine in descending order. The first three noble gases (Helium, Neon, and Argon) do not place on the Pauling scale for electronegativity as, reflected by Figure 3, these elements have zero valence.

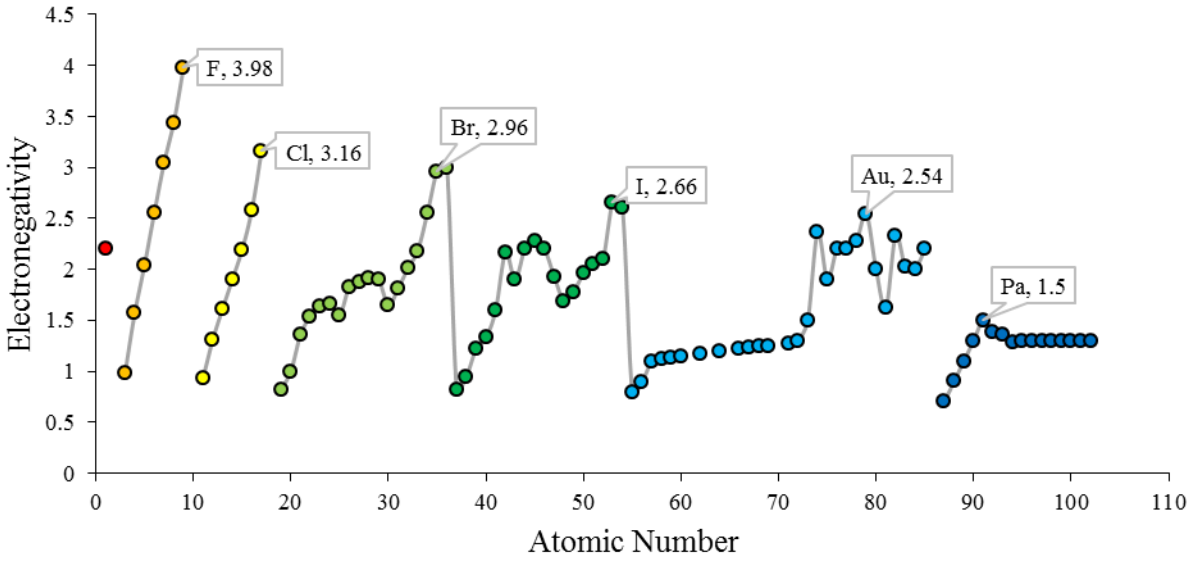

Figure 9. The electronegativity of the periodic elements. The elements with the highest electronegativity per period are labelled, except the first period.

Electron affinity is the amount of energy change when an electron is added to an element in gas phase, to form a negative ion (Figure 10). It is a measure of how likely an electron is to be added to an element. Halogen elements (Group 17) have the largest electron affinity as they require one more electron to have a stable outermost electron shell. Chlorine has the highest electron affinity of all the elements at 349 kJ/mol.

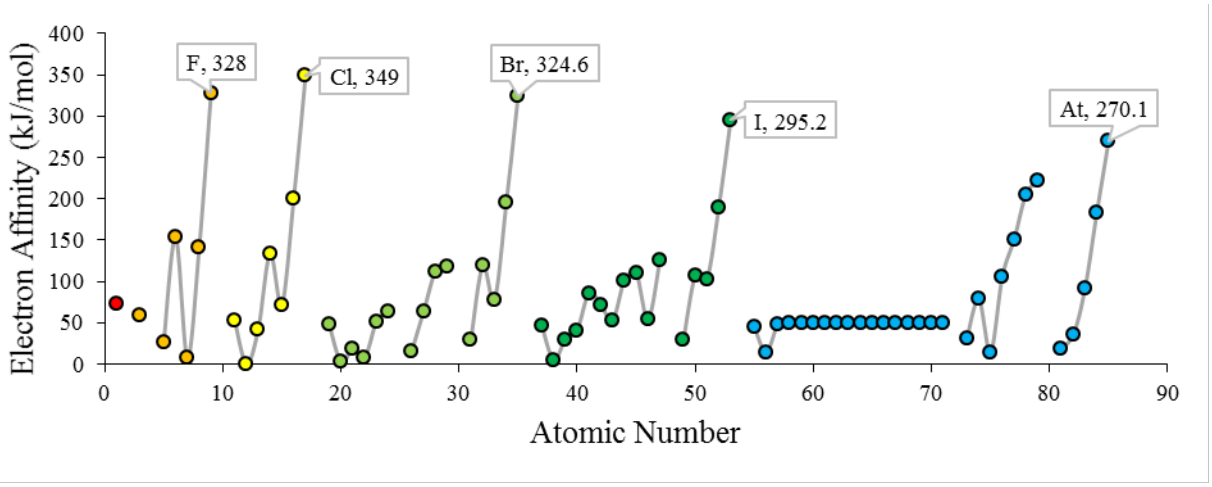

Figure 10. The electron affinity of the periodic elements. The elements with the highest electron affinities per period are labelled, with the exception of the first period.

The ionization energy (Figure 11) is the amount of energy required to remove the most loosely bound electron from the outermost electron shell, of a gaseous element, to form a cation. Noble gases (Group 18) are classified as the most stable elements as they have complete electron shells, and thus require the most amount of energy to remove an electron from its outermost shell.

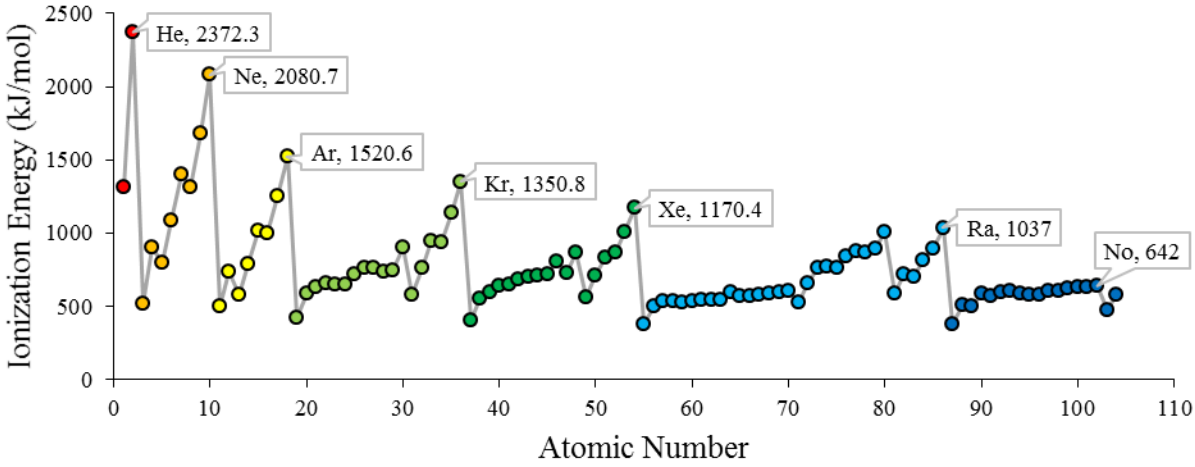

Figure 11. The first ionization energy of the periodic elements. Elements with the highest values per period are labelled.

The greatest covalent radii empirically measured of the atomic elements are held amongst the Group 1 elements, and a gradual decrease in radius length can be seen for each period as the group number increases for the respective elements by period (Figure 12).

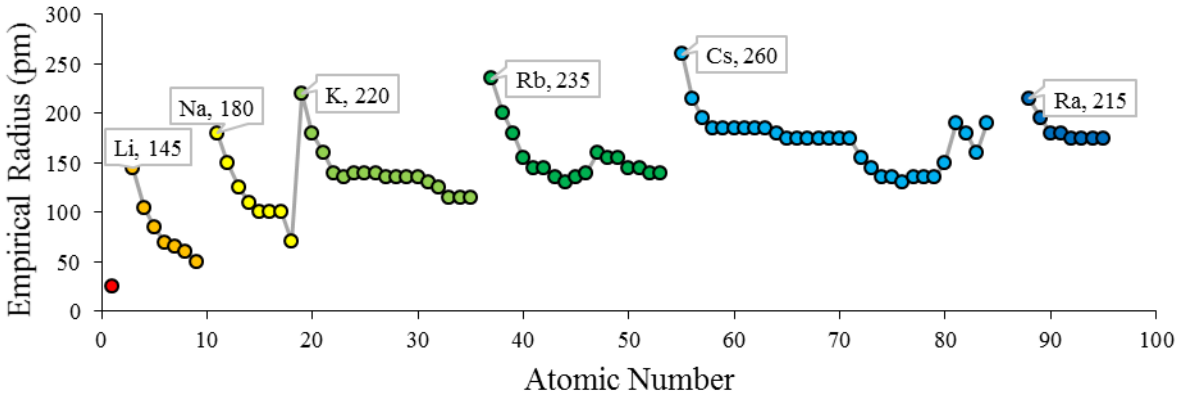

Figure 12. The empirical covalent radii (in picometers) of the periodic elements. The elements with the greatest radius per period are labelled, with the exception of the first period.

The refractive indices (how much light is refracted) of the periodic elements by period reveal a dispersion amongst most of the gas phase elements (Figure 13). Carbon in cubic diamond, which is not displayed on the figure below, has a refractive index of 2.4175. No other elemental refractive indices were measured from the source material as there was insufficient data.

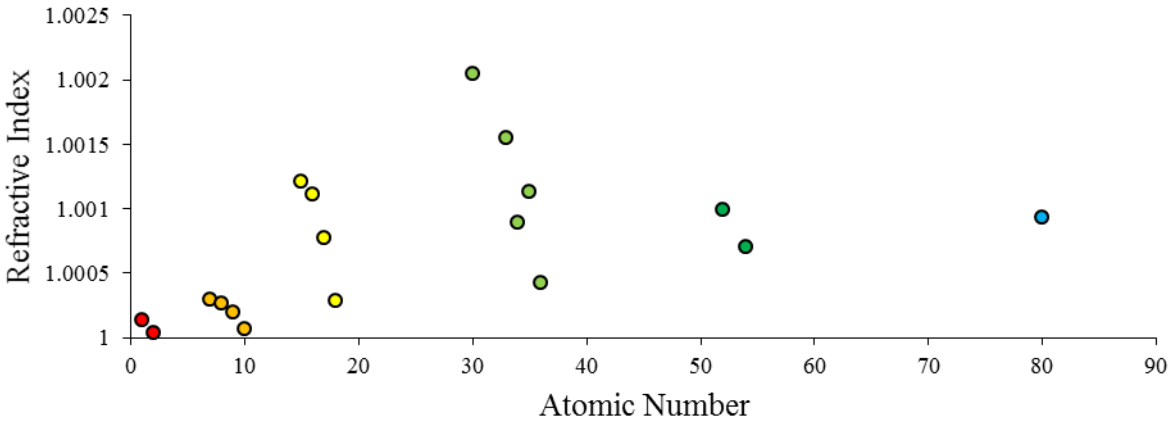

Figure 13. The refractive indices of the periodic elements.

The thermal conductivity of the periodic elements (Figure 14) measured in Watts per metre Kelvin are greatest within the Group 11 elements: Silver (430 W/m*K), Copper (400

W/m*K), and then Gold (320 W/m*K) in descending order of greatest thermal conductivity values.

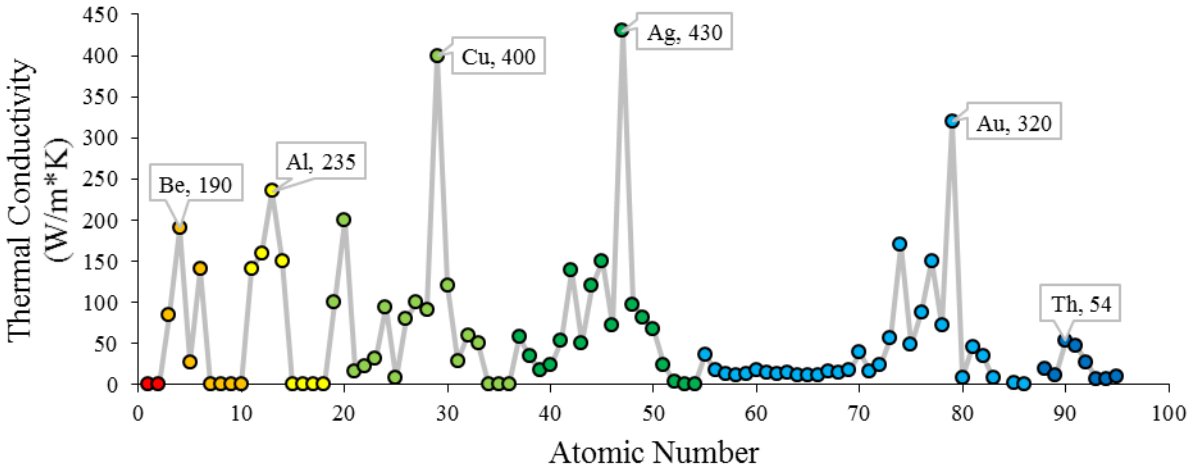

Figure 14. The thermal conductivity of the periodic elements. Elements with the greatest conductivities are labelled. The first period is excluded from labelled values.

The same general periodic trend can be observed of the periodic elements with electrical conductivity (Figure 15), measured in megaSiemens per metre, where Silver has the highest electrical conductivity (62 MS/m), followed by Copper (59 MS/m) then Gold (45 MS/m).

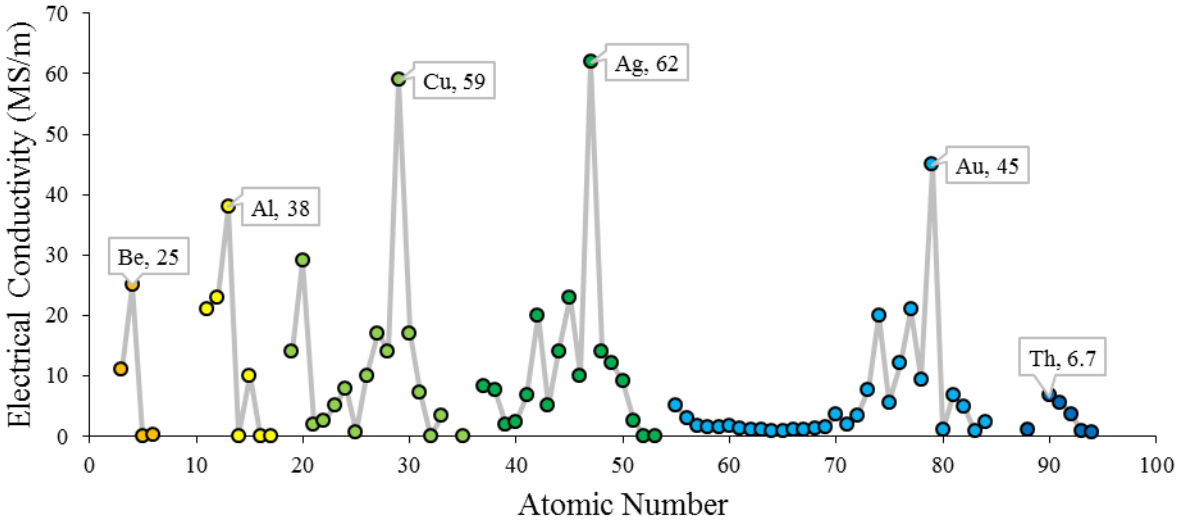

Figure 15. The electrical conductivity of the periodic elements. Elements with the greatest conductivity are labelled.

Figures 16, 17, and 18 display the periodic trends of the varying moduli that can be measured of the elements. Gaseous elements had missing data as only non-gaseous elements could be measured of their resistance to compression. Bulk modulus is a measure of resistance to uniform compression (Figure 16), shear modulus (Figure 17) is a ratio of shear stress, and Young modulus (Figure 18) is the ratio of stress along the axis of strain placed on a solid (elasticity). All measures of the moduli are in GigaPascal units; measures of pressure.

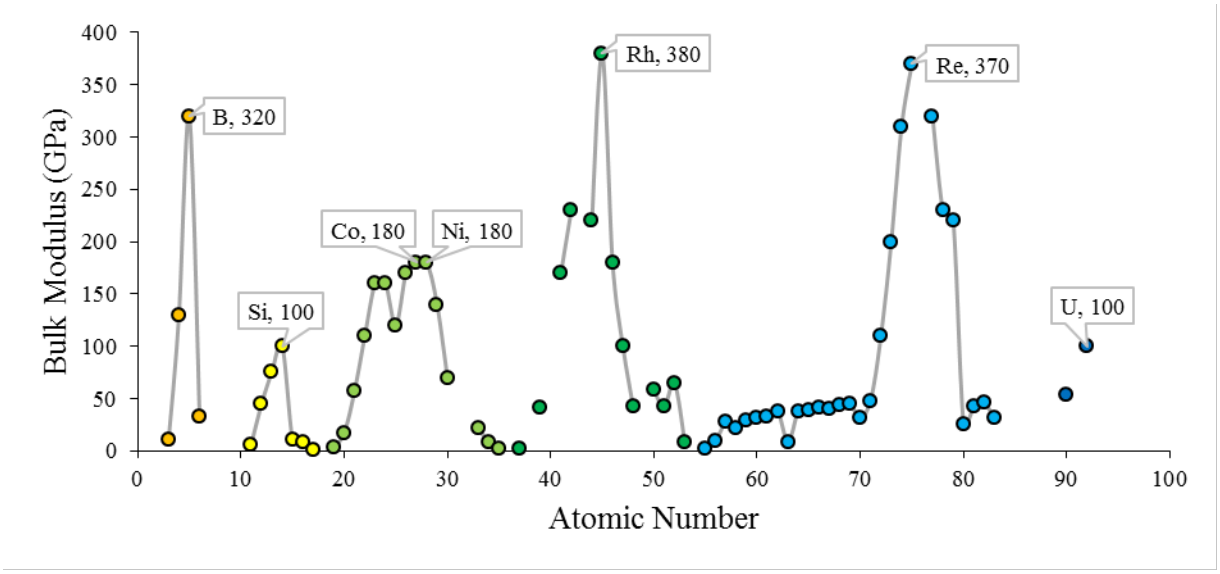

Figure 16. The bulk modulus of the periodic elements. Elements with the greatest moduli are labelled.

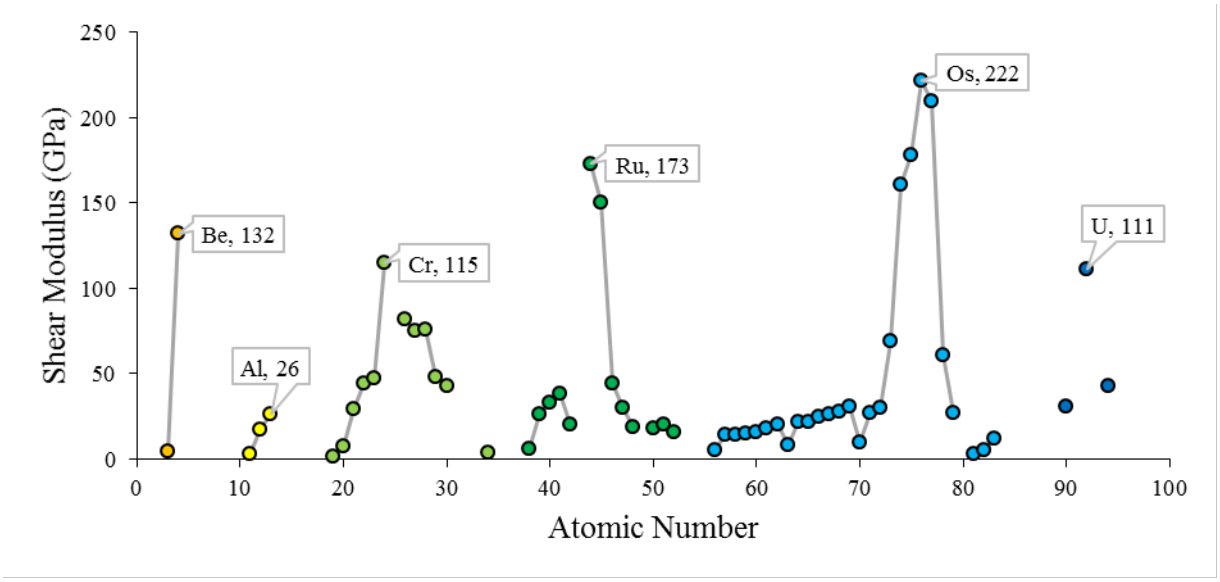

Figure 17. The shear modulus of the periodic elements. Elements with the greatest moduli are labelled.

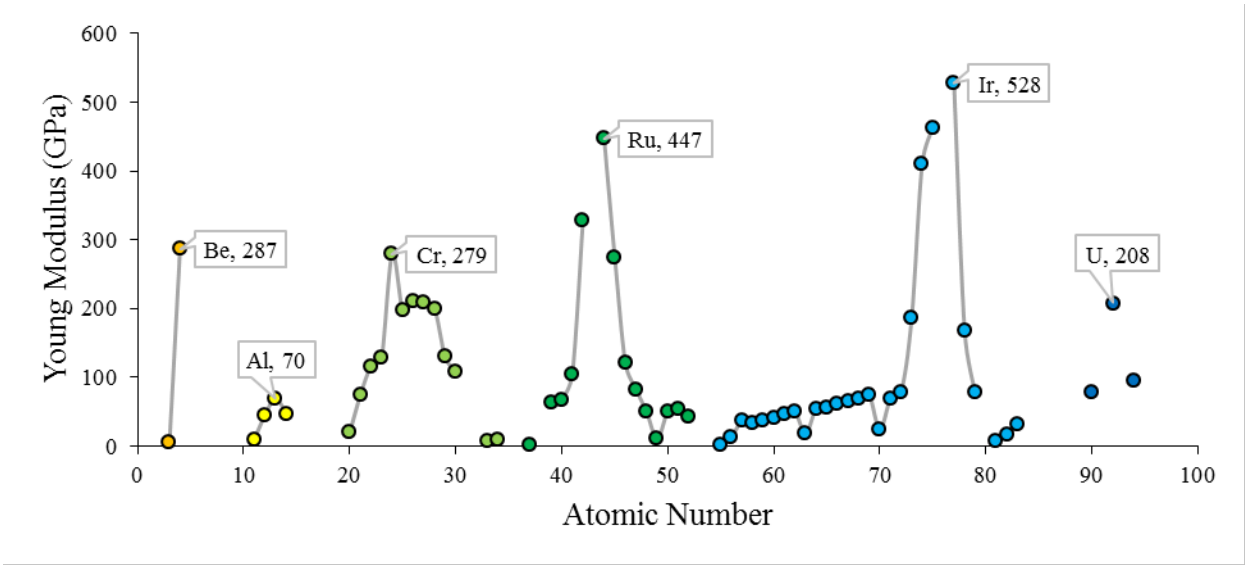

Figure 18. The Young modulus of the periodic elements. Elements with the greatest moduli are labelled.

Miscellaneous Data

Various data on the estimated abundance of the periodic elements within labelled systems were obtained and plotted on the figures below. The human body (Figure 19) contains more Oxygen than any other element, similar to the Earth's oceans (Figure 20). The human body is then mostly comprised of Carbon, followed by Hydrogen. Other parallels of chemical abundance

can be observed between the Earth's crust (Figure 21) and meteor composition (Figure 22), as well as the approximate equal ratios of elements within the Sun (Figure 23) and the observable Universe (Figure 24).

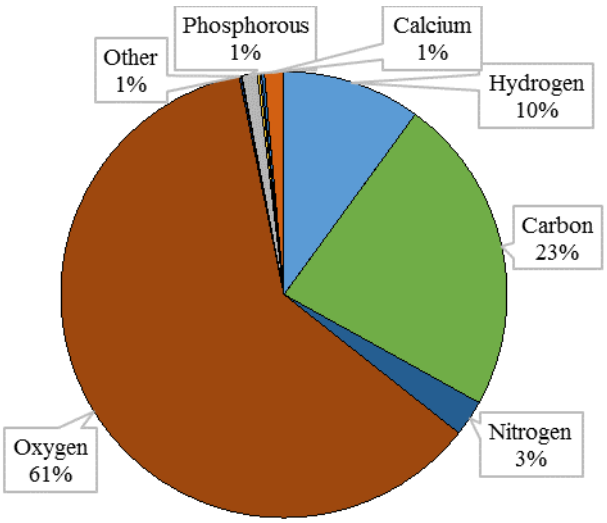

Figure 19. Abundance of the periodic elements in the human body.

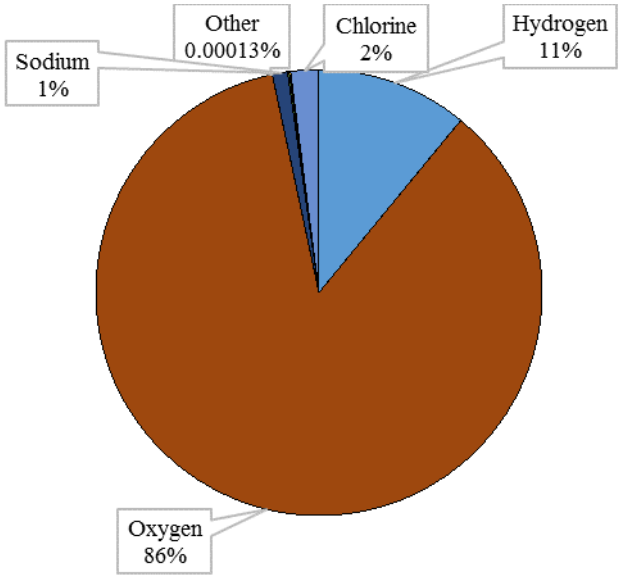

Figure 20. Abundance of the periodic elements in the Earth's oceans.

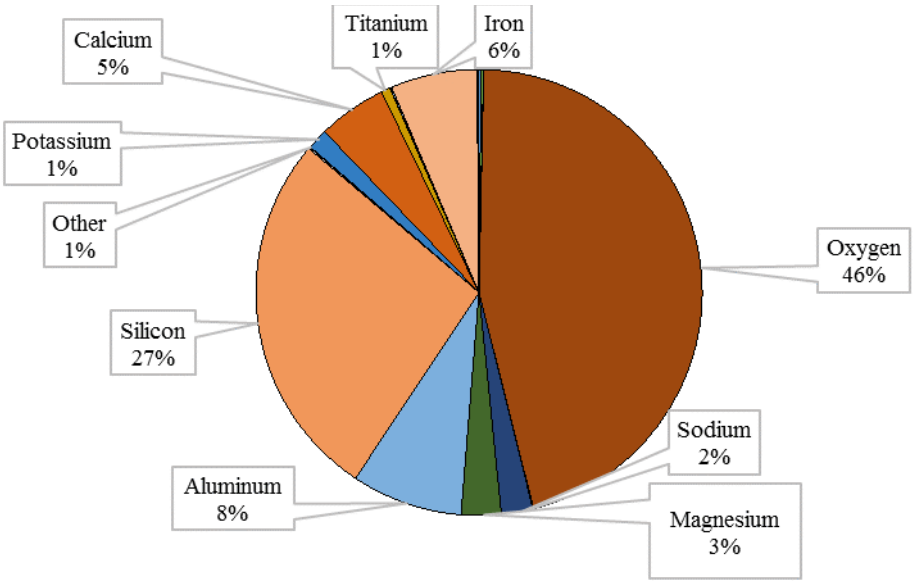

Figure 21. The abundance of the periodic elements in the Earth's crust.

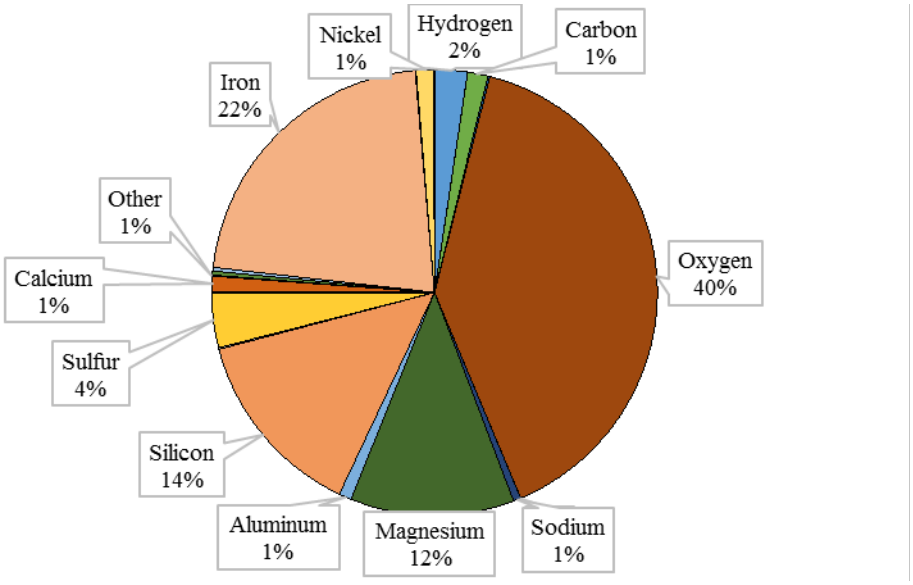

Figure 22. The abundance of the periodic elements in meteors.

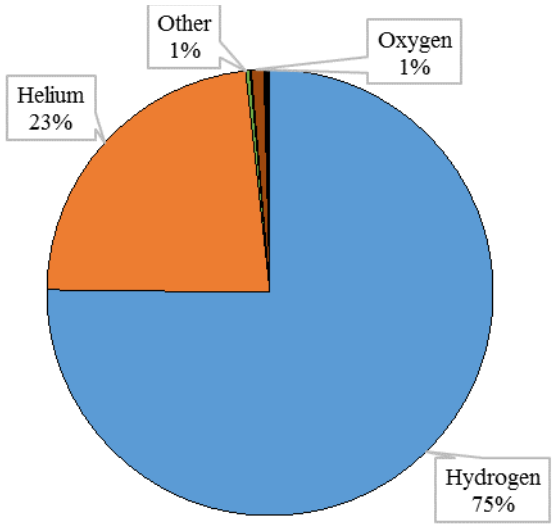

Figure 23. The abundance of the periodic elements in the Sun.

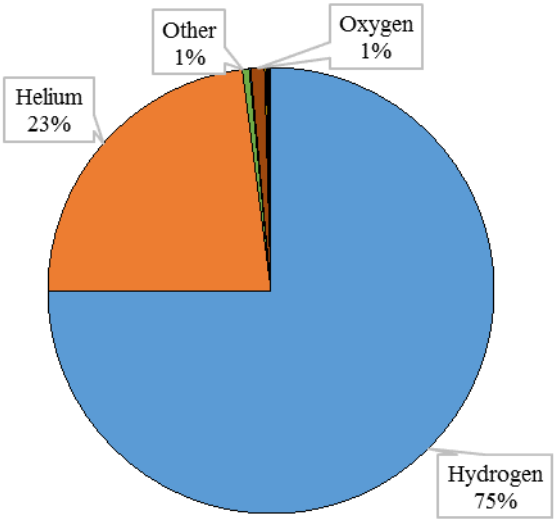

Figure 24. The abundance of the periodic elements in the Universe.

Relationships

A significant positive correlation was observed between melting and boiling points of the atomic elements, $r = 0.902$, $N=96$, $p<.001$ (Figure 25).

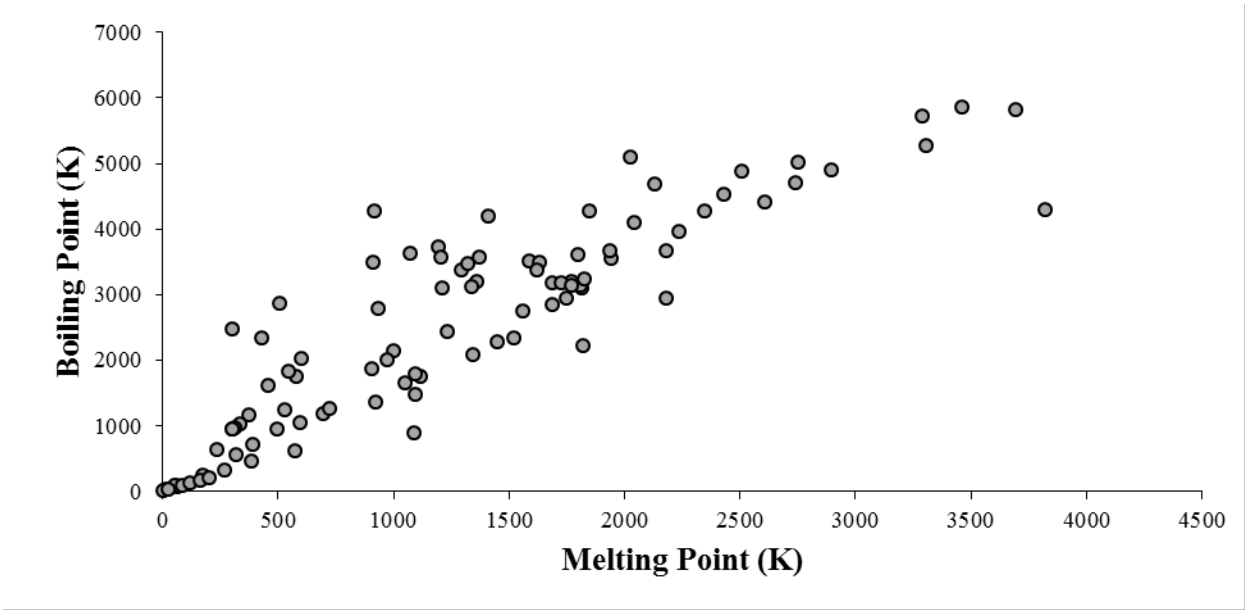

Figure 25. The relationship between melting and boiling points of the periodic elements.

A significant positive correlation was observed between the electronegativity and the electron affinity of the atomic elements, r = 0.702, N=70, p<.001 (Figure 26).

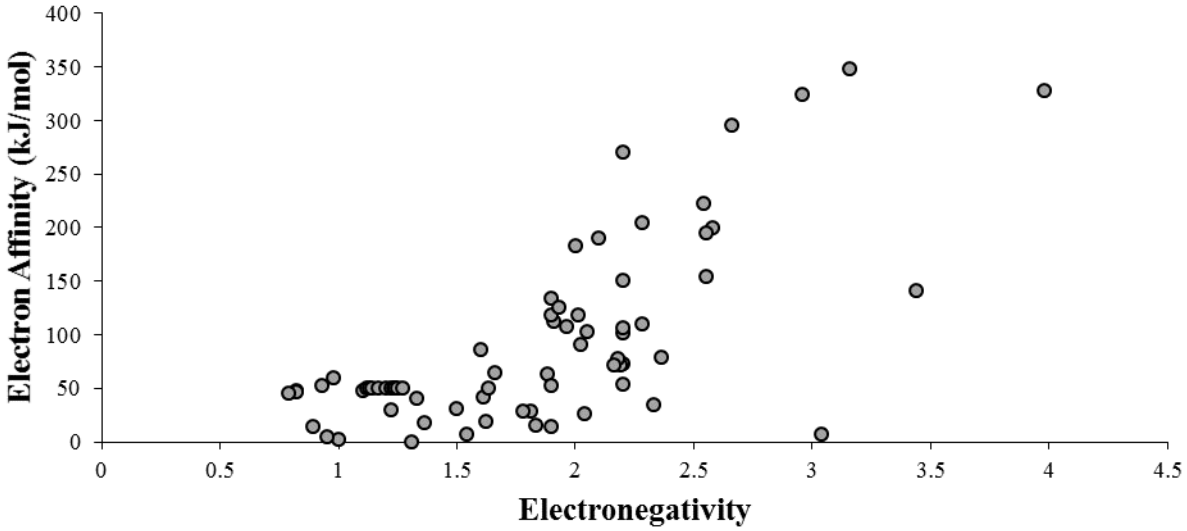

Figure 26. The relationship between the electronegativity and the electron affinity of the periodic elements.

When correlating the electronegativity of the atomic elements with the first ionization energy, a positive correlation is observed, r = 0.905, N=95, p<.001 (Figure 27).

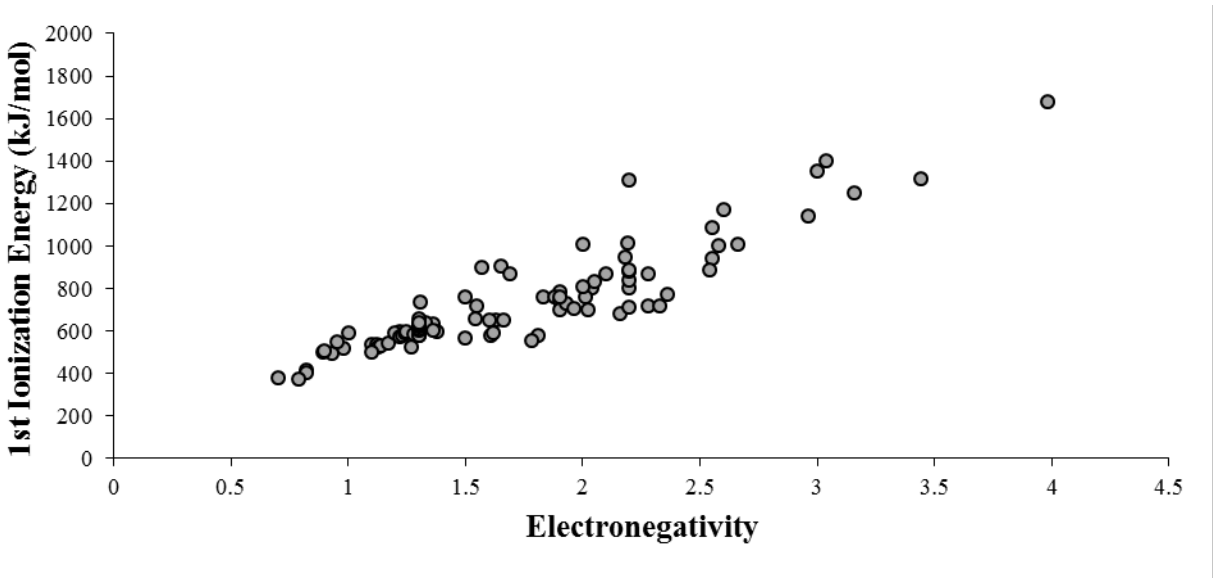

Figure 27. The relationship between the electronegativity and the first ionization energy of the periodic elements.

A strong negative correlation is found when relating the electronegativity of the atomic elements with their empirical radii, r = -0.798, N=83, p<.001 (Figure 28).

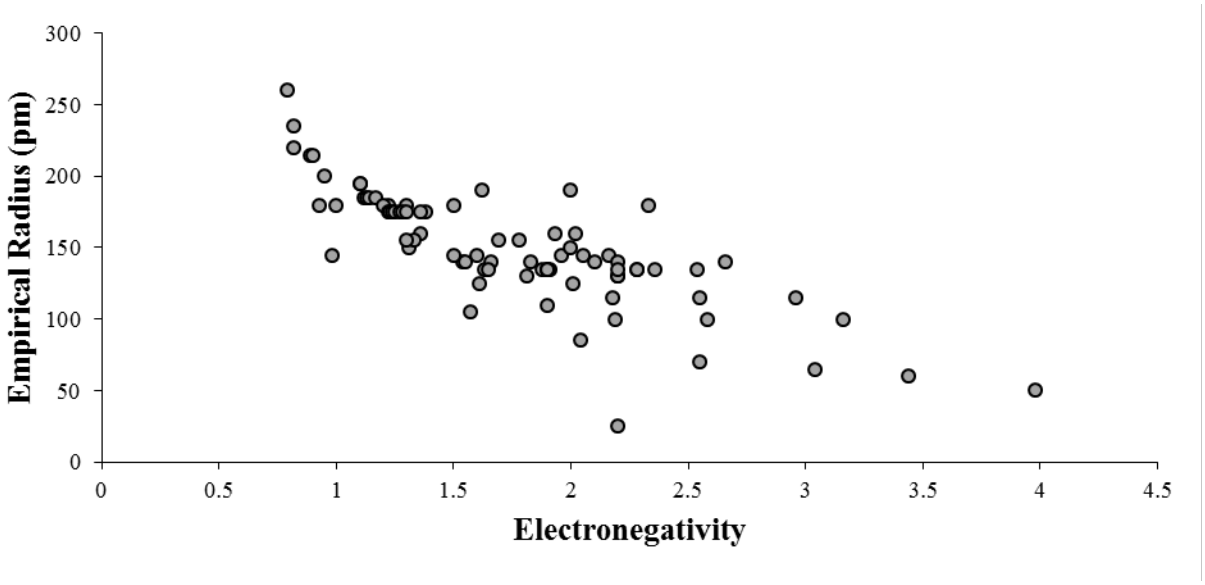

Figure 28. The relationship between the electronegativity and the empirical radii of the periodic elements.

A negative correlation was observed when relating the first ionization energy of the atomic elements and the empirical radii, r = -0.854, N=88, p<.001 (Figure 29).

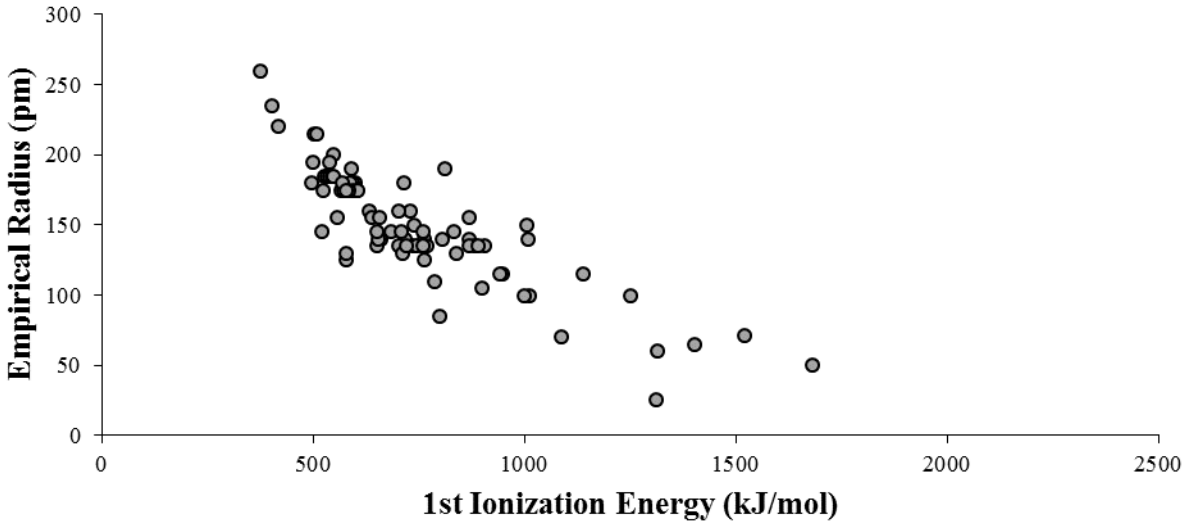

Figure 29. The relationship between the first ionization energy and the empirical radii of the periodic elements.

A strong, positive linear relationship was found between thermal and electrical conductivities of the atomic elements, r = 0.951, N=79, p<.001 (Figure 30).

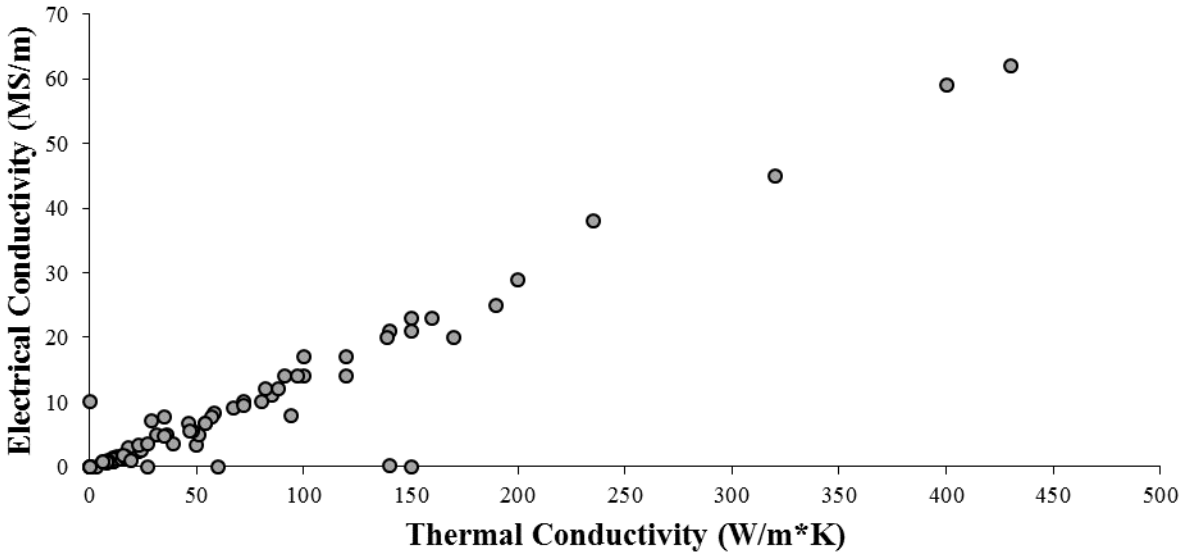

Figure 30. The relationship between the first ionization energy and the empirical radii of the periodic elements.

Pearson correlations revealed a positive linear relationship between the densities and the melting points of the atomic elements (Figure 31), r = 0.571, N=95, p<.001.

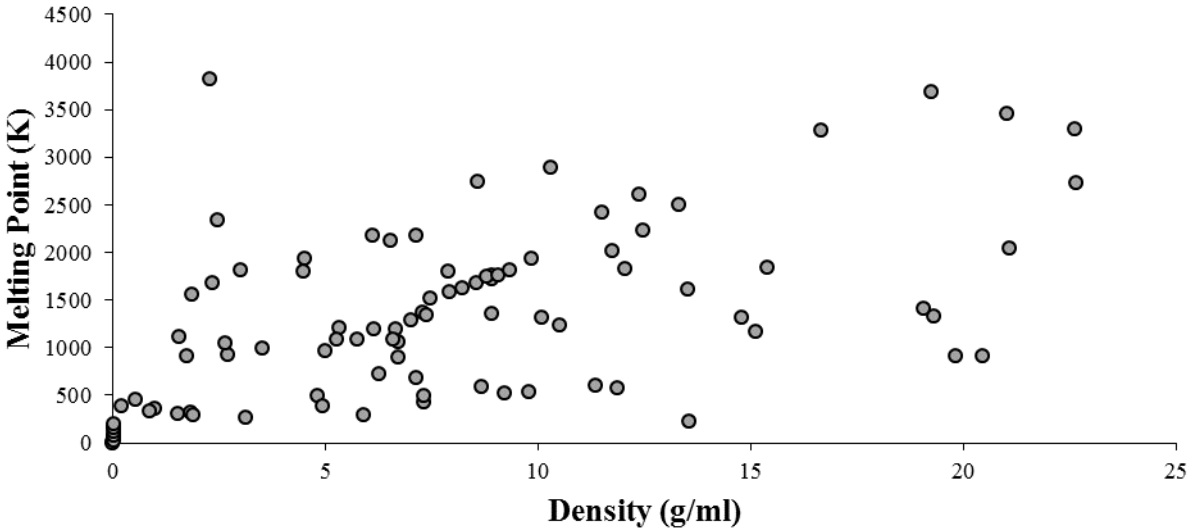

Figure 31. The relationship between density and the melting points of the periodic elements.

Conversely, in relation to the boiling points of the atomic elements, density is correlated with a higher coefficient than that of the melting point relationship (Figure 32), $r = 0.64$, $N=93$, $p<.001$.

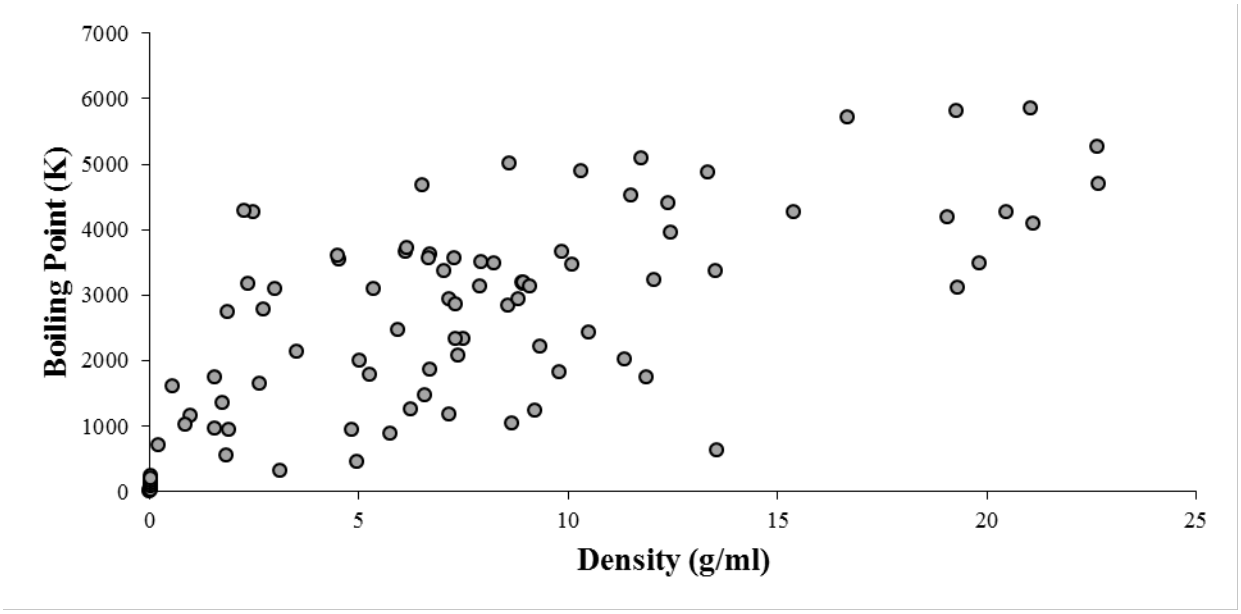

Figure 32. The relationship between density and the boiling points of the periodic elements.

A weak correlation between density and heat of fusion can be observed (Figure 33), r = 0.299, N=91, p=.004. Removing the element with the largest heat of fusion (Carbon) from the dataset, the correlation coefficient increases to r = 0.484.

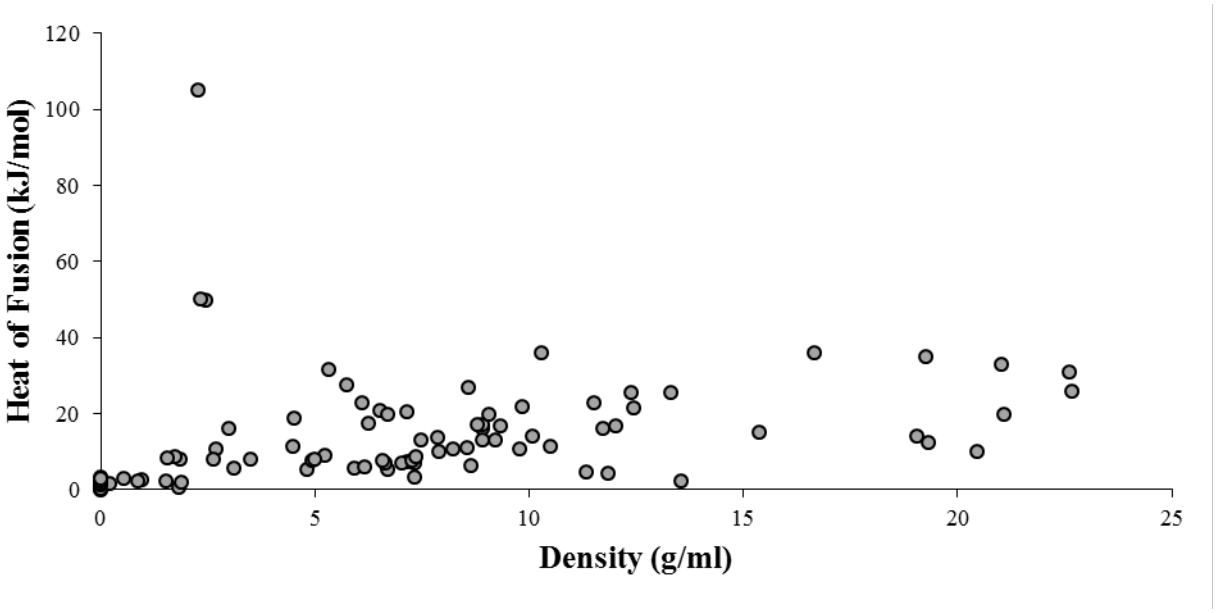

Figure 33. The relationship between density and the latent heat of fusion of the periodic elements.

A moderate correlation was observed between density and the latent heat of vaporization of the periodic elements (Figure 34), r = 0.646, N=92, p<.001.

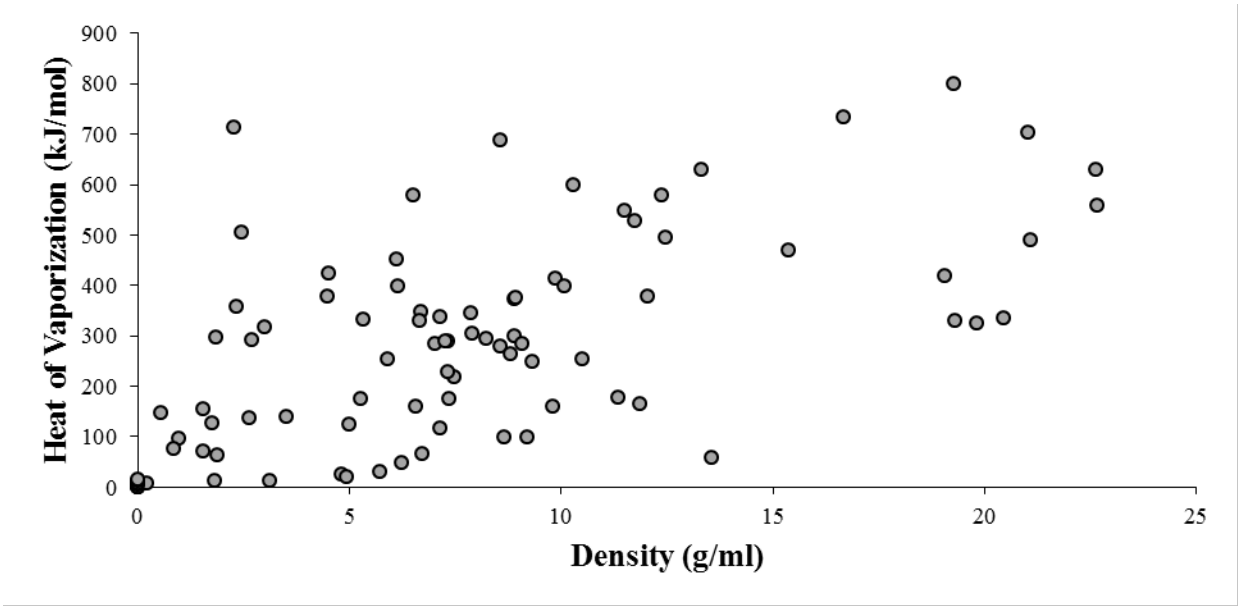

Figure 34. The relationship between density and the latent heat of vaporization of the periodic elements.

A linear relationship between the densities and first ionization energies of the atomic elements was observed (Figure 35), r = -0.331, N=95, p=.001. A logarithmic equation plotted over the same data strengthens the correlation coefficient (r = -0.781) where the equation would equate to:

$$y = -89.6\ln(x) + 862.6$$

The largest skew of the relationship between densities and first ionization energies of the elements derive predominantly from the noble gas elements, where they comprise the least dense elements and have the greatest first ionization energy.

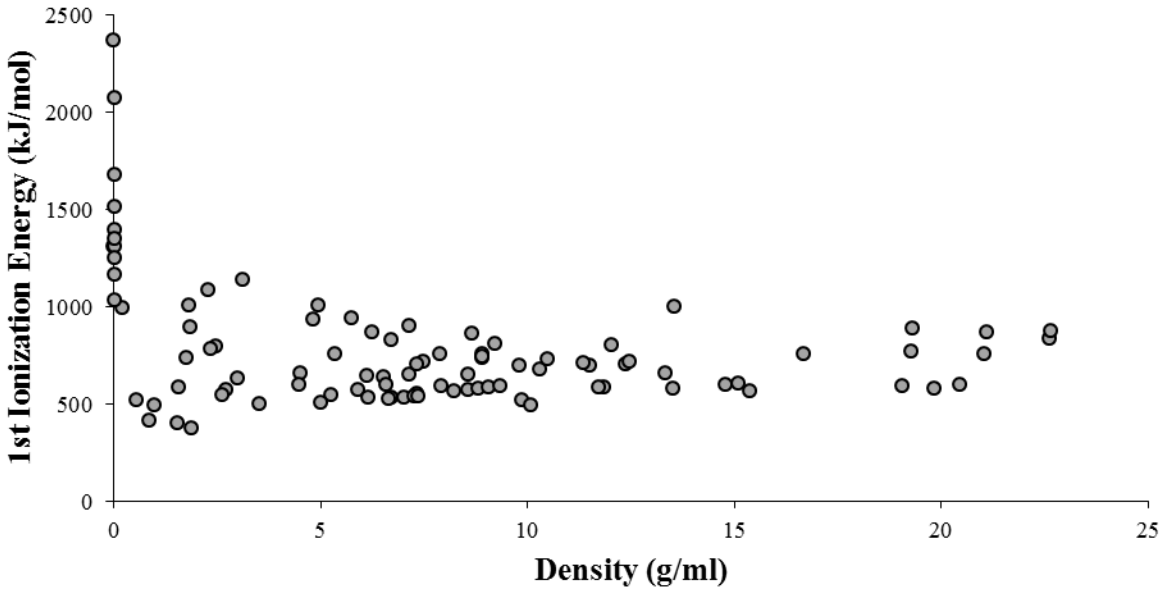

Figure 35. The relationship between density and the first ionization energies of the periodic elements.

A strong linear relationship between the boiling points and the heat of vaporization of the atomic elements was found (Figure 36), $r = 0.960$, $N=94$, $p<.001$.

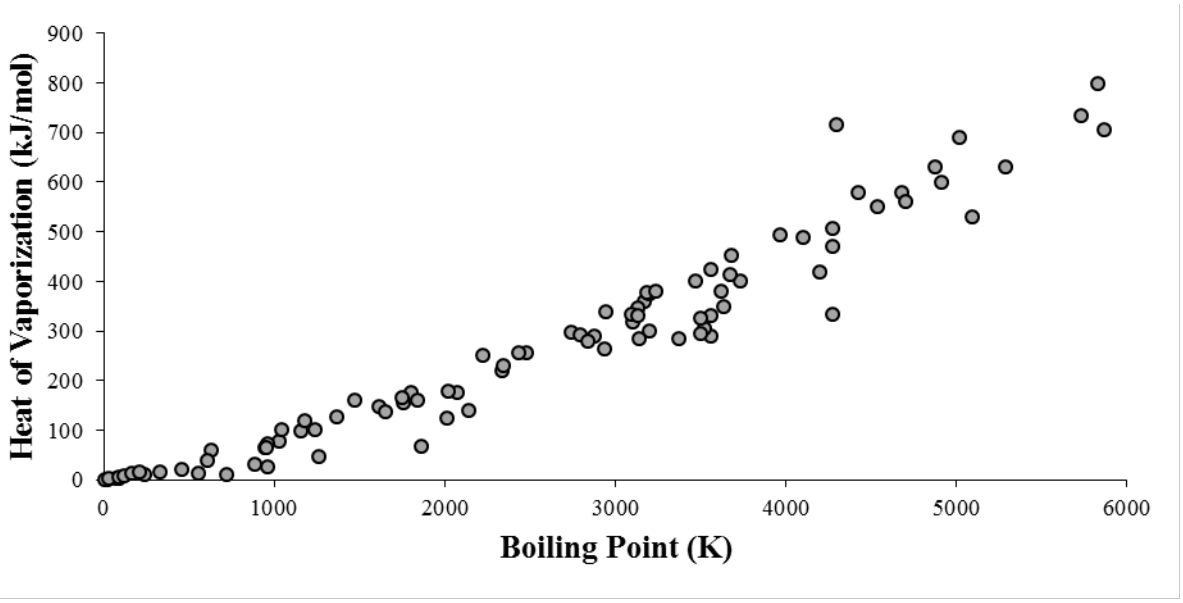

Figure 36. The relationship between the boiling points and the heat of vaporization of the periodic elements.

Discussion

It is clearly demonstrated from the data collected and analyzed, that atomic mass in accordance to the number of protons within each element is highly correlated. It is a simple deduction to assume that all elements are collections of protons and neutrons which constitute mass. As the atomic number increase, the amount of protons within the atomic nucleus increases. In this sense the simplest of all elements, Hydrogen, is noted as a single proton, and all other elements can be seen as a collection of Hydrogen atoms, when attributing mass equivalents. All other properties that are measured from the chemical elements are highly variable from one another. Such differences lie in the electrodynamics from the electron configurations and radii that define how the elements react with one another. The interactions have allowed the categorization of the periodic elements to be placed into groups and periods within the Periodic Table.

The neurological importance of some of the chemical elements can be hypothesized from the findings of physical and chemical dependent processes studied from neuroscientists in the last century. When periodic trends can be observed, the importance of specific element groups or periods can be deduced to have properties that drive biology and cellular processes. Organic life forms, those that contain Carbon, most notably would reveal some patterns to indicate that carbon is structural or dynamically different than other elements to be able to support the mechanisms underlying living biological organisms.

Schrödinger argued that life was significant from non-living structured systems in that living systems must oppose entropy in order to exist (Schrödinger, 1967). This argument directly observes that thermodynamic properties of life must be different than those that are not living. If it is assumed that the Carbon is present in most living organisms, and we observe the differences

of the thermodynamics of Carbon amongst the periodic elements, differences can be noted. The abundance of Carbon in the human body comprising of 23% has the highest latent heat of fusion amongst all of the elements; 105 kJ/mol. This is the amount of energy required to convert one mole of Carbon from its solid phase to its liquid phase. This high latent heat of fusion, as well as having one of the highest latent heat of vaporization, creates a high threshold for Carbon to maintain its physical structure. If Carbon bonds are prevalent within biological systems, such as in amino acids, it would be detrimental for the configuration of clusters of amino acids that produce proteins to break down and change phase consistently. A high latent heat of fusion in Carbon based life may not be coincidental, in that Carbon allows for parameters to exist to facilitate life. This high threshold may allow Carbon to 'absorb' energy greater than any other element, which when considering the neural applications, would be important for the consolidation and creation of new memories. This assumes that the amount of energy transfer is due to heat loss or acquisition similar to Landauer's principle in computing systems (Landauer, 1975). It may not be coincidental that the next element with the greatest latent heat of fusion is Silicon, which by modern technology standards, is used in creating computer processors.

Ion pumps along neuronal plasma membranes facilitate the movement of charge by the chemical exchange of ions from intracellular to extracellular concentrations. By assessing the properties of the most abundant ions within the human body, possible patterns may be observed. Biophotonic sources have been assumed by researchers such as Popp to be due to oxidative stress on cells through the mechanisms of reactive oxygen species (ROS) (Popp, 1979). However, oxidative stress allows Calcium (Ca^{2+}) influx to occur from the extracellular environment and endpoplasmic reticulum. Further calcium influx can directly inflcuence nucleic functions for gene transcription, and cell signalling in neural networks (Ermack & Davies, 2001).

It is evident from the results that calcium (Element 20 in the reported figures) has a moderate electrical and thermal conductivity that allows energy to be facilitated efficiently through it. Suppose there is a correlation between oxidative stress and calcium exclusively that may lead to photonic emission. Ca^{2+} carries a valence charge complementary to oxygen's O^{2-}, and can bind easily to form 2 molecules of CaO for every diatomic oxygen molecule. The separation of this molecule may briefly allow for a single oxygen radical (·O-) to occur during cellular changes due to calcium efflux. The remaining singlet oxygen may bind to form nitrogen monoxide for secondary messenger purposes, or towards the electron transport chain in the mitochondrion. The importance of caclium in cell signalling, and in apoptosis (when coupled to oxidative stress) leads to one of, if not the most important, charged elements in biophotonic emissions. Cellular calcium plays an important role in the conformational changes in cell membrane structure in the development in dendritic spine growth correlated to learning and memory formation (Yuste, Majewska & Holthoff, 2000). Calcium influxes used in vesicle release at the synaptic terminal may also share a source of photonic emission from the release of chemical neuropeptides in excitation. The many mechanisms that are influenced directly by cellular calcium must not be overlooked when considering the vital role it may take in cellular photonic emissions.

Thermal and electrical conductivity among the elements are highly correlated. The necessity for energy in any measurable state (ie. heat) to be facilitated through atomic compositions allows for elastic and inelastic radiation of energies to be measured in chemical systems reliably. As the many different elements differ based on mass and volume, the photoelectric dynamics would differ similar to the findings of Einstein (1917). The strong inverse relationship of the empirical covalent radius of atomic elements and the first ionization energy is revealing. The larger the electron space that can be shared within covalent bonds, the

less energy is required to remove a bound electron from it. While vice-versa, the smaller the electron space of an element the more energy is required to remove an electron. If the removal of electrons from external energy sources are in the form of photons as Einstein suggested, then the absorbance and emittance of photons is possible at this level of discourse. Predicting the photon's wavelength is possible if the amount of energy is known.

Each individual element emits and absorbs visible range photons uniquely based on their observable emission spectra. The energies associated with the visible wavelength photons (2.84×10^{-19} J to 4.97×10^{-19} J) and respective molar energy ranges of 171 kJ/mol (red) to 299 kJ/mol (violet) represent a spectrum for atomic elements to spontaneously emit photons within them. Any chemical data that pertains to this energy range include thermodynamic results within this energy range. Assuming this range of energy to be the visible range, only one of the first twenty elements fits within this emission of energy from the acquisition of an electron. This element is Sulfur (200 kJ/mol) with respect to electron affinity. Halogens have an energy change equivalent to the energy of ultraviolet radiation. The hydrogen halide reactions in chemistry usually require ultraviolet light in order to break the bonds to form radicals such as that of bromine and hydrogen for example. Many of the remaining elements have an energy change equivalent to infrared radiation including carbon and silicon which would be a recipient of heat absorption and possible emission, as stated previously. Although outside of the visible range, this calculated energy range fits closely within the biological range of photon emissions proposed by Popp (1979) of 300-1400nm in wavelength.

The patterns observed in chemical elements may provide the structural and dynamic bases that comprise larger systems in biology. Photon emissions are likely due to the electron states from the periodic elements when radicals are formed such as in research involving the

addition of hydroperoxides into rat livers both *in situ* and *in vivo* (Boveris *et al.*, 1980). Chemical electron interactions with neighbouring atoms, and molecules within biological systems such as the nervous system, play a pivotal role in the processes that dictate photon emissions measured in biophoton studies based on their states of excitability.

References

Boveris, A., Cadenas, E., Reiter, R., Filipkowski, M., Nakase, Y., Chance, B. (1980). Organ chemiluminescence: Noninvasive assay for oxidative radical reactions. *Biophysics*, 77(1), 347-351.

CRC Handbook of Chemistry and Physics (87 ed.), CRC Press, 2006

Dayah, M. (1997). Dynamic Periodic Table. Retrieved December 12, 2015, from Ptable: http://www.ptable.com

Einstein, A. (1917). The Quantum Theory of Radiation. *Physikalische Zeitschrift*, 18, 121.

Ermak, G., Davies, K.J.A. (2001). *Molecular Immunology*, 38, 713–721.

Landauer, R. (1975). Inadequacy of entropy and entropy derivatives in characterizing the steady state. *Phys. Rev. A Physical Review A, 12*(2), 636-638.

Popp, F. A. 1979. Photon storage in biological systems. *Electromagnetic bioinformation*. Urban and Schwarzenberg: N.Y. 123-149.

Schrödinger, E. (1967). What is life?: The physical aspect of the living cell & Mind and matter. *Cambridge: University Press*.

The Periodic Table by WebElements. (n.d.). Retrieved December 12, 2015, from http://webelements.com/

Yuste, R., Majewska, A., Holthoff, K. (2000). From form to function: calcium compartmentalization in dendritic spines. Nature Neuroscience, 3(7): 653-659.

Chapter 3 - Differential Spontaneous Photon Emissions from Cerebral Hemispheres of Fixed Human Brains: Asymmetric Coupling to Geomagnetic Activity and Potentials for Examining Post-Mortem Intrinsic Photon Information

Published in Neuroscience and Medicine

Abstract

The emissions of biophotons have been considered a ubiquitous property of living systems and their components. “Spontaneous” photon emissions from fixed whole and sectioned human brains were measured within hyper-dark settings. Significant differences in photon counts were measured from different spatial planes. The flux densities were in the order of 2×10^{-12} W per m^2. The right hemispheres but not the left hemispheres displayed more photon emissions whose spectral power density profiles exhibited a conspicuous amplitude peak between 7.9 and 8 Hz. Brains measured in the hyperdark ($\sim 10^{-12}$ W·m^{-2}) after removal from the typical lighting of the laboratory emitted more photons than those that had been maintained in the hyperdark for one week. The significant correlation between the numbers of photons emitted from the left hemisphere (but not the right) and global geomagnetic activity also exhibited energy equivalence between the photon flux densities and the geomagnetic shift within the cerebral volumes. These results indicate that what has been assumed to be fixed unresponsive human brain tissue still emits small numbers of photons that may be residuals from ambient light and can potentially interact with global geomagnetic activity. The medical implications for post-mortem intrinsic photonic information based upon the anisotropic microstructures within the hemispheres of the human cerebrum are discussed.

Introduction

The emissions of photons from living systems have been examined and verified quantitatively from multiple perspectives. The perspicacious formulations by Popp and his colleagues (Popp, 1979; Popp, 1988; Popp, F.-A., Li, Mei, Galle, & Neurohr, 1988) concerning the physical and chemical mechanisms for biophoton emissions have been demonstrated in other contexts. Photon counts near living tissue that exceed background flux densities have been measured from bacteria (Tilbury & Quickenden, 1988), cells (Dotta, Buckner, Cameron, Lafrenie & Persinger, 2011), hippocampal slices (Kobayashi *et al.*, 1999), and the brains of human subjects engaging in specific cognitions (Dotta, Saroka, & Persinger, 2012; Van Wijk, Van Wijk & Bajpai, 2006). This list is by no means exhaustive. The order of magnitude of these photon emissions is $\sim 10^{-12}$ $W \cdot m^{-2}$. The ubiquitous nature of photon emissions from likely multiple mechanisms (Bókkon, Salari, Tuszynski & Antal, 2010) within the living system suggests they may be more directly involved with communication between living units such as cells and bacteria (Fels, 2009; Trushin, 2004). Communication also implies the containment and generation of information. However, to current knowledge, there have been no studies that have examined the spontaneous photon emissions from fixed human brains. When fixed properly, the micromorphological detail of the cerebral cortices remains remarkably intact for decades as verified by histological examination at 1000×. For several years a "background" radiant flux density by a variety of digital and analogue photomultiplier units that discern an order of magnitude of $\sim 10^{-12}$ to 10^{-11} $W \cdot m^{-2}$ were measured (Persinger, 2012; Persinger, Lafreniere, & Dotta, 2012). These values are about 10 to 100 times greater than the estimated values for cosmic ray densities at ground level (Konig, Kreuger, Lonag, & Sonning, 1981). In this article, it is

shown that spontaneous photon emissions increased near fixed whole brains and sections, and that the power spectra of the amplitude modulations of these flux densities were not random and may reflect the capacity to retain photonic energies.

Materials & Methods

Photomultiplier Tube

A single photomultiplier tube (PMT) from Sens-Tech Sensor Technologies (Model DM0090C) was used in all experiments to measure temporal photon counts. The spectral response range was between 300 - 850 nm. Sens-Tech Counter Timer software recorded all data with a 50 Hz sampling rate for 5000 readings (20 msec data points for 100 seconds) on a Lenovo ThinkPad laptop. All measurements were taken within a cardboard box (7.5 cm × 72 cm × 51 cm) in which the brain samples and photomultiplier sensor unit were placed. All trials occurred within a hyperdark enclosed chamber, with USB connections from the photomultiplier unit connected through to an external room where the data-logging laptop was positioned.

Specimens

Photon counts were obtained from preserved whole-brains (n = 3), sagittal brain portions of both left (n = 2) and right (n = 2) hemispheres, and coronal brain slices (n = 3; different brain sources) that had been stored in the Neurochemistry laboratories for the Behavioural Neuroscience Program at Laurentian University. Whole brains were either light-deprived for 7 days or remained within a laboratory that was illuminated by overhead fluorescent lights (250 lux) during storage and between trials. The flux in front and behind the containers ranged from 5 lux to 50 lux. All specimens were removed from their plastic storage containers containing EFA

(ethanol-formalin-acetic acid) and placed into the box on folded paper towels. Whole and sagittal preparations were placed into the box directly. Coronal slices were placed in a tissue culture dish (15 cm in diameter) filled with EFA solution and were wrapped in a black nitrile glove to cover one hemisphere for measurements of each exposed hemisphere individually.

Procedure

Whole brains were placed into the cardboard storage box (Figure 37) approximately 9 cm from the aperture of the photomultiplier unit. Six aspects of the whole brains were used to record the photon counts: rostral, caudal, left, right, dorsal, and ventral aspects (Figure 38). When recording the dorsal and ventral aspects of the whole brain, the photomultiplier unit was suspended and placed onto supporting structures along the top of the box. The aperture of the PMT faced down onto the brain at a 9 cm distance. The whole brain was placed on its dorsal surface facing down (ventral aspect upwards) when recording the ventral aspect of the whole brain. Baseline recordings were taken with no brain present in the box and with the photomultiplier aperture facing downward into the box.

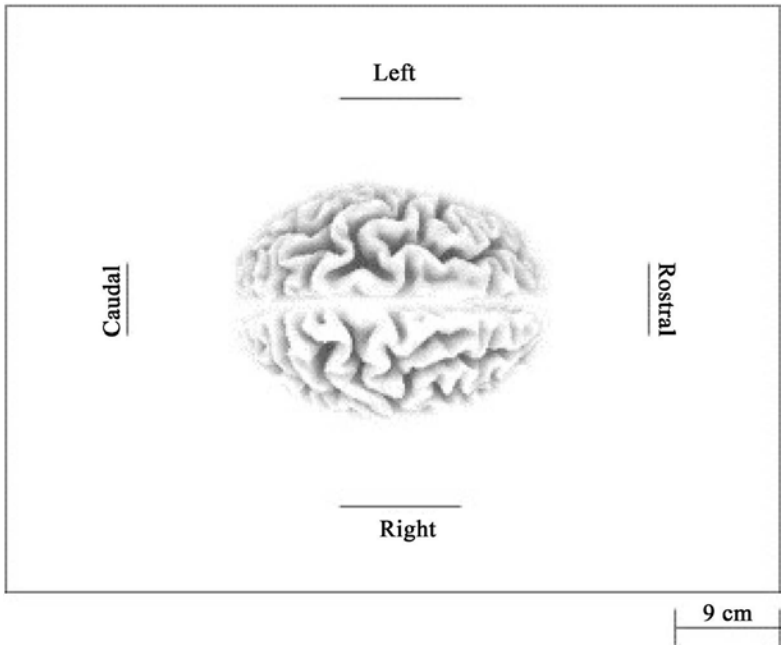

Figure 37. Dorsal view of the whole-brain placed within a box. Spatial orientation is provided where lines indicate the position and orientation of the PMT aperture. A 9 cm buffer zone was maintained between the brain and the measurement device.

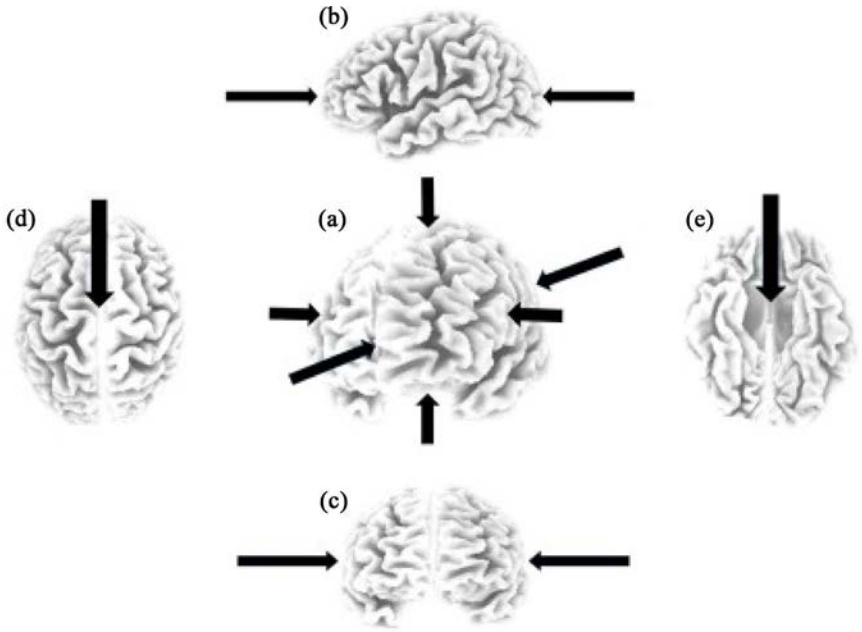

Figure 38. sLORETA template figures with arrows indicating the orientation of the PMT device during measurement procedure. All planes of space are represented (a) including rostral-caudal (b), left-right (c), as well as dorsal (d) and ventral (e) planes of space.

Sagittal brain measurements of both left and right hemispheres were recorded over both the lateral and medial aspects (Figure 39) while having the photomultiplier unit suspended and within 9 cm between the aperture and the brain sample. The lateral aspect of both hemispheres was recorded by placing the sagittal brain on its medial aspect face down onto folded paper towel in the center of the box. The medial aspect was recorded by placing the sagittal section in the box with the lateral aspect face down. Baseline recordings were taken with the photomultiplier tube facing downward into the box, with no sagittal brain present. Coronal sections were measured with the photomultiplier tube suspended above the tissue culture dish. Either the left or the right hemisphere was wrapped in a black nitrile glove (Figure 40). The photomultiplier unit was positioned over the exposed hemisphere when photon count recordings were ongoing. Baseline measures were taken with the EFA solution in the dish and without coronal brain samples present.

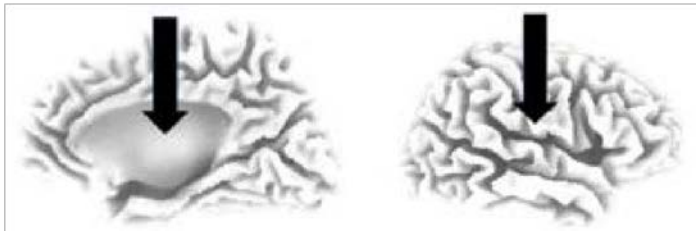

Figure 39. sLORETA 3D template representation of the medial (left) and lateral (right) aspects of a right sagittal section. Arrows indicate direction of the PMT during recordings.

Figure 40. Coronal brain slices were fitted with a black nitrile glove, and placed within plastic tissue culture dishes filled with EFA solution. The right hemisphere is exposed. An arrow displays direction of the PMT during recording over the exposed hemisphere.

Analyses

All data were imported into IBM SPSS Statistics v20 and analyzed. Time series data were Z-scored and spectral analyzed (SPECTRA) and then averaged into the respective conditions. Because the sampling was 50 times per sec (25 ms increments) the Nyquist Limit for the spectral power densities (SPD) for the amplitude variations was 25 Hz. All spectral analyzed data were then computed into binned intervals to analyze frequency differences employing mean comparisons and analysis-of-variance (ANOVA) measures. Averages (means) for photon counts per 25 ms from each recording were grouped into respective conditions in each experiment and analyzed through paired t-tests and ANOVA measures. Because there was day-to-day variation in the photon counts for some regions of the brain but not for background levels or other brain regions we examined the potential contribution from geomagnetic fluctuations upon the variance of photon counts. The maximum global K indices obtained from the Boulder Station for the day were downloaded from the appropriate website. These Kp values ranged primarily from 1 to 4 (there was one 8) during the 8 different days of photon measurement from the human brain samples. Previous experiments (Hunter *et al.*, 2010; Persinger, Dotta, Karbowksi, & Murugan, 2015) had demonstrated quantitative equivalents between biophoton emissions from brain activity and very small and proximal shifts in the earth's magnetic field.

Results

Whole-Brain

A factor analysis with varimax rotation revealed 2 components, cumulatively explaining 77% of the variance. The first factor, with factor loading scores greater than 0.5, consisted of photon counts from caudal (0.91), left (0.98) right (0.95), dorsal (0.80), and ventral (0.80) surfaces. The second factor consisted of background (0.66) and rostral (0.76) photon counts. Paired t-tests revealed that within-brain significant differences could be identified when comparing left (M = 150.64, SEM = 5.40) and ventral (M = 140.01, SEM = 4.55) photon counts, $t(11) = 3.17$, $p < 0.01$, $r^2 = 0.48$. Higher numbers of photon counts were recorded for the rostral (M = 159.36, SEM = 5.76) regions relative to ventral (M = 140.01, SEM = 4.55) counts, $t(11) = 2.86$, $p < 0.05$, $r^2 = 0.43$. Rostral photon counts were also higher relative to dorsal (M = 142.83, SEM = 4.86) photon counts, $t(11) = 2.58$, $p < 0.05$, $r^2 = 0.38$. Figure 41 demonstrates these effects. Over the range (0 to 25 Hz) of the amplitude fluctuations the SPDs were not random. There was an obvious increase within a sustained band between 7 and 9 Hz. Narrow-band factor analysis (varimax rotation) of photon count spectral power densities for the 7 Hz - 9 Hz interval revealed four components that cumulatively accommodated 70% of the variance. The first component, explaining 20% of the variance, consisted of rostral (0.71), caudal (0.71), and left (-0.54) photon counts. The second component, explaining ~18% of the variance, consisted of baseline (0.79) and right hemisphere (0.78) photon counts. This component displayed a conspicuous ($z > 4.5$) 7.9 Hz - 8 Hz peak (Figure 42). The third component, explaining 16% of the variance, consisted of ventral (0.87) and left (0.52) photon counts. The fourth and final component consisted of a single loading, dorsal (0.91) photon counts, explained the final ~16% of the variance.

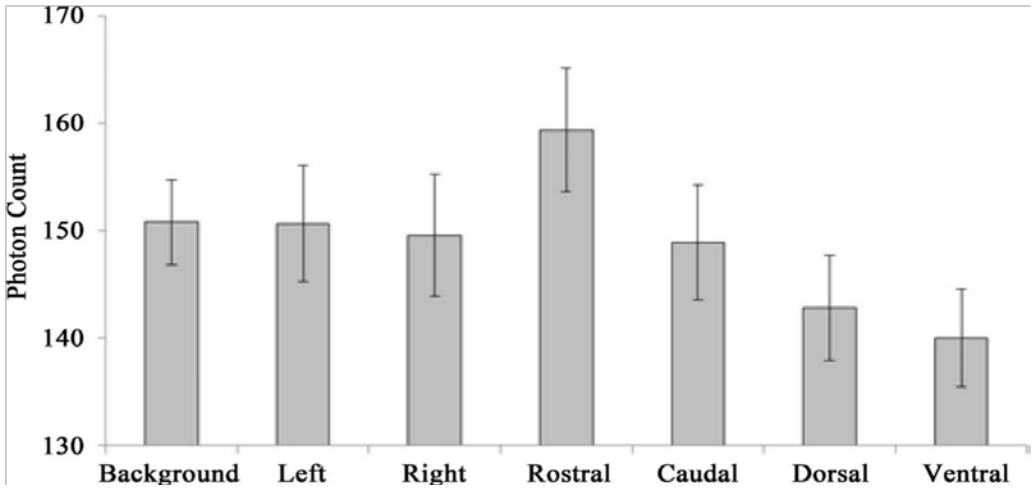

Figure 41. Photon counts obtained over various exposure aspects of whole human brain specimens including background values.

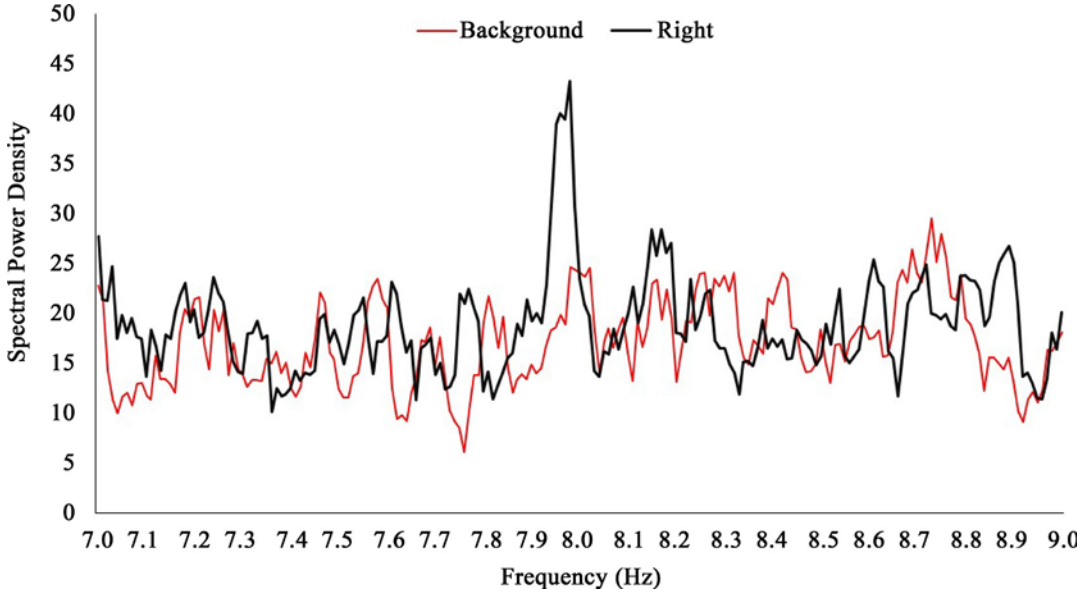

Figure 42. SPDs within the 7 Hz - 9 Hz band associated with background photon counts and those obtained over the right hemisphere of whole human brain specimens.

Light-Deprived Whole-Brain

If the whole-brain specimens had been placed in a hyper-darkened chamber (that was also a Faraday cage and acoustic chamber) for a week there were conspicuously lower photon counts over the ventral aspect of the brain (M = 132.50, SEM = 4.82) that differed significantly from those obtained over the left hemisphere (M = 149.76, SE = 5.62), right hemisphere (M =

145.35, SEM = 4.42), rostrum (M = 151.85, SEM = 7.32), caudal aspect (M = 144.13, SEM = 3.88), and dorsal aspect (M = 149.00, SEM = 5.16). The effect sizes, the amount of variance accommodated, ranged between 51% and 68%. Photon counts obtained over the rostral pole were higher relative to background values (M = 139.66, SEM = 6.36), $t(8) = 3.66$, $r^2 = 0.63$. These results are presented in Figure 43.

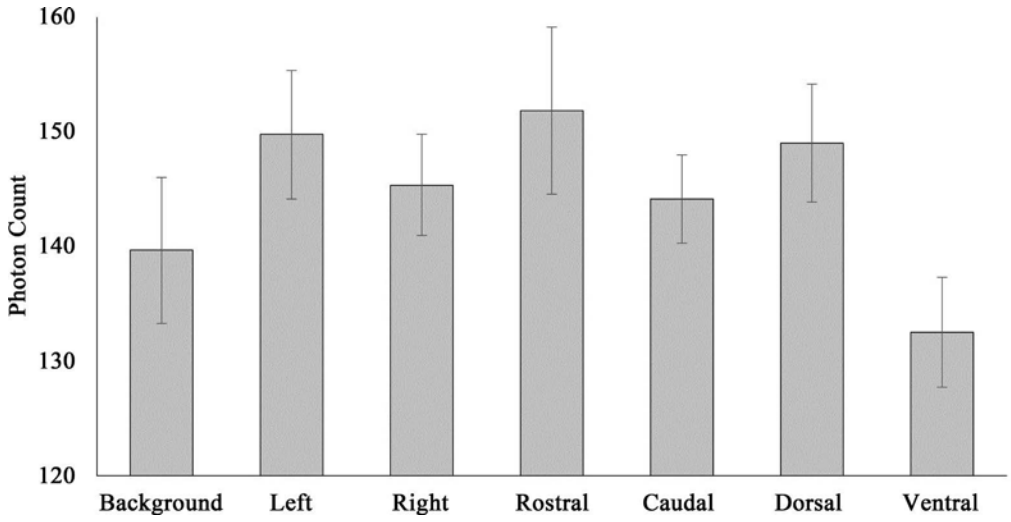

Figure 43. Photon counts obtained over various exposure aspects of light-deprived, whole human brain specimens including background values.

Sagittal Brain

Though no statistically significant differences in photon counts could be identified within hemispheres, there were clear and statistically significant between-hemisphere differences. They could be identified when medial and lateral surfaces were compared. Photon counts over the lateral surface of the sagittal sections were higher over the right hemisphere (M = 136.65, SEM = 3.50) relative to the left (M = 128.42, SEM = 1.58), $t(5) = 2.91$, $p < 0.05$, $r^2 = 0.63$. Photon counts over the medial surface of the sagittal sections were higher within the right hemisphere (M = 138.62, SEM = 4.24) relative to the left (M = 127.10, SEM = 1.13), $t(5) = 2.74$, $p < 0.05$, $r^2 = 0.60$. The lateral surface of the right hemisphere was associated with more photon counts relative to the medial surface of the left hemisphere, $t(5) = 3.52$, $p < 0.05$, $r^2 = 0.71$. These results

are presented in Figure 44. A plot of the right hemispheric SPDs between 7 Hz and 9 Hz revealed a number of peaks separated by increments of about 0.3 - 0.5 Hz. One of these peaks centered around 8.1 Hz (Figure 45). The difference in power for the 8.1 Hz peak was equivalent to a z-score of 2.37 and was only exceeded by one peak centered around 8.8 Hz. Its amplitude compared to all others was equivalent to a z-score of 3. This pattern of significant increases in power within the 7 Hz to 9 Hz was not evident for left hemispheric SPDs within the same range (Figure 46). These spectral differences are noted despite clear overlap in mean photon counts as indicated in Figure 47. In addition to simple hemispheric effects, a factor analysis employing varimax rotation involving SPDs computed within the 7 Hz - 9 Hz range revealed (loading coefficients in parentheses) that left-medial (0.71) and right-medial SPD (−0.72) loaded on the first of two components which cumulatively explained 61% of the variance. SPDs derived from photon counts obtained over the lateral surface of the left hemisphere loaded on the second factor (0.87) alone. SPDs derived from photon counts obtained over lateral surface of the right hemisphere did not load on either factor.

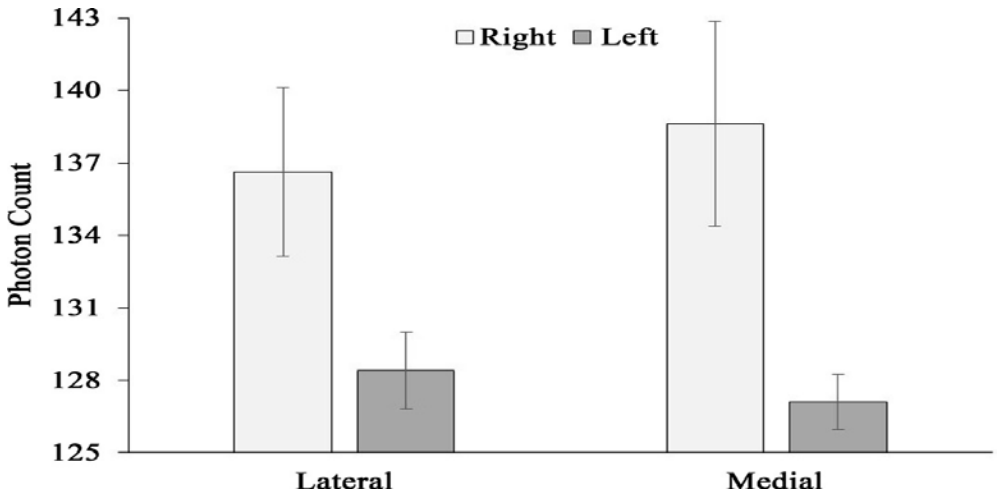

Figure 44. Photon counts as a function of medial-lateral surface aspect exposure obtained over right (light) and left (dark) hemispheres of sagittal sections.

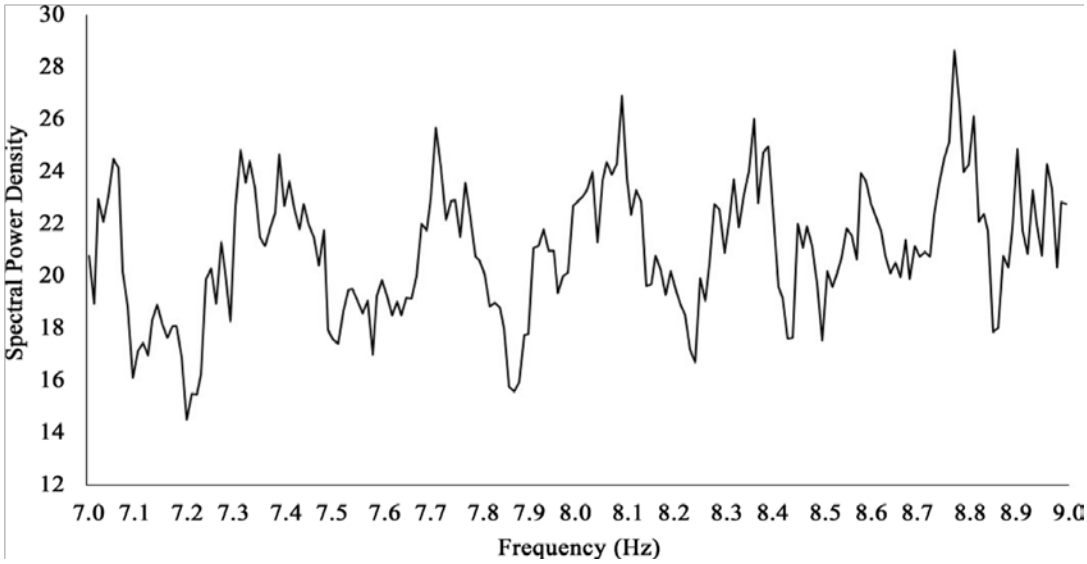

Figure 45. Average SPDs associated with photon counts over right hemispheric medial and lateral surfaces of sagittal sections within the 7 Hz - 9 Hz band.

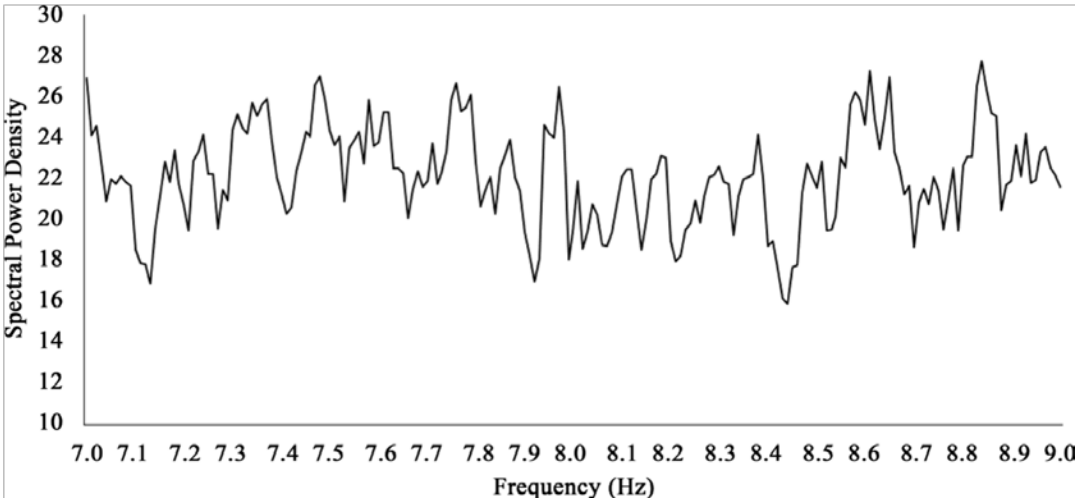

Figure 46. Average SPDs associated with photon counts over left hemispheric medial and lateral surfaces of sagittal sections within the 7 Hz - 9 Hz band.

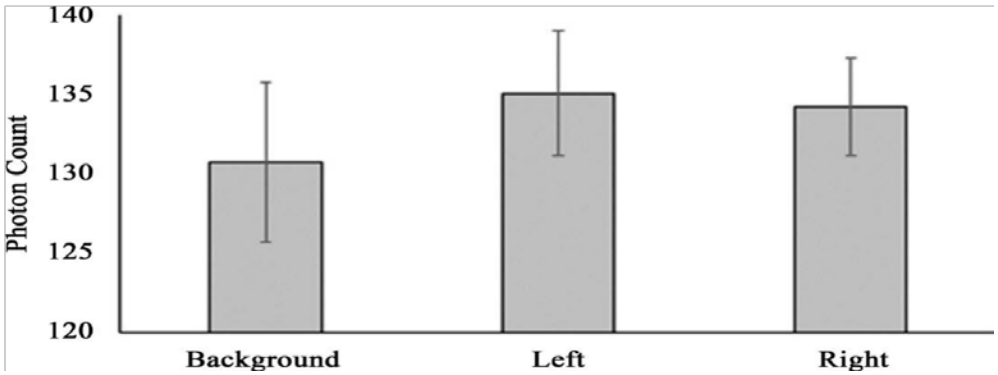

Figure 47. Mean photon counts obtained over left and right hemispheres of coronal human brain sections including background values. Means and standard errors are provided.

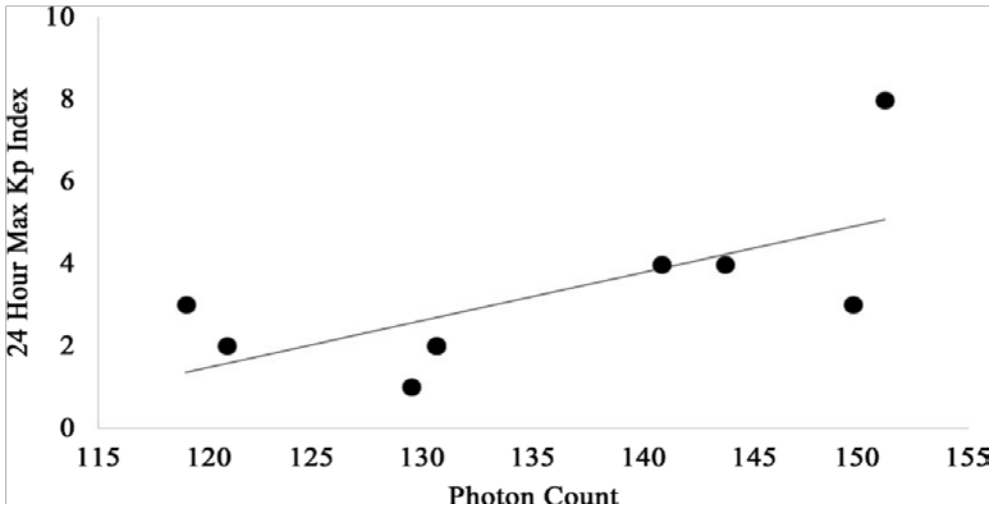

Figure 48. Significant positive correlation between 24 hour maximum Kp values and mean photon counts obtained over the left hemisphere of coronal sections of human brain.

However a strong correlation (rho = 0.88) between photon counts measured over left and right hemispheres was clearly evident. The magnitude of this correlation coefficient if it were a parametric value would suggest that ~23% of the variance associated with photon emissions could not be explained by this powerful interhemispheric relationship and instead would be associated with some other source of variance. The regression line in Figure 48 for the left hemispheric photon counts as a function of the maximum global Kp index on the day of the photon measurements indicated a range between 120 and 150 counts per 20 ms and range of 1 to 4 Kp units. According to Campbell's classic text (Campbell, 1997), a Kp of 1 is a variation (of the most disturbed component of the geomagnetic field) of about 4 nT while a Kp of 4 would be

about 27 nT. Energy (E) within a volume immersed within a magnetic field can be calculated from:

$$E = B^2 (2\mu)^{-1} m^3 \quad (1)$$

where B is the strength of the field; μ is magnetic permeability ($4\pi \times 10^{-}7$ N·A$^{-}2$) and m^3 is the volume of the sample. A difference of about 23 nT within a volume of the coronal section of the left hemisphere (50 cc to 100 cc or 5×10^{-5} to 10^{-4} m^3) is ~10^{-14} Joules.

On the other hand, the shift in photon counts (150 - 120) would be about 30 counts per 25 ms or 750 photons per s. Assuming a mid-value of ~5×10^{-19} J per photon the increase in photon energy output between the least and most geomagnetic activity and energy (excluding the outlier) within the volume of the sections would be 3.8×10^{-16} J per s per cm^{-2} (the width of the aperture). If this area were expanded over the volume of the section the total energy would be in the order of 10^{-14} J. This would be within the same order of magnitude as the "intrinsic" energy within the brain section volume associated with the increased geomagnetic variations.

Discussion

The results of the measurements indicate that the human brain generates differential numbers of photons that may reveal some intrinsic structural capacity that remains after clinical death and following protracted fixation. Although the differences in photon counts measured from the rostral compared to the ventral regions of the whole brain were about 20 counts per 20 ms (1000 photons per s), the discrepancy may be significant. This is equivalent to about 5×10^{-16} J per s (W) and considering the aperture of the photomultiplier unit would be about 2×10^{-12} W·m^{-2}. This order of magnitude has been considered a persistent flux density that has been

measured with both analogue and digital units. The value, which is about a factor of 10 above the background flux density of cosmic rays at ground level (Konig, Kreuger, Lonag, & Sonning, 1981) and is meaningful, is indicated by its consistent inverse correlation with shifts in ambient geomagnetic fields in the order of 1 nT (Hunter *et al*., 2010; Persinger, Dotta, Karbowksi, & Murugan, 2015).

If the emissions were "random", one would not expect the two distinct factor loadings for the amplitude fluctuations of the spectral power densities. They would have been less influenced by the nuances of net photon numbers. One involved shared profiles of photon power densities over the rostral, caudal, and left regions of the whole brain. The other involved the shared variance between the power densities over the right hemisphere and the baseline (no tissue present) conditions. This discrepancy is important for two reasons. First it suggests that there is a structural difference that is still present within the two human cerebral hemispheres many years after clinical death within appropriately fixed tissue. The greater number of photons emitted from the right hemisphere compared to the left was evident for the coronal and sagittal sections. The right hemisphere emitted about 500 "spontaneous" photons per s more than the left hemisphere.

Second, the conspicuous peak between 7.9 and 8 Hz for that power density is remarkably similar to both the peak range of power within the living quantitative electroencephalographic profile of older people (which was the likely source of these brains) as well as the fundamental frequency of the Schumann Resonance that is generated between the earth's surface and the ionosphere (Nickolaenko & Hayakawa, 2014). There may be an intrinsic organization within the right hemisphere that facilitates intercalation between this region of the living human brain and the Schumann power spectra. Recently Saroka *et al.* (2016) and Persinger and Saroka (2015)

reported quantitative evidence for this relationship as well as the theoretical bases for the concordance in large populations.

There was quantitative evidence that the whole brain deprived of exposure to ambient light (~102 lux) in the standard laboratory setting for about 12 - 18 hrs per day (before the lights are extinguished for the night) emitted about 5 to 8 more photons per 20 ms than the same whole brains that were maintained in the hyper-dark environment for a week. Although potentially spurious, the energy associated with this small number of photons is equivalent to a wavelength that overlaps with the Bohr orbit within a temporal frame (~20 to 25 ms) coupled with the recurrent rostral-to-caudal transcerebral cortical fields associated with consciousness (Llinas & Ribardy, 1993) is relevant. This effect was repeated several times. Although the differential values for photon counts from the different planes of the whole brains remained relatively consistent the absolute numbers of photons were less in the brains that had been deprived of ambient light. The diminishment of photons when the brains had been exposed for a week in the hyper-dark settings approached the likely background level associated with cosmic ray flux density at sea level.

From another perspective, the measurements suggest that fixed brain tissue in the laboratory exposed to ordinary lighting has the capacity to “store” photons in some manner, perhaps analogous to Popp’s virtual concepts (Popp, 1979), that is then re-emitted within the hyperdark setting. Karbowski *et al.* (2016) have shown that living melanoma cells in culture display this capacity. They found that when pulsed 470 nm (LED) light was coupled to a specific weak magnetic field (designed from geomagnetic sudden impulses) the cells maintained the photon energy and re-emitted it during the subsequent 30 to 60 min after the cells had been removed from the fields and the light but maintained in the dark. The total energy associated

with the delayed photon emissions was directly related to the energy available within the cellular volume from the intensities of the applied magnetic fields. One experiment that might demonstrate an equivalent effect within fixed, dead human brain tissue would involve exposure to appropriately patterned weak magnetic fields that simulate natural geomagnetic activity with concomitant same-patterned pulses of specific LED (light emitting diodes) photons. The re-emission of these wavelengths in a manner similar to the Karbowski *et al.* (2016) experiments would support the capacity for the fixed human brain to retain potentially photonic information.

A surprising result in the present study was the statistically significant correlation between the numbers of photon emissions from the left hemispheres only for the various sessions and the indices of global geomagnetic activity. Over the median range of approximately 27 nT there was an increase of about 30 counts per 20 ms. Calculations indicated that the photonic energy released was in the same order of magnitude as the energy that would have occurred within the volume of the brain from the increased geomagnetic variation. This correlation only occurred from the photons that were measured over the left hemisphere and not the right hemisphere. The application of either weak, physiologically patterned extremely low frequency magnetic fields (Persinger, 1999) or 0.1 to 1 GHz microwave sources (Stocklin & Stocklin, 1981) over the left hemisphere but not the right hemisphere has been shown experimentally to modify the power within the alpha range of electroencephalographic activity in human beings. The power densities in the latter experiments were equivalent to ~10^{-11} W·m^{-2}. The normal discrepancy between hemispheres in living brains reduces the probability the effects observed in the present experiments were adventitious and suggests that intrinsic differences in cerebral structure, still present after years of fixation, might respond differently to environmental energy sources. Of the approximately 176 sulci and gyri that comprise the left and right hemispheres of

the human brain only a few, such as the central sulcus, Sylvian fissure on the lateral side, the calcarine sulcus and the cingulate sulcus are similar in both hemispheres (Van Essen & Drury, 1997).

There are significant implications for the interface between medicine and neuroscience. For example, although microtubule preparations exposed to weak, physiologically patterned magnetic fields may exhibit increased photon emissions the more critical feature was the shifts in spectral power patterns of photon flux densities. These patterns represented information being transferred between microtubules. Trushin (2004) has suggested photons may be a fundamental means by which bacteria, one of the most persistent and universal life forms, “communicate”. Bokkon (2005) had postulated that sequences of visual imagery within the human cerebrum were photon fields rather than phenomenological correlates of action potentials. He and his colleagues (Bókkon, Salari, Tuszynski, & Antal, 2010; Bokkon, Dai & Antal, 2010) calculated there were more photons within neurons and that those that were emitted may contain representative information. Experiments by Dotta *et al.* (2012) showed that instructing subjects sitting in hyperdarkness to imagine white light was associated with increased photon emissions from their right (but not their left) hemispheres. These specific increases did not occur when the same subjects engaged in banal ideation. The potential for discerning what type of information can be extracted from fixed cerebrums must still be examined empirically.

References

Bokkon, I. (2005). Dreams and Neuroholography: An Interdisciplinary Interpretation of Development of the Homeotherm State in Evolution. *Sleep and Hypnosis*, **7**, 61-76.

Bókkon, I., Salari, V., Tuszynski, J.A. & Antal, I. (2010). Estimation of the Number of Biophotons Involved in the Visual perception of a Single-Object Image: Biophoton Intensity Can Be Considerably Higher inside Cells than outside. *Journal of Photochemistry and Photobiology B*: *Biology*, 100, 160-166.

Bokkon, I., Dai, J. & Antal, I. (2010). Picture Representation during REM Dreams: A Redox Hypothesis. *Biosystems*, **100**, 79-86.

Campbell, W.H. (1997). Introduction to Geomagnetic Fields. Cambridge University Press, Cambridge.

Dotta, B.T., Buckner, C.A., Cameron, D., Lafrenie, R.F. & Persinger, M.A. (2011). Biophoton Emissions from Cell Cultures: Biochemical Evidence for the Plasma Membrane as the Primary Source. *General Physiology and. Biophysics*, 30, 301-309.

Dotta, B.T., Saroka, K.S. & Persinger, M.A. (2012). Increased Photon Emissions from the Head While Imagining Light in the Dark Is Correlated with Changes in Electroencephalographic Power: Support for Bokkon's Biophoton Hypothesis. *Neuroscience Letters*, 513, 151-154.

Fels, D. (2009). Cellular Communication through Light. *PLos ONE*, 4, e5086.

Hunter, M.D., Mulligan, B.P., Dotta, B.T., Saroka, K.S., Lavallee, C.F., Koren, S.A. & Persinger, M.A. (2010). Cerebral Dynamics and Discrete Energy Changes in the Personal Physical Environment during Intuitive-Like States and Perceptions. *Journal of Consciousness Exploration & Research*, 1, 1179-1197.

Karbowski, L.M., Murugan, N.J. & Persinger, M.A. (2016). Experimental Evidence that Specific Photon Energies Are "Stored" in Malignant Cells for an Hour: The Synergism of Weak Magnetic Field-LED Wavelength Pulses. *Biology and Medicine*, 8, BM-162-16.

Kobayashi, M., Takeda, M., Sato, T., Yamakazi, Y., Kaneko, K., Ito, K.-I., Kato, H. & Inaba, H. (1999). *In Vivo* Imaging of Spontaneous Ultra-Weak Photon Emission from a Rat's Brain *in Vivo*. *Journal of Neuroscience Methods*, 34, 103-113.

Konig, H.L., Kreuger, A.P., Lonag, A.P. & Sonning, W. (1981). Biologic Effects of Environmental Magnetism. Springer-Verlag, New York.

Llinas, R.R. & Ribardy, U. (1993). Coherent 40-Hz Oscillations Characterizes Dream State in Humans. *Proceedings of the National Academy of Sciences of the United States of America*, 90, 2078-2081.

Nickolaenko, A. & Hayakawa, M. (2014). Schumann Resonance for Tyros. Springer, Tokyo.

Persinger, M.A. (1999). Increased Emergence of Alpha Activity over the Left but Not the Right Temporal Lobe within a Dark Acoustic Chamber: Differential Response of the Left but Not the Right Hemisphere to Transcerebral Magnetic Fields. *International Journal of Psychophysiology*, **34**, 163-169.

Persinger, M.A. (2012). Annual Variation of Local Photon Emissions' Spectral Power within the mHz Range Overlaps with Seismic-Atmospheric Acoustic Oscillations. *International Journal of Geosciences*, 3, 192-194.

Persinger, M.A., Lafreniere, G.F. & Dotta, B.T. (2012). Marked Increases in Background Photon Emissions in Sudbury Ontario more than One Week before the Magnitude > 8.0 Earthquakes in Japan and Chile. *International Journal of Geosciences*, 3, 627-629.

Persinger, M.A., Dotta, B.T., Karbowksi, L.M. & Murugan, N.J. (2015). Inverse Relationship between Photon Flux Densities and NanoTesla Magnetic Fields over Cell Aggregates: Quantitative Evidence for Energetic Conservation. *FEBS Open Bio*, 5, 413-418.

Persinger, M.A. & Saroka, K.S. (2015). Human Quantitative Electroencephalographic and Schumann Resonance Exhibit Real-Time Coherence of Spectral Power Densities: Implications for Interactive Information Processing. *Journal of Signal and Information Processing*, 6, 153-164.

Popp, F.-A. (1979). Photon Storage in Biological Systems. In: Popp, F.-A., Becker, G., Koenig, H.L. and Peschka, W., Eds., *Electromagnetic Bio-Information*, Urban & Schwarzenberg, Munich, 123-148.

Popp, F.-A. (1988). Biophoton Emission. *Experientia*, 44, 543-544.

Popp, F.-A., Li, K.H., Mei, W.P., Galle, M. & Neurohr, R. (1988). Physical Aspects of Biophotons. *Experientia*, 44, 576-585.

Saroka, K.S., Vares, D.A.E. & Persinger, M.A. (2016). Similar Spectral Power Densities within the Schumann Resonance and a Large Population of Quantitative Electroencephalographic Profiles: Supportive Evidence for Koenig and Pobachenko. *PLoS ONE*, 11, e0146595.

Stocklin, P.L. & Stocklin, B.F. (1981). Low Power Microwave Effects on the Human Electroencephalogram: Supporting Results of Bise. *Physiology, Chemistry and Physics*, **13**, 175-177.

Tilbury, R.N. & Quickenden, T.I. (1988). Spectral and Time Dependence Studies of the Ultra-Weak Bioluminescence Emitted by the Bacterium *Escherichia coli*. *Photochemistry and Photobiology*, 47, 145-150.

Trushin, M.V. (2004). Light-Mediated Conversation among Microorganisms. *Microbiological Research*, 159, 1-10.

Van Essen, D.C. & Drury, H.A. (1997). Structural and Functional Analyses of Human Cerebral Cortex Using a Surface-Based Atlas. *The Journal of Neuroscience*, **17**, 7079-7102.

Van Wijk, R., Van Wijk, E.P.A. & Bajpai, R.P. (2006). Photocount Distribution of Photons Emitted from Three Sites of the Human Body. *Journal of Photochemistry and Photobiology B*: *Biology*, 84, 46-45.

Chapter 4 – A Possible Flux Density Value of 10^{-12} W·m^{-2} for "Spontaneous" Photon Emissions in Fixed Human Brain Tissue: Was Spinoza Correct?

Published in Research in Neuroscience

Abstract

The equivalence between universal values of 10^{-20} J and 10^{-12} W·m^{-2} involves the product of the inverse of diffusivity of wave impedance distributed over the hydrogen wavelength divided by the magnetic permeability of free space. These two values reflect the increment of energy associated with action potentials (a major correlate of cognition) and the power densities of photon emissions during imagination as measured experimentally. The human brain, alive or dead (if structurally maintained) has similar mass and occupies space. The hypothesis was tested that these two properties would be sufficient to produce enhanced "spontaneous" photon emission compared to empty space. The photon flux density from different volumes (masses) of fixed human brain ranging between 20 mg and 1100 g were measured. Compared to the 20 mg masses that did not differ from dark counts (background), the average flux density for 100 to 1000 g volumes was ~$2 \cdot 10^{-12}$ W·m^{-2}. These results are consistent with the possibility that mass occupying space reflects it fundamental properties that relate to an intrinsic relationship between energy (J) and flux density (kg·s^{-3}). Within the human cerebrum the energy density would be about 10^{-11} W·m^{-3} or 10^{-14} J·s^{-1}. This is equivalent to the discharge of ~10^{7} cortical neurons which is within the range of experiencing a percept in the living human brain. These results also support the Hameroff and Penrose concept of "consciousness" as well as Spinoza's implicit argument that cerebral properties indicates it is a subset of all space. There is quantitative evidence by calculation the mediating variable may be related to the neutral hydrogen line which exhibits ubiquitous presence in the universe.

Introduction

Hameroff and Penrose (2013) have developed a cogent and convincing argument for consciousness in the universe that results from discrete physical events. They have argued that "such events have always existed in the universe as non-cognitive, proto-consciousness events, these acting as part of precise physical laws not yet fully understood. Eddington's (1928) approach to astronomy and the nature of the universe was implicitly that its perception and conception were influenced by the physics, chemistry and physiology of the human brain. Some assumptions of quantum physics indicate that observation or more specifically measurement can affect the outcome of photon interactions (Kofman & Kurizki, 2000). The phenomenon of entanglement (Aczel, 2002) would allow two complex systems to be excessively correlated such that a change in one component produces a complimentary change in the other regardless of distance. "Entanglement energies" or those associated with "excess correlations" (Dotta, Murugan, Karbowski & Persinger, 2013) that are associated with non-local effects are within the same magnitude (~10^{-20} J) as those associated with action potentials (Persinger, 2010) of the neurons whose patterns are strongly correlated with human consciousness (Dotta, Buckner, Cameron, Lafrenie & Persinger, 2011; Hunter *et al.*, 2010). The most frequently considered unit by which the phenomena of excess correlation might be mediated is the photon (Dotta & Persinger, 2012).

Recently Dotta and his colleagues (2012) have shown that normal people engaging in vivid imagination of light display reliable increases in photon emissions equivalent to about 10^{-12} $W \cdot m^{-2}$ from their right hemispheres. Additional calculations by Persinger (2015[a]) indicated that this quantity of power density could be coupled to the basic unit of energy (10^{-20} J per s) through the inverse of diffusivity of the wave impedance distributed over the neutral hydrogen

wavelength when this value was divided by the magnetic permeability of space. If this is valid then the presence of mass, such as the human brain, should exhibit this order of magnitude of flux density. Empirical evidence is presented here that different masses of fixed human brain tissue emit "spontaneous" photons that reflect the 10^{-12} $W \cdot m^{-2}$.

Multiple philosophies have assumed the presence of a universal field or substance that reflects the structure of space. Different increments of mass occupy different volumes of space and reflect these characteristics. One inference of this assumption is that the human cerebrum which occupies about 10^{-3} m^3 will reflect a feature of this space. Because billions of human brains are similar in volume they will all display a commonality by which coherence and "condensate" like properties could emerge under specific situations (Persinger, 2013). Spinoza (Grene, 1973), without the benefit of quantification, had argued that the human brain's special abilities (including cognition and consciousness) was a reflection of the universal property being represented within cerebral space. There is quantified support for this supposition. If the averaged energy density of the universe is about 10^{-9} $J \cdot m^{-3}$ and a percept is associated with about 10^7 neurons (Rouleau & Dotta, 2014) distributed through the cerebral cortices each discharging ~10 Hz, then the total energy from 10^{-20} J per action potential is 10^{-12} J per s. Because the human cerebrum is about 10^{-3} m^3 this is equivalent to 10^{-9} $J \cdot m^{-3}$ which is the same order of magnitude (Persinger, 2015[b]; Persinger, Koren, & Lafreniere, 2008).

Calculations

According to Persinger (2015[a]) the relationship between $W \cdot m^{-2}$ and $J \cdot s^{-1}$ can be equated by:

$$W \cdot m^{-2} = (s \cdot m^{-2}) \cdot (J \cdot s^{-1}) \cdot s^{-1} \quad (1),$$

or as stated semantically the flux power density is equal to the product of joules per second, the inverse of diffusivity and frequency. It would be expected of the values for these quantities to be universal. It is assumed that s^{-1} is the rotational Bohr frequency for an electron ($6.59 \cdot 10^{15}$ s^{-1}).

For inverse diffusivity assume that the wave impedance of 376.73 Ω applied across the hydrogen wavelength ($2.12 \cdot 10^{-1}$ m), or $7.99 \cdot 10^{1}$ Ω·m. When divided by magnetic permeability in a vacuum, which is $1.26 \cdot 10^{-6}$ $N \cdot A^{-2}$, the diffusivity would be $6.34 \cdot 10^{7}$ $m^2 \cdot s^{-1}$. The inverse value is $0.16 \cdot 10^{-7}$ $s \cdot m^{-2}$. The product of $1.5 \cdot 10^{-20}$ J, the basic quantity that emerges as a property of water (Karbowski, & Persinger, 2015) and the energy per Planck's voxel (Persinger, 2014; Persinger, Koren & Lafreniere, 2008), the inverse diffusivity term and the Bohr frequency is $1.6 \cdot 10^{-12}$ $W \cdot m^{-2}$.

The hydrogen wavelength, perhaps the most ubiquitous signature that traverses space-time, is required for the balanced solution between two fundamentals: the quantity of energy per unit of interaction and what appears to be the optimal photon flux density to produce many of the magnetic pattern effects that have been measured for cells, mice and humans. For example for every 1 nT decrease in the earth's magnetic field around the heads of people who are imagining, the photon emissions increased by about 10^{-12} $W \cdot m^{-2}$ (Dotta, Saroka & Persinger, 2012). A similar relationship has been found with direct measurements over aggregates of melanoma cells (Persinger, Dotta, Karbowski & Murugan, 2015) as well as within background measurements (Vares & Persinger, 2013).

The inclusion of the neutral hydrogen line in these calculations was not for convenience. W. Ross Adey (1981) once described an interesting relationship between voltage and band width which was:

$$V^2=4kTBR \quad (2),$$

where k was the Boltzmann constant, T=temperature, B was band width and R was resistance. If instead B (band width) is solved and 40μV is assumed to be the potential difference across ~11 cm (the cube root of the volume) of cerebral cortical space, the band width is within a few percent of 1.42 GHz. This is the intrinsic neutral hydrogen (21 cm) frequency.

Measurements

Specimens were obtained from the Laurentian University Behavioural Neuroscience Program's Brain Library. All brains had remained fixed in ethanol-formalin-acetic acid for 10 to 20 years. This fixative maintains the general detail of neuronal soma as verified by direct histological examination. Fixed brain photon data from four months of research were compiled into a single dataset and analyzed based on rank order from least to greatest average photon counts. Previous photon data were recorded from various cuts of fixed brain tissue from: 0.02 gram portions of white and grey matter of cerebral cortex, 3 coronal sections, 2 of left and right sagittal brain sections, and 3 whole human brains respectively by rank order. All photon recordings took place in a dark, enclosed chamber using a single photon recording device placed 1-9 cm away from the fixed brain tissue.

A single photomultiplier tube (PMT) from Sens-Tech Sensor Technologies was used in all experiments to measure temporal photon counts, with a spectral response range between 300-

850 nm. Sens-Tech Counter Timer software recorded all data with the photomultiplier tube at a 50 Hz sampling rate for 5000 readings (20 msec data points for 100 seconds) on a Lenovo ThinkPad laptop. Dark counts which were defined as the photon measurements within the special hyperdark room when only air (no tissue) was present averaged 109 per 20 ms. Dark counts are presumed to originate from the intrinsic components of the photomutilplier circuits. Consequently the actual photon counts from any mass in adjacent to the sensor aperture would be that value minus the dark counts.

Results

The means and standard errors of the means (SEM) for the numbers of photon counts per 20 ms (the raw data) for the different types of human brain tissue are shown in Figure 49. The grey-white matter samples which involved 20 mg quantities were not significant statistically from the dark counts which involved measurements with no tissue present. As can be seen in Figure 50, when compared to the smallest mass 20 mg which did not differ from dark counts, the brain masses between 100 g and 1100 g (whole brain) displayed a similar number of photon counts. The average difference from dark counts was 26 photons per 20 ms or $1.3 \cdot 10^{3}$ photons per s. Assuming each photon was a median value of $5 \cdot 10^{-19}$ J, the power would have been $6.5 \cdot 10^{-16}$ W. Because the width of the PMT aperture was about 2 cm the area would have been $3.14 \cdot 10^{-4}$ m^2. Consequently the flux power density would be ~$2.1 \cdot 10^{-12}$ $W \cdot m^{-2}$.

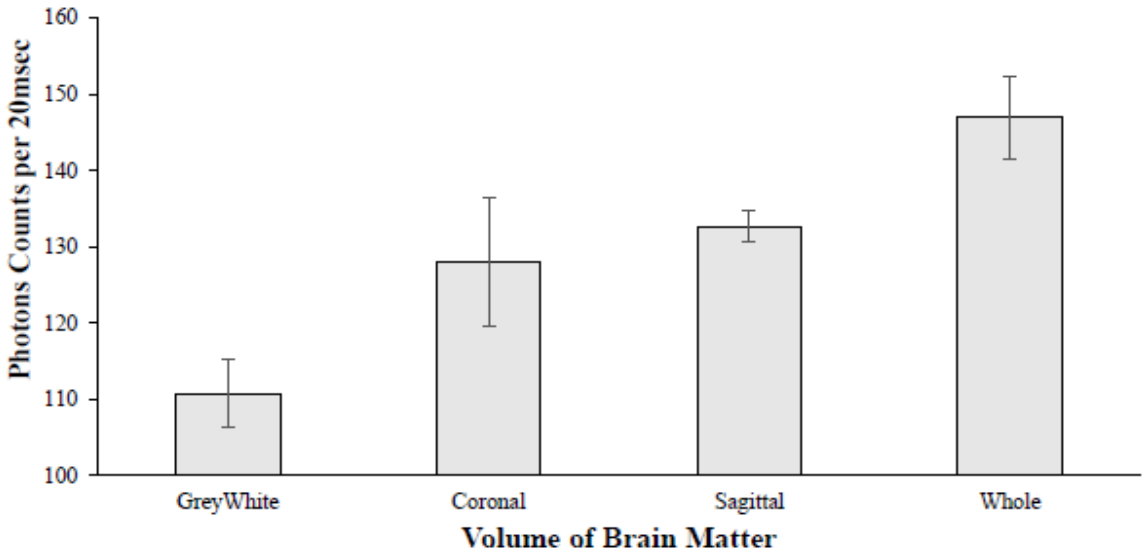

Figure 49. Raw photon counts per 20 ms for different sections (volumes) of fixed human brain tissue. The grey-white tissue (20 mg) values did not differ from background or dark counts.

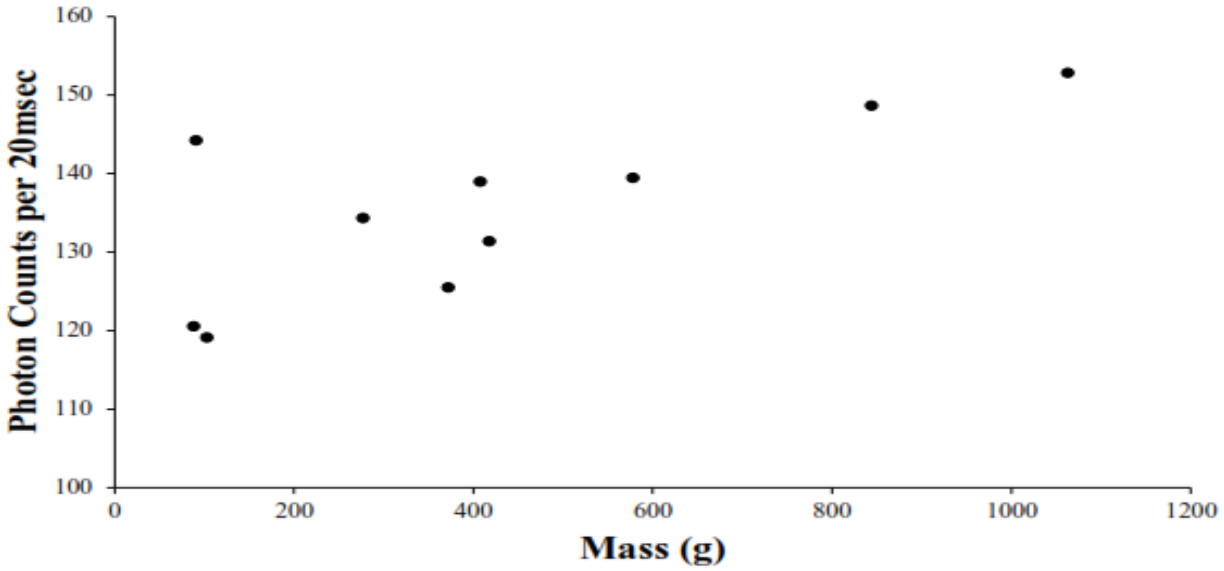

Figure 50. Raw photon counts for the actual mass of each component of human brain tissue measured. The values from the dark counts which were similar to the 20 mg tissue samples (not shown) ranged between 108 and 112 counts per 20 ms.

Discussion

The results of these measurements support the concept that fundamental properties within space may be manifested when the mass that occupies that space is present. Assuming the more or less consistent measurement of ~$2.1 \cdot 10^{-12}$ $W \cdot m^{-2}$ across the 100 to 1100 g of various fixed brain masses is not an artifact of the restricted limit, the presence of human cerebral tissue enhanced photon detection over dark (background) counts by the value that is related quantitatively to 10^{-20} J. This emerges when a term composed of the product of inverse diffusivity of wave impedance over the neutral hydrogen wavelength is divided by the magnetic permeability in a vacuum.

When bold conjectures are considered quantitative solutions become even more important for verification or in the least support of the proposition. If the human brain, even when it is fixed, occupying space is associated with enhanced manifestations of ~$2.1 \cdot 10^{-12}$ $W \cdot m^{-2}$ then the energy within the volume can be estimated. Within the ~10^{-3} m^3 of the human cerebrum, the energy density would be $2.1 \cdot 10^{-12}$ $W \cdot m^{-2}$ divided by $1.1 \cdot 10^{-1}$ m or $2 \cdot 10^{-11}$ J per s per m^3. Within the specific dimensions of the 10^{-3} m^3 cerebrum, this is $2 \cdot 10^{-14}$ J per s. Assuming 10^{-20} J per action potential (Persinger, 2010) and the energy required to sequester most ligands to receptors, the numbers of neurons would be between 10^6 (at 10 Hz) to 10^7 (at 1 Hz). As discussed by Rouleau and Dotta (2014) and verified by estimates from fMRI (functional Magnetic Resonance Imaging) data, the typical numbers of neurons in an intracerebral "network" associated with a percept or a thought is about that magnitude.

This convergence elicits important philosophical questions. First, is there something specific if not unique about the average human brain volume that enhances its congruence with the universal properties? Eddington (1928), who was in our opinion inappropriately demeaned

for his views, integrated the brain mediated perception of the universe as its essential properties. Implicitly he argued that the properties of the universe as we measure them (even with the most sophisticated tools that are extensions of our basic senses) are reflections of intrinsic brain structure. This concept had been articulated earlier by Immanuel Kant (1966) who emphasized that the perception of three-dimensional space and time are innate properties of the human brain.

Second, if there is an intrinsic feature of space and the mass that occupies this space amplifies its properties then Spinoza's concepts may have experimental support. His philosophy was similar to the physical assumptions of Ernst Mach (1919) whose principle of the Immanence of the Universe indicated that any part of the universe is affected by all of the other parts and visa-versa. These concepts create the conditions for both holographic models and the possibility of entanglement where by any two points within the universe can be mutually affected regardless of the distance. In other words, the occupation of a space by a specific mass could indicate that that the mass becomes a subset set of the total set in terms of both properties and microfunction.

Third, if fixed human brain tissue spontaneously displays photon emissions whose quantities simulate those associated with consciousness and the experience of percepts within the human brain, what differentiates the living from the non-living human cerebrum? In biology and chemistry, structure dictates function. Histologically, the neuronal somas are remarkably intact within the cerebral cortices of these brain specimens. Whether or not there are residual properties still remaining within fixed human brains that could contribute to entanglement or to other fundamental properties has rarely been considered or investigated.

Two questions that might be examined are: 1) what is the role of this prominent frequency as a carrier of phase and frequency modulations between 1 Hz and 1.42 GHz (like

communication carrier waves), and, 2) can we measure this frequency from the human brain? The Adey (1981) solution for width of the wave band within the human brain according to our calculations is the neutral hydrogen frequency. This indicates that frequency or phase modulation from the lowest value up to the limit of 1.42 GHz could be a major source for the communication of information within brain space. It may not be spurious that velocity of light within an aqueous environment such as the brain divided by the averaged diameter of the cerebrum (assuming a sphere) is within the range of variability for human brain volumes for 1.42 GHz.

Whether or not the human brain volume generates a small compliment of the neutral hydrogen line would have significant implications for interpretations within physical neuroscience as well as for the integration of biological, chemical, physical and astronomical relationships. The energy associated with the hydrogen line is associated with a shift in electron spin which occurs within an individual hydrogen ion once every approximately 10 million years or 10^{14} s. There are 10^{27} proton mass equivalents within the human cerebrum that weighs about 1.5 kg.

Assuming a pH of about 6 within the cerebral volume, there would be $6 \cdot 10^{17}$ hydronium ion (with an extra proton) per mole or 18 cc and because the average cerebral volume is 1350 cc, the total numbers of protons would be $4.5 \cdot 10^{19}$. When divided by the time for a single electron spin shift, the numbers of proton-electrons involved would be $4.5 \cdot 10^{5}$ per s. The $2 \cdot 10^{-20}$ J increment associated with each proton results in $9 \cdot 10^{-15}$ W. When divided by the cross sectional area of the human cerebrum of 10^{-2} m^2 the power density would be $\sim 10^{-12}$ $W \cdot m^{-2}$. This does not prove that hydrogen line emissions are being generated by the human brain volume. However, if it is detected the energy levels by inference would be sufficient to be discerned.

Conclusion

The fixed human brain at different volumes displays “spontaneous” photon emissions whose flux densities are the same order of magnitude as the value of wave impedance and magnetic permeability produces the equivalence to 10^{-20} J. The quantitative equivalence involves an important role of the energies associated with the neutral hydrogen line that might be of sufficient quantity to be discerned by sensitive equipment from human brain. The persistence of spontaneous photon emission within mass equivalents of human brain that are associated with cognitive functions and ideation supports the concepts of Eddington, Mach, and Spinoza and suggests that structured matter, anywhere within the universe, may simply reflect the intrinsic properties of that total set.

References

Aczel, A. D. (2002). Entanglement: The greatest mystery in physics. *Raincoast Books*, Vancouver.

Adey, W. R. (1981). Tissue interactions with nonionizing electromagnetic fields. *Physiol. Rev.*, 61: 435-514.

Dotta, B.T. Buckner, C. A., Cameron, D. Lafrenie, R. F., Persinger, M. A. (2011). Biophoton emission from cell cultures: biochemical evidence for the plasma membrane as the primary source. *Gen. Physiol. Biophys.*, 30:301-309.

Dotta, B. T., Persinger, M. A. (2012). "Doubling" of local photon emissions when two simultaneous spatially, separated, chemiluminescent reactions share the same magnetic field configurations. *J. Biol. Chem.*, 3:72-80.

Dotta, B. T., Saroka, K. S., Persinger, M. A. (2012). Increased photon emission from the head while imagining light in the dark is correlated with changes in electroencephalographic power: support for Bókkon's biophoton hypothesis. *Neurosci. Lett.*, 513: 151-154.

Dotta, B. T., Murugan, N. J., Karbowski, L. M., Persinger, M. A. (2013). Excessive correlated shifts in pH with distal solutions sharing phase-uncoupled angular accelerating magnetic fields: macro-entanglement and information transfer. *Int. J. Phys. Sci*., 8: 1783-1787.

Hunter, M. D., Dotta, B. T., Saroka, K. S., Lavallee, C. F., Koren, S. A., Persinger, M. A. (2010) Cerebral dynamics and discrete energy changes in the personal physical environment during intuitive-like states and perceptions. *J. Cons. Explor. Res.*, 1: 1179-1197.

Eddington, A. (1928). The nature of the physical world. *University of Michigan Press.*

Hameroff, S., Penrose, R. (2013). Consciousness in the universe: a review of the "Orch OR' theory. *Phys. Life Rev*.

Grene, M. (ed.) (1973). Spinoza: A collection of critical essays. Anchor/Double Day, N.Y.

Kant, I. (1966). Critique of Free Judgment (translated by J. H. Bernard), *Hafner Publishing*, New York.

Karbowski, L. M., Persinger, M. A. (2015). Variable viscosity of water as the controlling factor in energetic quantities that control living systems: Physicochemical and astronomical interactions. *Int. Lett. Chem. Phys. Astron.*, 4, 1-9.

Kofman, A. G., Kurizki, G. (2000). Acceleration of quantum decay processes by frequent observations. *Nature*, 405: 546-549.

Mach, E. (1919). The science of mechanics. *The Open Court Publishing Co*, Chicago.

Persinger, M. A. (2010). 10^{-20} Joules as a neuromolecular quantum in medicinal chemistry: An alternative approach to myriad molecular pathways? *Cur. Med. Chem.*, 17: 3094-3098.

Persinger, M. A. (2013) Billions of human brains immersed within a shared geomagnetic field: Quantitative solutions and implications for future adaptations. *Open Biol. J.*, 6:8-13.

Persinger, M. A. (2014). A possible explanation for the vacuum catastrophe. *Int. J. Astron. Astrophys.*, 4:178-180.

Persinger, M. A. (2015[a]). The prevalence and significance of ~10^{-20} J and ~10^{-12} W·m^{-2} as convergent/divergent nodal units in the universe. *Int. Lett. Chem. Phys. Astron*., 61: 94-100.

Persinger, M. A. (2015[b]). Thixotropic phenomena in water: Quantitative indicators of casimir-magnetic transformations from vacuum oscillations (virtual particles). *Entropy*, 17:6200-6212.

Persinger, M. A., Koren, S. A., Lafreniere, G. F. A (2008). neuroquantological approach to how human thought might affect the universe. *Neuroquantology*, 6, 262-271.

Persinger, M. A. Dotta, B. T., Karbowski, L. M., Murugan, N. (2015). Inverse relationship between photon flux densities and nanotesla magnetic fields over cell aggregates: Quantitative evidence for energetic conservation. *J. FEBS Open*, 5:413-418.

Persinger, M. A., St-Pierre, L. S. (2015). The physical bases to consciousness: Implications of convergent quantifications. *J. Sys. Integrat. Neurosci*., 1: 55-64.

Rouleau, B., Dotta, B. T. (2014). Electromagnetic fields as structure-function zeitgebers in biological systems: environmental orchestrations of morphogenesis and consciousness. Front. Integrat. Neurosci., 8, article 84.

Vares, D. A. E., Persinger, M. A. (2013). Predicting Quantum Random Events from Background Photon Density Two Days Previously: Implications for Virtual-to-Matter Determinism and Changing the Future. *J. Non-Locality*, II: 2.

Chapter 5 – Lagged Coherence of Photon Emissions and Spectral Power Densities between the Cerebral Hemispheres of Human Subjects during Rest Conditions: Phase Shift and Quantum Possibilities

Published in World Journal of Neuroscience

Abstract

Photon counts about 15 cm from the left and right sides of the head while subjects sat quietly during baseline conditions within a hyper-dark chamber were measured by photomultiplier units. Lag/lead analyses for photon emissions between the two hemispheres indicated a weak but statistically significant correlation between the amplitude fluctuations that were separated by about 800 to 900 ms. Analyses of the spectral power densities of photon amplitude variations from the left and right hemispheres revealed peak values between 2 and 3 Hz which were equivalent to a difference of about 900 ms. The radiant flux densities were estimated to be in the order of 10^{-12} $W \cdot m^{-2}$ and to include the equivalence of about 10^{7} neurons. Our calculations, which accounted for the small magnitude of the strength of the interhemispheric coefficients, suggest that the coherence could be strongly correlated with processes associated with the unmyelinated axons with diameters between 400 to 800 nm, the visible wavelengths, within the corpus callosum. When the ratio of the phase shift was applied to the Aharanov-Bohm equation, the time required for a photon-related electron to be within a cerebral magnetic field was the same duration as a single orbit of an electron and a photon's traversal latency across a neuronal plasma membrane. It is suggested that the peak photon decoherence between the two cerebral hemispheres may reveal a neuronal-quanta substrate to the conditions associated with consciousness.

Introduction

The measurements of ultraweak light emissions from the right hemisphere of a human subject sitting in hyper-dark settings (10^{-12} $W \cdot m^{-2}$) during periods of imagining white light compared to more mundane cognitions (Dotta, Saroka, & Persinger, 2012) indicated that complex neuronal processes associated with consciousness could be coupled to biophotons (Dotta, Saroka, & Persinger, 2012; Dotta, Buckner, Lafrenie, & Persinger, 2011; Saroka, Dotta, & Persinger, 2013). The strong correlation between quantitative electroencephalographic activity over the left prefrontal region and the flux density of photons emitted from the right hemisphere during these conditions suggests that intention and other forms of self-monitoring behaviours could potentially modify photon emissions. Biophotons are emitted from bacteria (Tilbury & Quickenden, 1988), cells (Inaba, 1988), and hippocampal slices (Isojima, Isoshima, Nagai, Kikuchi, & Nakagawa, 1995). These electromagnetic emissions within the visible wavelength may be forms of intercellular communication rather than simply metabolic artifacts (Sun, Wang & Dai, 2010).

The seminal research of Popp (1979; 1988) and the Van Wijks (1988; 2006) has shown that photon emissions are measureable from several loci of the body, including the hands and head. The magnitudes, often measured in the order of 10^7 photons per meter-squared per second, are effectively the same flux density measured from cells and the heads of human volunteers. Although photon emissions from the head might be attributed to sources within the hair or scalp rather than the cerebrum this explanation would not accommodate the reliable, reversible increase and decrease in photon counts or radiant flux densities coupled to imagining white light compared to mundane thoughts. These intervals are determined by the instruction of the experimenter and hence are less likely to be spurious associations.

To reduce the possibility of artifact and to further pursue the relationship between the characteristics of photon emissions from the left and right hemispheres an experiment was desgined where photon emissions from both sides of the head were measured simultaneously. The primary goal was to discern if there is temporal coherence between the two hemispheres. In previous studies Saroka, Caswell, Lapointe & Persinger (2014) had found that electroencephalographic coherence between the left and right temporal lobe structures was affected by global geomagnetic activity, suggesting that relatively small amounts of energy could be involved with this enhanced intercalation. Here evidence is presented for the first time that the amplitude variations in photon emissions from the left and right hemispheres are coherent but phase-lagged during resting (baseline) conditions.

Materials and Methods

To test this relationship seven subjects (3 men, 4 women) between 20 and 26 years of age volunteered as subjects after the protocol was approved by the university's research ethics committee. This small sample was considered sufficient because each person was employed as his or her "own" control and have shown biophoton emissions from cerebral activity to be reversibly controlled by external instruction (Dotta, Saroka, & Persinger, 2012). Photon emissions were measured from the left and from the right hemisphere simultaneously. The purpose of the experiment was to discern the temporal correlation between amplitudes of photon emissions, as measured by photomultiplier units, from the left and the right hemisphere. Vivid cognition or the act of imagining white light while sitting blind folded in a hyper-dark chamber (10^{-12} $W \cdot m^{-2}$) has been shown to significantly increase photon emissions. Consequently, bilateral photon emissions during baseline conditions when no active or at least instructed cognition was

in progress were compared. In other words is there an intrinsic decoherence or coherence in spectral density profiles between the two cerebral hemispheres of human beings when they simply sit in the dark and engage in cognition commensurate with the default network?

The procedures were very similar to those reported by Dotta, Saroka, & Persinger (2012). Each participant sat within a comfortable arm chair within a hyper-dark (10^{-12} $W \cdot m^{-2}$) acoustic chamber (13 m^3). Digital photomultiplier devices were placed on the left and right side of the subject's head approximately 15 cm from the temporal lobes. The information from each device was captured by its own software and IBM laptop computer that was housed outside the chamber in a room that was also dark. The photons were sampled at 10 times per second for 1 min. To control for idiosyncratic features of a given photomultiplier unit, the location of the units (right or left side of the head) were counterbalanced for different subjects.

The numbers of photons per 100 ms (10 Hz sampling) for the middle 60 s (600 cases) of the baseline from the left and right side of the head for each subject were extracted and analyzed by SPSS (16) software. For each subject the photon numbers from the left and from the right side of the head were correlated. In order to discern potential temporal displacement between the two hemispheres the photon counts from the left and right hemisphere were lagged by 20 increments (100 to 2000 ms) and then correlated with the reference unit for the other hemisphere.

Results

The results are shown in Figure 51. Although the strengths of the correlation coefficients were small and explained less than 1% of the variance the strongest significant relationship was the increase in photon radiant power from the left hemispheres about 900 ms before increased emissions from the right hemispheres. In fact the correlations with most of the other lags for the

right hemisphere with respect to the left hemisphere and vice versa were significantly weaker as indicated by the overlap with the standard errors of the means. It may be relevant that the numbers of corpus callosum fibers, each emerging from a single neuron, within the human brain constitute 1% or less of the total numbers of cortical neurons which average about 23 billion (Aboitiz, Scheibel, Fischer, & Zaidel, 1992). If the source of the approximately 1 s lag between the left and right hemispheric photon emissions was related to interhemispheric processing superimposed upon background biophoton emissions than one would expect this magnitude of strength of association. The upper limit for the estimated recurrent interhemispheric times for unmyelinated (0.1 to 1 μm) axons as described by Aboitiz *et al*. (1992) would be about 900 ms which is well within the range of what was observed.

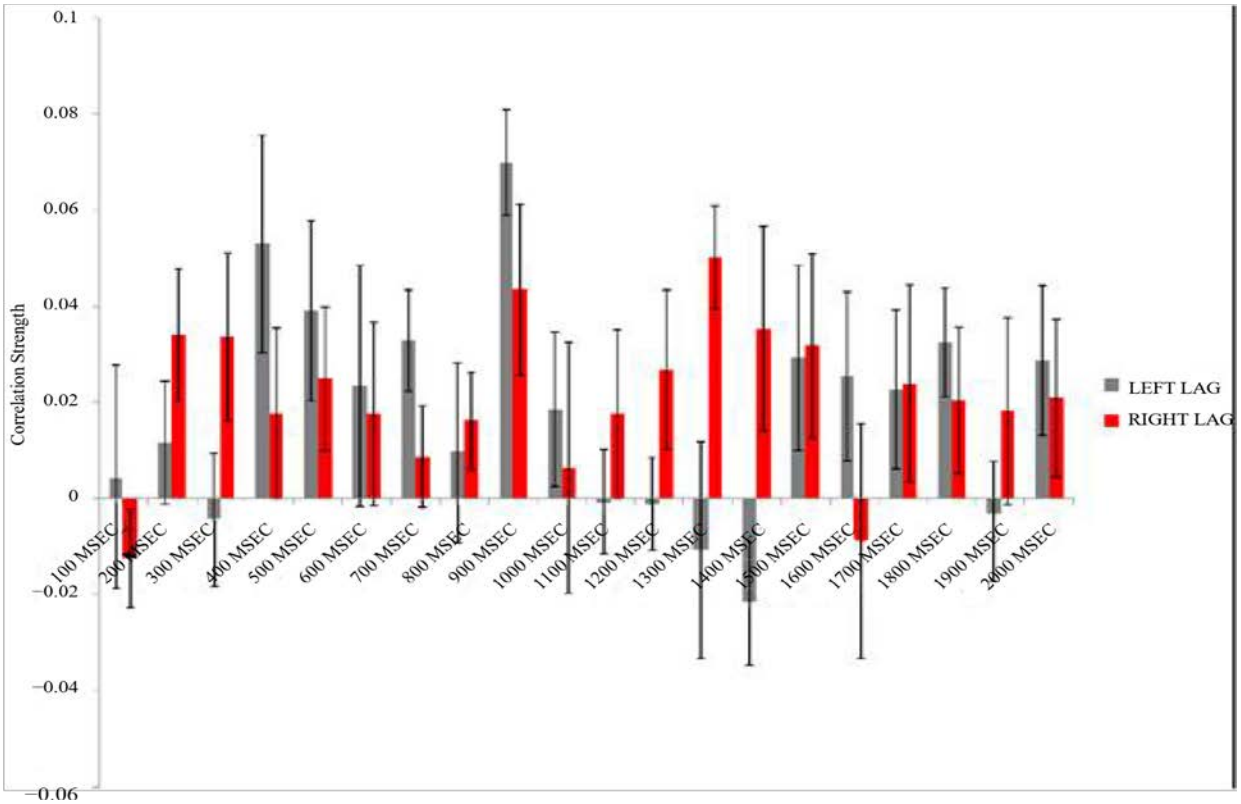

Figure 51. Correlation coefficients between the amplitude variations in photon emissions from the left and right hemisphere while subjects sat quietly in a hyper-dark room. The gray bars indicate the left hemisphere is temporally lagged behind the right hemisphere photon values. The red bars indicate the right hemisphere was lagged behind the left hemisphere. The horizontal axis indicates increments (in ms) of the lags. Vertical bars represent standard errors of the mean.

It is reasoned that if this temporal displacement were valid then spectral analyses of the amplitude fluctuations in photon emissions should verify the effects. Spectral analyses (SPSS 16, Spectra) were completed for each of the seven subjects. The spectral power for the fluctuations in photon spectral power density from the right and left hemisphere for a sample participant is shown in Figure 52. All subjects displayed similar patterns. Spectral analyses revealed a peak in power density at 2.7 Hz for the left hemisphere and 1.85 Hz for the right hemisphere. There were no statistically significant correlations between the power densities. In order to allow direct comparison the photon numbers from each hemisphere were z-scored before the spectral densities were calculated. The spectral power densities were compared. Lag correlations by the increments of Δf (in this case $\Delta f = 0.016$ Hz, the Nyquist Limit for the spectral power densities) were then computed for the spectral densities as a function of frequency bin for the data from each hemisphere. When they were lagged by 0.98 Hz to 1.15 Hz statistically significant negative correlations were clearly evident with a peak value of $r = -0.23$. The results of the lag analyses are shown in Figure 53. This indicated that the average "out of phase" would be have been about 800 to 890 ms which is within the range of the lag measured from the standardized scores of the power density of the photon emission every 100 ms.

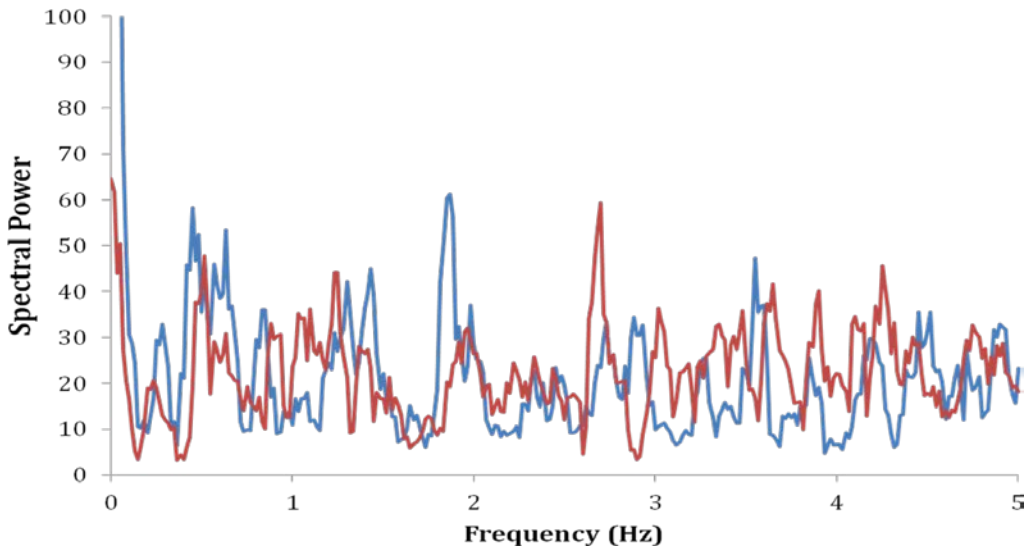

Figure 52. Spectral power denisties for the amplitude of photon emissions during baseline (rest) conditions for the left (blue) and right (red) hemispheres. Note the singular peak in power for time frequency in the left hemisphere around 1.8 Hz (blue) and in the right hemisphere around 2.8 Hz (red).

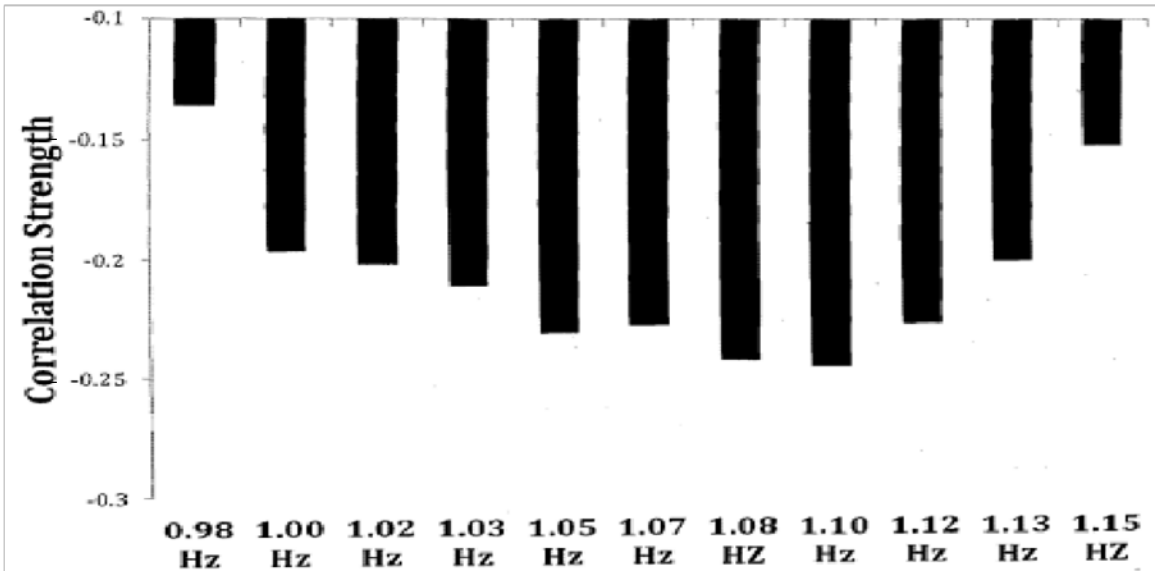

Figure 53. Strength of correlations between spectral power densities for different frequency lags. All lags between 0.98 and 1.15 Hz were statistically significant at the $p < 0.05$ level.

Discussion

These results support measurements from previous studies that photon emissions can be measured at distances more than direct contact to the human skull during a brief (1 min) baseline sampling if the person is sitting in a hyper-dark setting. There is strong evidence that the power densities of the photon emissions for each hemisphere are not temporally coherent but lagged by approximately 1 s. This was evident from the lag analyses for the standardized photon counts as well as the results of the comparisons of the spectral densities for the left and right hemisphere of the volunteers.

The discrepancy could be considered a phase lag analogous to the Aharanov-Bohm phenomenon that has been attributed to electrons moving near a special magnetic field condition. The degree of phase shift is related to the intrinsic voltages and the time within the field. The relationship can be set to solve for t (the time within the field) as:

$$t = (\Psi \cdot \hbar) \cdot (V \cdot q)^{-1} \quad (1)$$

where Ψ is the phase lag; $\hbar$ is the modified Planck's constant; V is the voltage and q is the unit charge. If the phase lag is reflected by the ratio of 1.8 Hz (for the left hemisphere) and 2.8 Hz (for the right hemisphere), that is 0.64, and the energy Vq is that associated with the median energy of the photons discerned by the photomultiplier units, 5×10^{-19} J, then t, the time each electron that might be related to the photon emission within the field is 1.34×10^{-16} s.

This duration is remarkably proximal to the time required for an electron to complete one Bohr orbit (1.52×10^{-16} s). This is the same order of magnitude and comparable coefficient for the time required for a photon moving 1/3rd the velocity of light in a vacuum to traverse a plasma cell membrane of the neuron which averages around 10 nm. This convergence at least sets the

conditions for the photon to intercalate with the completion of a single electron orbit. The energy associated with the mass of an electron moving at the square of the fine structure velocity in the time of one orbit is effectively Planck's regular constant, particularly when the ratio of the spin and orbital magnetic moment of the electron is accommodated.

In previous studies we had shown that the amplitude of the photon emissions from the right hemisphere but not the left hemisphere increased during imagining white light but not during engagement of more mundane cognitive tasks (Dotta, Saroka, & Persinger, 2012). For these no-imagine, imagine, no-imagine, and imagine procedures, the net increase compared to the previous no imagine interval was about 5×10^{-12} $W \cdot m^{-2}$. It was estimated that based upon the cross sectional area of the lateral cerebral hemispheres (about 10^{-2} m^2), this would be equivalent to about 10^{-14} J per second. Assuming the neurons contributing to this energy were each discharging on average at 10 Hz and each action potential involved 10^{-20} J, the source population would be in the order of 10^6 to 10^7 neurons.

Aboitiz *et al.* (1992) as confirmed by Bojak and Liley (2010) indicated that the numbers of unmyelinated axons within the human corpus callosum between 0.4 and 1 μm diameter would involve about 1.6×10^7 neurons compared to the estimated 200 million within the entire structure. This would involve a maximum of about 6.5% of the total population of fibers. For comparison these diameters if they were electromagnetic wavelengths (400 to 1000 nm) would include the range of visible photons. Dotta *et al.* (2011; 2014), while measuring malignant cells that had been removed from incubation, showed that the typical wavelengths associated with metabolic and replication activity concentrated within the interfaces between ultraviolet-visible and visible-infrared.

The source of the photon emission interaction between the left and right hemispheres may primarily involve the non-myelinated axons with widths between 400 and 800 nm. If the approximately 6.5% of the total corpus callosal fibers were mediating the effect and were determining effect size then any correlation between the two hemispheres would be the square root of that value or equivalent to a r value of 0.25. This is within error variation of what was measured in this experiment.

There are relatively sound biophysical bases to this number. Assuming the coherence of voltage across the major area of the cerebral cortices is in the order of 0.2 $mV \cdot m^{-1}$ or 2×10^{-4} $V \cdot m^{-1}$ (Saroka & Persinger, 2014) and the extracellular fluid resistance of 2 $\Omega \cdot m$ (Barnes, 1986) the current density would be 10^{-4} $A \cdot m^{-2}$. Over the total surface area of the cerebral cortices of 1.8×10^{-1} m^2 the electric current would be 1.8×10^{-5} A. Given that there is 1.6×10^{-19} $A \cdot s$ per unit charge, this means that a total of 1.1×10^{14} charges per second would be involved. Typical estimates average 10^6 to 10^7 charges per action potential. Hence 10^{14} charges per s would be equivalent to 10^6 to 10^7 axons discharging between 1 to 10 Hz. Assuming the dominant contribution from $\sim 4 \times 10^7$ action potentials per second each with a unit energy of 10^{-20} J, the energy (Persinger, 2010) would be 10^{-13} $J \cdot s^{-1}$ (W). When distributed over the area of the average cerebral cortices (1.8×10^{-1} m^2) the radiant flux density would be $\sim 2 \times 10^{-12}$ $W \cdot m^{-2}$ which would be within the range of the measurements recorded in this study.

The repeated observations in previous experiments (Dotta, Saroka, & Persinger, 2012; Saroka, Dotta, & Persinger, 2013) that instructions to imagine or not imagine types of imagery was associated with increased photon emissions from the right side of the brain and not the left side of the brain (Dotta, Saroka, & Persinger, 2012) minimized the likelihood of artifact. In addition, a powerful correlation was found accommodating more than 80% of the variance

between quantitative electroencephalographic power within the beta range over the left prefrontal lobes of the participants and the power density of the photon emissions from the right hemisphere during the experiment (Dotta, Saroka, & Persinger, 2012). One interpretation of this strong association is that intention or some factor associated with this process might influence the power density of biophoton emissions from the right hemisphere.

In the present experiment the lag of the peak correlation strength between the power density of photon emissions from the left and right hemisphere during baseline conditions when both measures occur simultaneously suggests that either each hemisphere is operating independently or that a discrete amount of time is required before the processes that are responsible for photon emissions in one hemisphere affect the processes associated with photon emissions from the other. Whatever process is involved the strongest cross-spectral correlation of about $r = 0.25$ indicates that only 6.5% of the variance in shared distributions of power density occurs between the two hemispheres when the optimal lag is implemented.

The ratio of 1.8 Hz and 2.8 Hz spectral power density peaks were employed for the left and right hemispheres, respectively, to obtain the inferred ratio for the phase shift in an Aharanov-Bohm effect if it were valid at macroscopic contexts (Persinger & Koren, 2016). The equivalent time would sufficiently overlap with the latency for a photon to traverse a neuronal plasma membrane and the orbit of a single electron. This creates the condition for an exchange of quantum bits of information moving from the membrane into space or from space into the membrane. Consider the upper boundary (433 ms) of the latency required for transmission along unmyelinated axons between the two hemispheres to be supportive of the absolute lag in hemispheric time (900 ms) if a complete circuit is considered. Considering the average transmission velocity to be 8.7 mm per ms per μm and the median width of an axon to be 500

nm, the single traversing time would be 25 to 30 ms or 33 to 40 Hz. This is the classic frequency band associated with human consciousness and awareness.

References

Aboitiz, F., Scheibel, A.B., Fischer, R.S. & Zaidel, E. (1992) Fibre Composition of the Corpus Callosum. *Brain Research*, 598, 143-115.

Barnes, F.S. (1986) Interaction of DC Electric Fields and Living Matter. In: Polk, C. and Postow, E., Eds., *Handbook of Biological Effects of Electromagnetic Fields*, CRC Press, Boca Raton, 99-120.

Bojak, I. & Liley, D.T.J. (2010) Axonal Velocity Distributions in Neural Field Equations. *PLoS Computational Biology*, 6, e1000653.

Dotta, B.T., Buckner, C.A., Lafrenie, R.M. & Persinger, M.A. (2011) Photon Emissions from Human Brain and Cell Culture Exposed to Distally Rotating Magnetic Fields Shared by Separate Light-Stimulated Brains and Cells. *Brain Research*, 1388, 77-88.

Dotta, B.T., Buckner, C.A., Cameron, D., Lafrenie, R. & Persinger, M.A. (2011) Photon Emissions from Cell Cultures: Biochemical Evidence for the Plasma Membrane as the Primary Source. *General Physiology and Biophysics*, 30, 301-309.

Dotta, B.T., Saroka, K.S. & Persinger, M.A. (2012) Increased Photon Emission from the Head While Imagining Light in the Dark Is Correlated with Changes in Electroencephalographic Power: Support for Bókkon's Biophoton Hypothesis. *Neuroscience Letters*, 513, 151-154.

Dotta, B.T., Murugan, N.J., Karbowski, L.M., Lafrenie, R.M. & Persinger, M.A. (2014) Shifting Wavelengths of Ultraweak Photon Emissions from Dying Melanoma Cells: Their Chemical Enhancement and Blocking Are Predicted by Cosic's Theory of Resonant Recognition Model for Macromolecules. *Naturwissenschaften*, 101, 87-94.

Inaba, J. (1988) Super-High Sensitivity Systems for Detection and Spectral Analysis of Ultraweak Photon Emission from Biological Cells and Tissues. *Experentia*, 44, 530-559.

Isojima, Y., Isoshima, T., Nagai, K., Kikuchi, K. & Nakagawa, H. (1995) Ultraweak Biochemiluminescence Detected from Rat Hippocampal Slices. *NeuroReprot*, 6, 658-660.

Persinger, M.A. (2010) 10 - 20 Joules as a Neuromolecular Quantum in Medicinal Chemistry: An Alternative Approach to Myriad Molecular Pathways? *Current Medicinal Chemistry*, 17, 3094-3098.

Persinger, M.A. & Koren, S.A. (2016) The Aharanov-Bohm Phase Shift and Magnetic Vector A Potential Could Accommodate the Optical Coupler, Digital-to-Analogue Magnetic Field Excess Correlations of Photon Emissions within Living Aqueous Systems. *Journal of Advances in Physics*, 11, 3333-3339.

Popp, F.-A. (1979) Photon Storage in Biological Systems. Electromagnetic Bioinformation. Urban and Schwarzenberg, N.Y., 123-149.

Popp, F.-A. (1988) Biophoton Emission. *Experientia*, 44, 543-544.

Saroka, K.S., Dotta, B.T. & Persinger, M.A. (2013) Concurrent Photon Emission, Changes in Quantitative Brain Activity over the Right Hemisphere, and Alterations in the Proximal Geomagnetic Field While Imagining White Light. *International Journal of Life Sciences and Medical Research*, 3, 30-34.

Saroka, K.S., Caswell, J.M., Lapointe, A. & Persinger, M.A. (2014) Greater Electroencephalographic Coherence between Left and Right Temporal Lobe Structures during Increased Geomagnetic Activity. *Neuroscience Letters*, 560, 126-130.

Saroka, K.S. & Persinger, M.A. (2014) Quantitative Evidence for Direct Effects between Earth-Ionosphere Schumann Resonances and Human Cerebral Cortical Activity. *International Letters of Chemistry, Physics and Astronom*, 20, 166-194.

Sun, Y., Wang, C. & Dai, J. (2010) Biophotons as Neural Communication Signals Demonstrated by *in Situ* Biophoton Autography. *Photochemical and Photobiological Sciences*, 9, 315-322.

Tilbury, R.N. & Quickenden, T.I. (1988) Spectral and Time Dependence Studies of the Ultraweak Bioluminescence Emitted by the Bacterium *Escherichia coli*. *Photochemistry and Photobiology*, 47, 145-150.

Van Wijk, R. & Schamhart, D.H.J. (1988) Regulatory Aspects of Low Intensity Photon Emission. *Experientia*, 44, 586-593.

Van Wijk, R., Van Wijk, E.P. & Bajpai, R.P. (2006) Photocount Distributions of Photons Emitted from Three Sites of the Body. *Journal of Photochemistry and Photobiology B*: *Biology*, 84, 46-55.

Chapter 6 – Marked Peak Frequencies of Spectral Power Densities from Magnetic and Photic Stimulated Cells: a Possible Verification of Information Storage in Biological Systems

Abstract

Mouse melanoma cells were exposed to frequency-modulated photic and/or magnetic sources and compared to cells that were not. Recorded cell photonic emissions were statistically greater than background flux densities but did not differ between the various stimulation conditions. Spectral as well as discriminant analyses were able to discern specific peak frequencies for cells exposed to either 7Hz pulsing white light, 7Hz magnetic fields or the combination of the two. Peak frequencies were not found in other frequency ranges with similar explained variance explained by discriminant analyses. This method of frequency encoding may provide a stronger correlation toward information storage in biological tissues.

Introduction

Photon emissions have been measured from cells (Dotta, Buckner, Cameron, Lafrenie & Persinger, 2011), bacteria (Tilbury & Quickenden, 1988), and neurological tissues (Kobayashi *et al.*, 1999). The significance and mechanisms underlying these processes have been debated. Common results show that increases or decreases in photon intensity are due to cell activity, stress, and external factors (Popp, 1988). These factors can be easily manipulated by changing the cellular environment, disrupting the system, and thus altering the cellular behaviour. However, classification of photon dynamics to discern between these factors are rarely studied. Photon intensity measures may determine broad structural and physical changes occurring in

cells. However, it is unclear what process is specifically occurring. A recent study had used the photon emission profiles of cells to infer cell activity by use of filters for specific wavelengths of light based on the Cosic Resonant Recognition Model (Dotta, Murugan, Karbowski, Lafrenie & Persinger, 2014; Cosic, 1994). The study reliably classified which protein pathways were most probably active for each wavelength of visible light recorded.

Popp (1979, 1988) had suggested that photons are stored within biological tissue. This storage of photons may provide a non-chemical bases to the system to maintain its structure and mediate specific functions. These same biological photonic emissions found in neurological settings may be used as a form of communication (Sun, Wang & Dai, 2010). Any "communication function" between cells must be able to receive, store, and transmit 'information' for communication to exist. By manipulating the source signal through photonic or magnetic stimuli, it may be possible to measure how transmitted (emitted) information may be briefly stored and released as photons. A novel approach is used by exposing frequency-modulated magnetic and light sources to cells to encode 'information' during stimulation periods. The representative photon emissions from cells are then directly measured after exposure. Fourier analysis was employed to find high specificity to the target modulated fields used.

Materials and Methods

Cell cultures

Dishes containing B16-BL6 mouse melanoma cells were divided amongst six conditions to be subject to various frequency modulated pulsed stimulation of either photic or magnetic

origin, neither, or both in a dark enclosed chamber (Figure 54) for approximately 8 minutes. Immediately after stimulated and non-stimulated plates were then placed inside a box containing a single photomultiplier tube (PMT) individually to record temporal photon counts (30 seconds between stimulation and photon recording). The photomultiplier tube was placed on directly on top of the closed dish for direct photon measures. A separate condition where empty dishes were placed inside the box housing the photomultiplier unit were used as a negative control representing the background counts attributed to the volume of the dish in the absence of cell cultures.

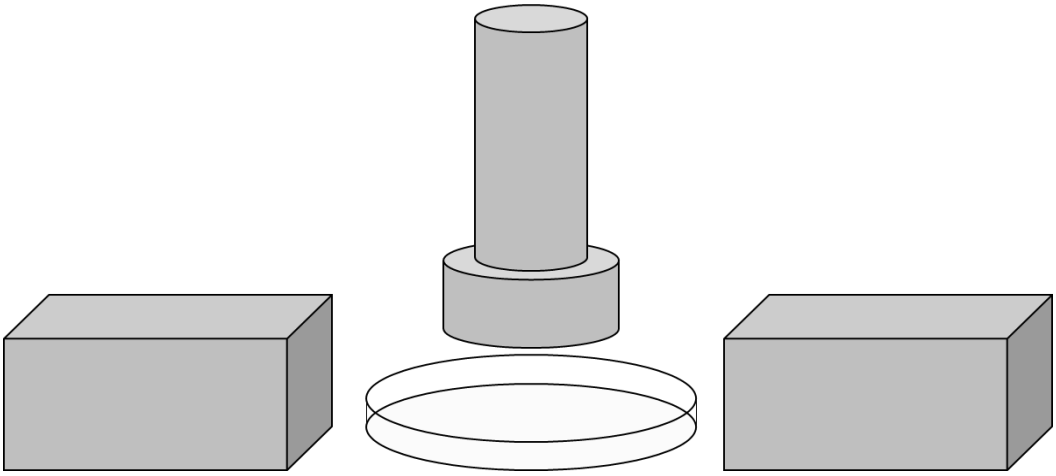

Figure 54. The design of the stimulation portion of the experiment. A petri dish (bottom centre) placed in between two solenoid housed units (left and right of dish), and under a flashlight (top centre). Solenoid units and flashlight were either on or off dependent on condition.

Photic stimulation

The photon source used in the stimulation of the cell cultures was a flashlight coupled to a Heath Schlumberger analog wave function generator that allowed the flashlight to flicker white light at a 7Hz frequency. Luxmeter readings recorded approximately 80 lux from the flashlight when measured directly against the flashlight head. The flashlight was placed directly on top of the dish of cells within the dark enclosed chamber for all conditions. The flashlight was turned

on only for those cell cultures that were placed in the photic stimulation or both magnetic field and photonic conditions.

Magnetic field stimulation

Two housed solenoid units were used to apply 1μT electromagnetic fields (EMF) onto the cell cultures along a single axis (5mm away from the dish of cells on either side). A digital waveform using a DAC system on an external connected computer was used to generate the EMFs via the solenoids. Waveforms of 1 and 7Hz sine waves were used in separate magnetic field conditions while either light was not present or was present along with the presentation of EMF stimulation.

Photomultiplier Unit

The photomultiplier unit (DM0089C Model) from Sens Tech Technologies of a spectral range of 280-630nm was used to record photon emissions within the visible range of the electromagnetic spectrum. The photomultiplier tube which was connected to an external Lenovo ThinkPad laptop using Sens Tech Counter Timer software, recorded 32000 readings of 20 msec data points (sampling rate of 50Hz for approximately ten minutes). The photomultiplier unit was placed directly on top of the petri dishes when recording photon counts so as to limit any external radiation within the volume of the box housing the PMT.

Analyses

Raw average photon counts were used for simple Oneway ANOVA analyses for mean count comparisons compared to the negative control, ‘Air’ condition. All data were then

detrended by subtracting raw values by the calculated natural logarithmic regression of each recording (Figure 55), with the exception of the negative controls where no downward trend was present. Detrended measures were used to account for photon count drift due to the progression of subsequent recordings and increase reliability in Fourier analysis. The compiled detrended data were imported into IBM SPSS v20 for subsequent analyses comparing average photon count differences between conditions. Spectral analysis and factor analysis measures were employed to assess the spectral power densities between conditions. A 'true' frequency variable was calculated by taking the frequency of the spectral analysis (0-0.5) and multiplying it by the sampling frequency of the photomultiplier unit (50Hz). The resulting frequencies, due to the Nyquist limit, would be between the ranges of 0-25Hz.

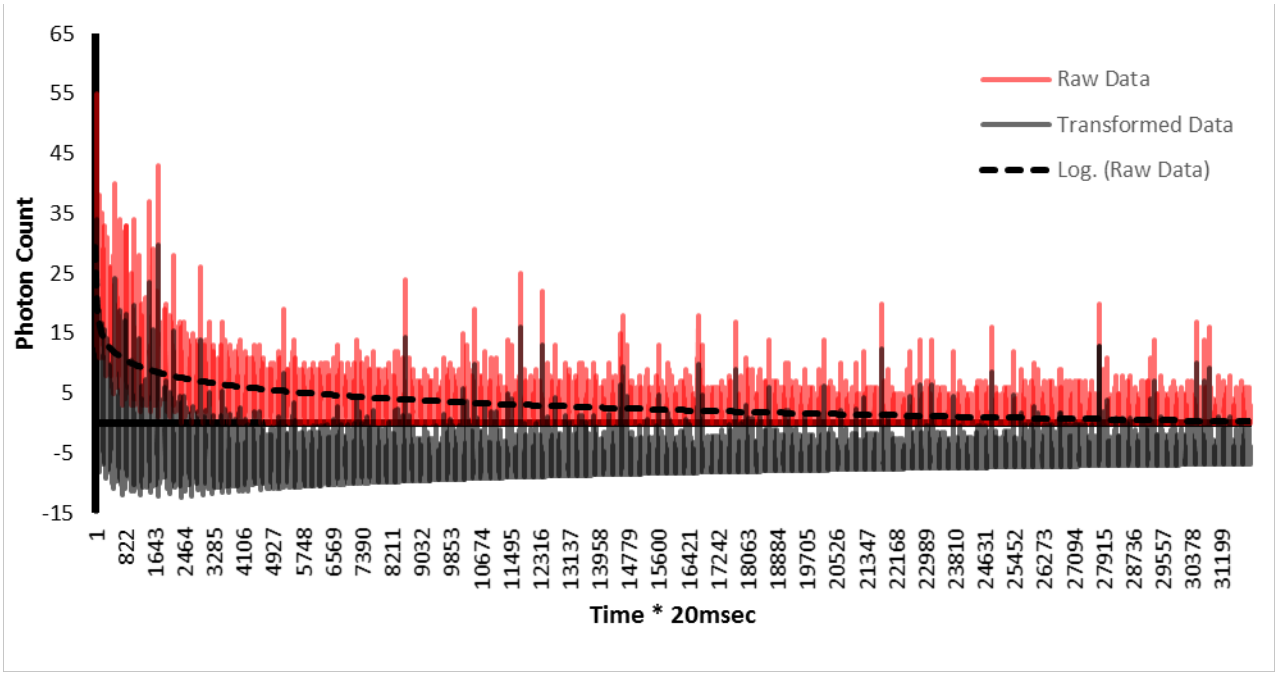

Figure 55. A sample recording of raw data (red) and subsequent detrended data (black) as a result of the difference of the raw data from the calculated natural logarithm trend (dotted black line).

Results

Raw Count Mean Comparisons

Oneway ANOVA analyses on raw average photon counts revealed significant differences $F_{(6,59)}$=2.525, p=.03 between cells not exposed to any stimulation (M=4.32, SD=2.34), cells stimulated with a 1 Hz magnetic field (M=3.91, SD=2.34), cells stimulated with a pulsating 7 Hz light flash (M=3.63, SD=1.24), cells receiving both 1 Hz magnetic field exposure and 7 Hz light flash (M=3.99, SD=2.36), cells receiving 7 Hz magnetic field exposure(M=3.27, SD=2.00) cells receiving both 7 Hz magnetic field exposure and 7 Hz pulsating light flashes (M=3.49, SD=3.73), and the 'Air' condition where no cells were placed inside the box (M=0.38, SD=0.03). When computing a grand average of all conditions that measured from cell sources (M=3.85, SD=2.22, N=60) and comparing it to the condition containing no cells (Air) (N=6), an independent t-test analysis revealed significant differences to differentiate conditions with and without cells, t(59.23)=-12.09, p<.001. Figure 56 displays the average counts between conditions with and without cells per second, which is calculated by multiplying the average of each recording by 50.

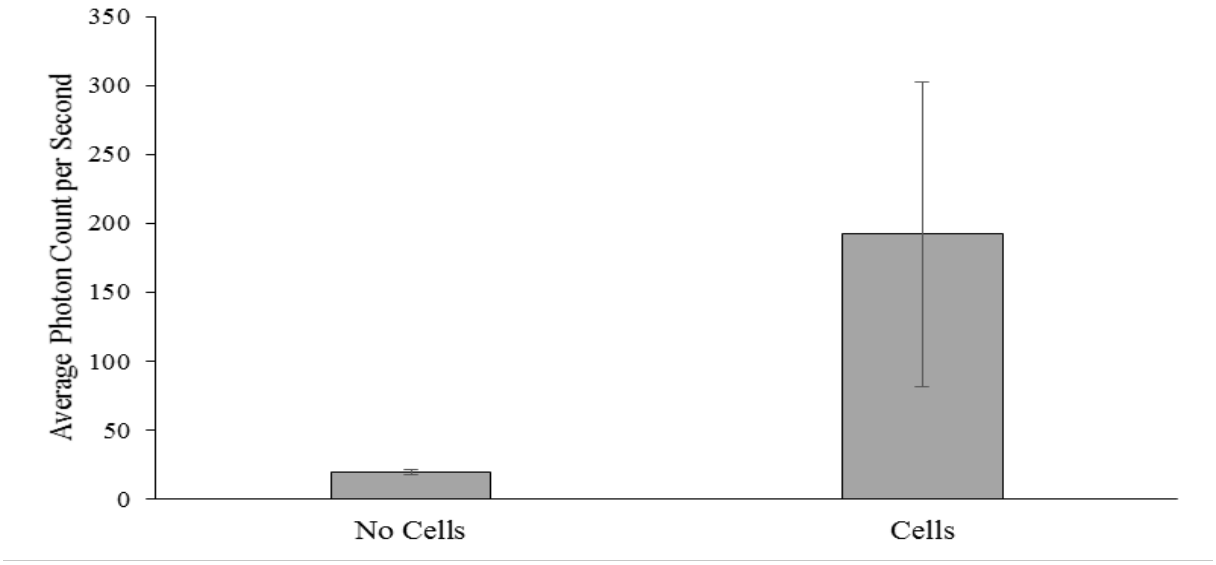

Figure 56. Grand averages of photon counts per second between conditions with cells and without cells, standard deviation bars are displayed.

Spectral Analyses

Detrended analyzed data were subjected to spectral analysis were binned into 0.1 Hz averages for comparisons between conditions of stimulated and non-stimulated cells between 0 and 25Hz of the calculated true frequency. Individual discriminant analyses were able to classify separate experimental conditions, specifically between cells that received 7 Hz photic stimulation and baseline conditions, as well as cells that were exposed to 7 Hz electromagnetic field stimulation compared to baseline conditions (Figure 57). Discriminant scores for photon emission spectral profiles of cells that received photic stimulation had a classification accuracy of 88% and were defined by the equation:

$$7\ \text{Hz Light} = 0.573*(7.5\ \text{Hz}) - 0.209*(14.9\ \text{Hz}) - 6.297$$

Discriminant scores for cells that received 7 Hz electromagnetic field pattern stimulation had a classification accuracy of 81%, represented by the equation:

7 Hz EMF = 0.363*(7.3 Hz) - 0.282*(20.7 Hz) - 1.444

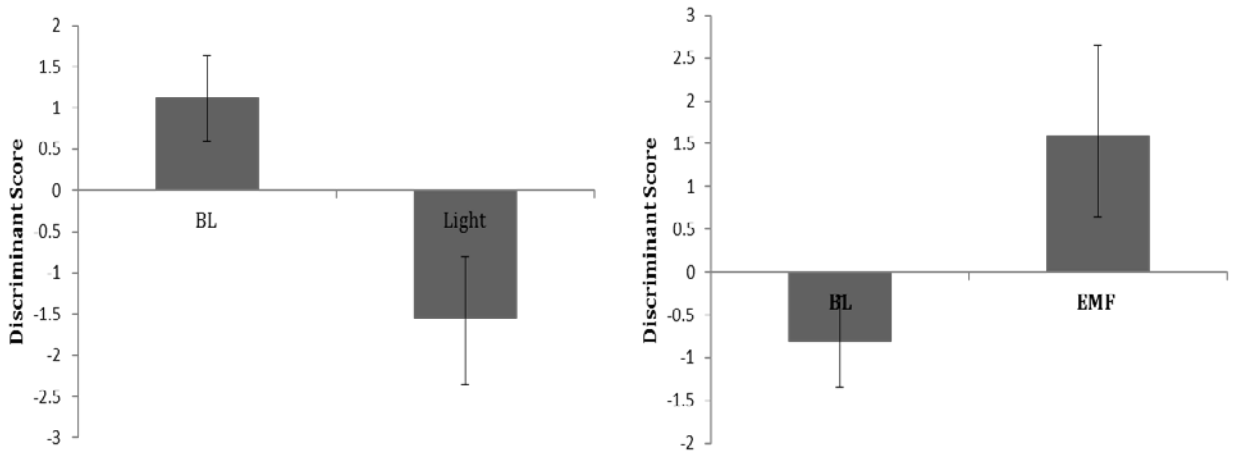

Figure 57. Discriminant scores of photon emission spectral profiles between 7 Hz light stimulated cells and baseline (BL) conditions (Left graph), and 7 Hz magnetic field stimulated cells and baseline (Right graph). Confidence intervals are represented.

From the calculated function represented for each of the stimulated cell conditions, the first factor of both light and magnetic field stimulation conditions occurred within the 7-8 Hz range. In other words this same frequency that had been applied was reemitted. Discriminant functions indicate that the light pulses (7Hz) suppressed the spectral power density while the 7Hz (but not 1Hz) magnetic field pulses enhanced the spectral power density. 0.1 Hz binned frequencies displayed in Figure 58 demonstrate these findings. A significant increase of spectral power density was observed at 7.3 Hz, $F_{(2,28)}$=8.086, p=.002. Post-hoc analysis testing revealed that the differences were driven by the magnetic field condition solely when compared to the light and baseline conditions. Significant differences were observed between the conditions at the 7.5 Hz frequency bin, $F_{(2,28)}$=12.875, p<.001, where significant differences were driven by the 7 Hz light condition. These analyses confirm the discriminant equations for each condition of magnetic and photic stimulation respectively.

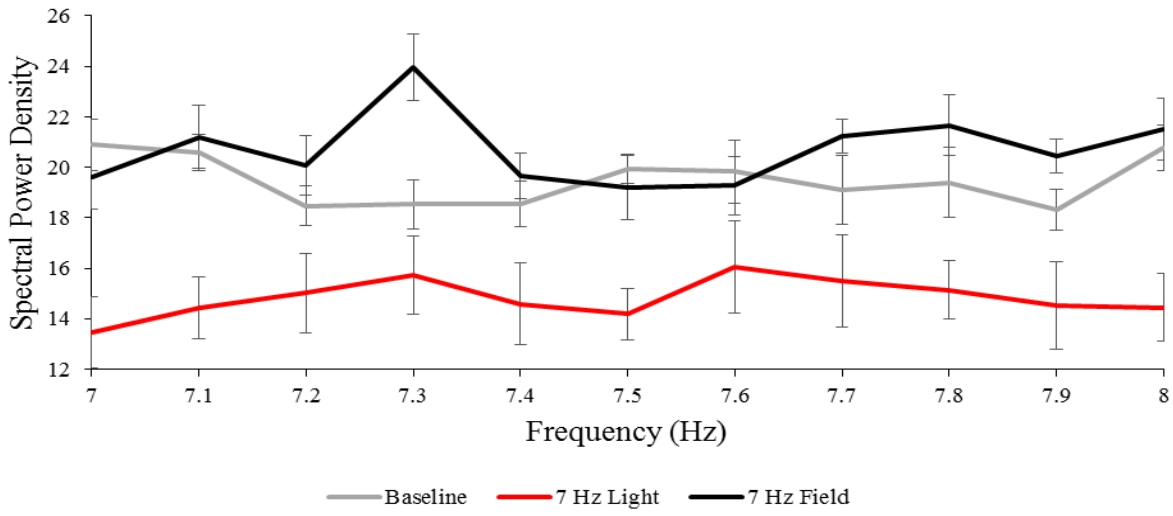

Figure 58. Marked photon spectral power density peaks within the 7-8Hz band between cells stimulated with either 7 Hz light pulses (red) or magnetic fields (black) compared to cells without stimulation (grey). Standard error bars are displayed.

In order to demonstrate the frequency specificity of the spectral power density, the 1-2Hz band was examined as a reference. An analysis of the 1-2Hz frequency band did not display peaks similar to that of the 7-8Hz true frequency range (Figure 59), where both photic and magnetic field stimulated cells did not show increased peak frequencies comparative to baseline ($p>.05$). The conditions for both light and magnetic field combined stimulation did not significantly differ in these frequency ranges and are not displayed due to the marked contrasts of the components making the combinations (7Hz light and EMF).

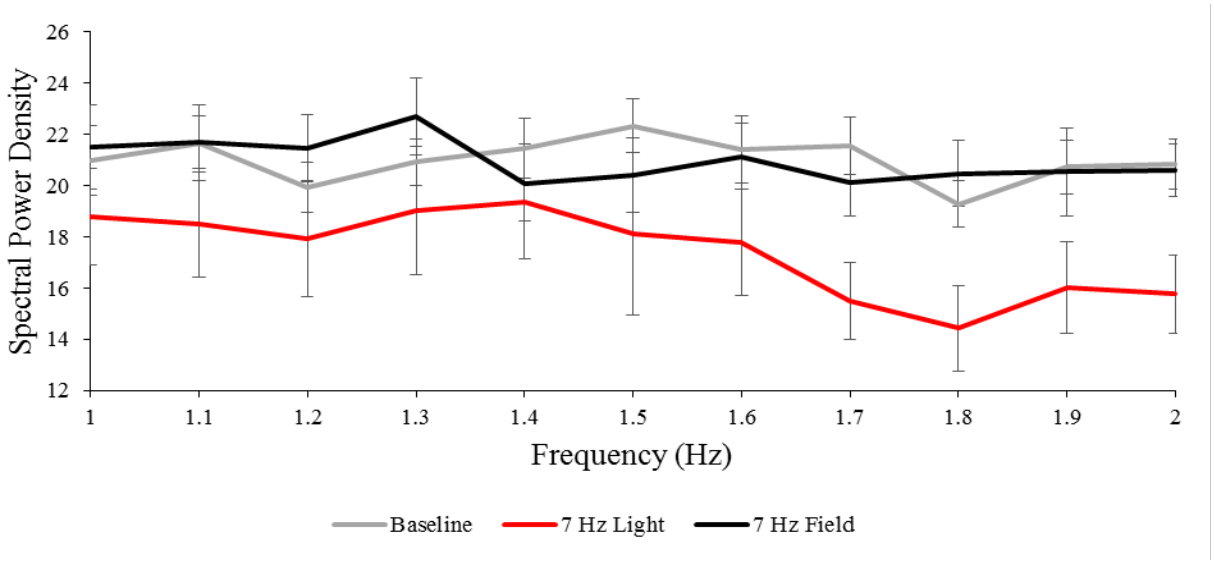

Figure 59. Photon spectral power density peaks within the 1-2Hz band between cells stimulated with either 7 Hz light pulses (red) or magnetic fields (black) compared to cells without stimulation (grey). Standard error bars are displayed.

Discussion

Melanoma cells removed from incubation show marked increases of photon emissions within the visible range for up to 24 hours after removal in previous experiments (Dotta, Murugan, Karbowski, Lafrenie & Persinger, 2014). The results of the present experiment showed no discernable differences in raw photon count between cells stimulated by the various stimuli. The major effect occurred with spectral power density.

Wavelengths within the visible photon spectra have been used to predict cellular functions using the Cosic Resonant Recognition model by the use of filters (Dotta, Murugan, Karbowski, Lafrenie & Persinger, 2014; Cosic, 1994). No filters were used on the photomultiplier unit to specify cellular function, as used in the experiment of Dotta *et al.* (2014), and cells were placed outside of incubation settings for under 1 hour. However, temporal changes within time series analyses presented provides a greater insight of the storage of

'information' rather than specific cellular functions related to cell proteins and signalling pathways. A representation of externally applied energy whether light or magnetic in origin from the electromagnetic spectrum may be represented in the cellular processes of aggregates of cells.

In this experiment 7Hz light or magnetic field stimulation were used as a frequency encoding paradigm. Shifts within spectral frequencies of the recorded photonic emissions from treated cells were directly associated with the temporal frequencies of the stimulation field patterns. This method of frequency encoding has been useful in neuroimaging applications such as retinotopic (Engel, Glover & Wandell, 1997), somatotopic (Servos *et al.*, 1998), and tonotopic (Talavage *et al.*, 1996) mapping in functional magnetic resonance imaging studies.

Presenting cellular aggregates of approximately 10^6 cells with cyclic frequency-modulated fields of both photic and magnetic origins, photonic emissions post-stimulation indicates that 'information' can be stored and later represented in the emission profiles of the cells comparative to baseline conditions. The discriminant analyses of the entire spectral range between 0-25Hz of the true frequency for each condition explained greater than 80% of the variance was explained by the 7.5Hz frequency of light stimulated cells, and 7.3Hz for magnetic field stimulated cells over all other frequencies. The implications of a cyclic 7Hz stimulation pattern of both photic and magnetic origin showing pronounced specificity within the broader 7-8Hz range may not be coincidental.

Similar to neuroimaging techniques such as the MRI employing strong magnetic fields to align and detect pertubances in proton spin, direct photic stimulation of pulsating white light at approximately 80lux might provide disturbances in natural photonic emissions of the same wavelengths. Photon counts from cells that received no stimulation significantly differed from cells that received photic stimulation. Magnetic field exposures have been shown in previous

studies to alter photic emissions in melanoma cells (Persinger. Dotta, Karbowski & Murugan, 2015) as well as 'holding' effects of pH in chemical solutions (Murugan, Karbowski, Dotta & Persinger, 2015). In fact, magnetic field stimulated cells shared similar spectral profiles with cells that did not receive any stimulation.

The punctate spectral frequency peak of 7.3Hz in magnetic field stimulated cells condition provides a strong possibility that the holding of 'information' through means of applied energy is present. The combined condition of both 7Hz light and magnetic field stimulation did not significantly differ from baseline, untreated cells in spectral power throughout the frequency range. The combination of two frequency-modulated sources of electromagnetic energy did not show a 'doubling' effect even though the two shared the same frequency modulation. The combination of the two sources may provide an emission profile similar to that of baseline activity, as each form of stimulation may cancel the effects of each other (light stimulation lowers spectral power, whereas EMF stimulation maintains or increases spectral power in 7.3Hz). These results coincide with the findings of Persinger *et al.* (2015) in which slight increases of magnetic field intensities were correlated with decreases in photonic emissions of cell aggregates exposed to magnetic fields.

The methods used provided very specific results by employing Fourier transforms to reveal spectral power density profile signatures correlated to temporal and frequency dependent measures. Although the choice of employing simple 7Hz fields for both photic and magnetic sources do not provide a wide range of peak frequencies in multitude, the specificity of peak frequencies within the discriminant analyses of the spectral profiles provided suggests simple information storage within cellular aggregates. The amount of cells within a culture dish ($\sim 10^6$) exposed to these sources of energy are similar to the amount of neurons required for imagery of

about 10^7 neurons (Dotta & Persinger, 2012). If specific patterns of externally applied stimuli are represented in the cellular aggregates of tissue, then the manifestations of conscious thought may be explored via the spectral peaks representative in frequency encoded photon emissions.

References

Cosic, I. (1994). Macromolecular bioactivity: is it resonant interaction between macromolecules? Theory and application. *IEEE Trans BioMed Eng*, 41: 1101–1114

Dotta, B.T., Buckner, C.A., Cameron, D., Lafrenie, R.F. & Persinger, M.A. (2011). Biophoton Emissions from Cell Cultures: Biochemical Evidence for the Plasma Membrane as the Primary Source. *General Physiology and. Biophysics*, 30, 301-309.

Dotta, B. T., Persinger, M. A. (2012). "Doubling" of local photon emissions when two simultaneous spatially, separated, chemiluminescent reactions share the same magnetic field configurations. *J. Biol. Chem.*, 3:72-80.

Dotta, B. T., Murugan, N. J., Karbowski, L. M., Lafrenie, R. M., & Persinger, M. A. (2014). Shifting wavelengths of ultraweak photon emissions from dying melanoma cells: their chemical enhancement and blocking are predicted by Cosic's theory of resonant recognition model for macromolecules. *Naturwissenschaften*, 101(2): 87-94.

Engel, S. A., Glover, G. H., Wandell, B. A. (1997). Retinotopic organization in human visual cortex and the spatial precision of functional MRI. *Cerebral Cortex*, 7:181-192.

Kobayashi, M., Takeda, M., Sato, T., Yamakazi, Y., Kaneko, K., Ito, K.-I., Kato, H. & Inaba, H. (1999). *In Vivo* Imaging of Spontaneous Ultra-Weak Photon Emission from a Rat's Brain *in Vivo*. *Journal of Neuroscience Methods*, 34, 103-113.

Murugan, N. J., Karbowski, L. M., Dotta, B. T. & Persinger M. A. (2015). Delayed Shifts in pH Responses to Weak Acids in Spring Water Exposed to Circular Rotating Magnetic Fields: A Narrow Band Intensity-Dependence. *International Research Journal of Pure & Applied Chemistry*, 5(2): 131-139.

Persinger, M. A. Dotta, B. T., Karbowski, L. M. & Murugan, N. (2015). Inverse relationship between photon flux densities and nanotesla magnetic fields over cell aggregates: Quantitative evidence for energetic conservation. *J. FEBS Open*, 5:413-418.

Popp, F. A. (1979). Photon storage in biological systems. In: Popp FA, Becker G, Konig HL, Pescha W (eds). *Electromagnetic bioinformation.* 123– 149

Popp FA (1988) Biophoton emission. *Experientia* 44:543–630

Servos, P., Zacks, J., Rumelhart, D. E., et al. (1998). Somatotopy of the human arm using fMRI. *Neuroreport*, 9: 605-609.

Sun, Y., Wang, C. & Dai, J. (2010) Biophotons as Neural Communication Signals Demonstrated by *in Situ* Biophoton Autography. *Photochemical and Photobiological Sciences*, 9, 315-322.

Talavage, T. M., Ledden, P. J., Sereno, M. I., et al. (1996). Preliminary fMRI evidence for tonotopicity in human auditory cortex. *Neuroimage*, 3: S355.

Tilbury, R.N. & Quickenden, T.I. (1988). Spectral and Time Dependence Studies of the Ultra-Weak Bioluminescence Emitted by the Bacterium *Escherichia coli*. *Photochemistry and Photobiology*, 47, 145-150.

Chapter 7 – Concluding Remarks

Summary

Photon emissions from chemical and biological sources, and from brain matter both living and non-living, were explored in this thesis. Photic energy displayed throughout these levels of magnitude follows the law of conservation. Energy cannot be destroyed nor created. The energy within a system remains constant. The 'systems' measured were controlled from external influences. Photon counting measures were completed in dark settings. Photomultiplier heating/cooling drift was accommodated. If the energy within the system remains constant, then calculations that account for specific traits of the elements, nervous tissue, and cellular aggregates, would provide an accurate prediction of the amount of energy that can exist within the measured system. Common traits that can be calculated amongst systems include mass, volume, and amount of particles. As the magnitude of the system increases, the amount of variables that need to be controlled increases. However this allows for greater degrees of freedom. For example, brain matter can be measured from different lobes, gyri, subcortical, cortical, cerebellar, tract systems both ascending and descending, and unmyelinated/myelinated axons. Comparatively, chemical sources of a pure element can be measured between phases, and of its thermo- and electro-dynamic properties. Measurements that are shared between all levels of discourse are most optimal to make comparisons of the photon sources.

To relate all photon sources from the reported chapters a reductionist approach is taken to dissect the more complex systems into the smaller systems that comprise the entire system. Assume that the human brain from a physiological standpoint is made up of cellular aggregates. Some are morphologically different from others. They are composed of individual cells that are

composed of organelles, and those organelles are aggregates of proteins. The proteins are chains of amino acids and amino acids are made up of chemical elements of which are the simplest forms of matter to measure. If the reductionist method is applied then all systems can be assumed to be, at simplest, large aggregates of atoms that only differ in magnitudes in the amount of atoms being measured. If macrocosm reflects microcosm, then the above assumption can be made.

Assuming the most basic units of matter within the periodic table of elements can be used to find such parallels of photonic emissions of that seen in cellular aggregates, the hypothesis must be met with calculations to conceptualize the phenomena. The hydrogen atom (proton) is the simplest unit of the chemical elements, and assuming that all chemical elements are composed of aggregates of protons and electrons, can arguably be a collection of hydrogen-like protons.

Given that the value of Van der Waals radius of the hydrogen atom, 120 picometers or 1.2 angstrom, the volume is calculated such that a single hydrogen atom occupying space has a volume:

$$\frac{4}{3}\pi\,(r)^3 = \frac{4}{3}\pi\,(1.2 \times 10^{-10}\,m)^3 = 7.24 \times 10^{-30}\,m^3$$

If the average width of the neuron is 10 micrometers, we calculate the volume:

$$(1.0 \times 10^{-5}\,m)^3 = 1.0 \times 10^{-15}\,m^3$$

Dividing the volume of an average neuron by the volume occupied by a hydrogen atom equates to approximately 1.38×10^{14} hydrogen atoms, or protons. This value is markedly similar

to the value observed by (Pakkenberg *et al.,* 2003), representing the amount of cortical synapses (1.5×10^{14}) in the human brain, and within the range of the gross estimate, by volume, of cells in the human body (Bianconi *et al.,* 2013*)* of $\sim 10^{13}$. The human brain arguably functions, largely, by the amount of viable connections from its synapses. The large amount of synapses within the cortex allows for activity to occur between neurons electrically, chemically (Purves et al. 2001), and by photonic processes (Dotta *et al.,* 2011). Activity within individual neurons are mediated by action potentials along the cell membranes that are coupled to any of these processes.

The volume of protons in the above calculation assumes no covalent bonds. It is used as a lower limit of the amount of hypothetical atoms that constitute an average neuron. However, these values serve as a reflection that the subunits that make up the entirety of the whole unit have similarities among differing levels of discourse. The subunits that make up the whole unit may serve as a critical threshold in order for energy to be represented in 4-dimensional space time. As a reiteration of the non-living brain matter studied in this document, spontaneous photon emissions were recorded when masses were equivalent to live human brains at the calculated amount of 10^7 cortical neurons.

This finding is markedly similar to the amount of neurons required for imagery of about 10^7 neurons (Dotta & Persinger, 2012; Rouleau & Dotta, 2014). The structure of matter may reflect the intrinsic properties of the entire set, as evident from the observed flux power densities correlating to the same power densities associated with action potentials in the brain; $\sim 10^{-12}$ W/m^2. A critical threshold of light emitting matter must be present in order for the spontaneous photonic emissions to be measured. However, non-living brain matter displays emission characteristics that differ from living tissue such that the amount of matter displays a linear relation to the volume that it occupies. It does not oppose entropy as living systems do

(Schrödinger, 1967). The emissions display elastic scattering of photons; energy is conserved from the interaction of photonic transfer from matter to the environment.

Living tissues arguably display an inelastic process in which the complexities of the living system does not conserve (in the kinetic aspect) and display the same energy from its interaction of photons. At the cellular discourse, it has been shown that photon emissions coupled to processes can be derived from the cell plasma membrane (Dotta, Buckner, Cameron, Lafrenie & Persinger, 2011). As the cell membrane serves as the barrier from the intracellular organelles, and the environment, it is the most important structure of the cell to oppose entropy. For the neuron, the membrane acts as a gradient and a structural transmitter of voltage and chemical related potentials (Lodish et al., 2000). It is through action potentials where photonic processes may most likely occur.

The proposed neuroquantum of 10^{-20} J by Persinger is the product of the change in voltage of 1.2×10^{-1} V of an action potential and unit charge of 1.6×10^{-19} Coulombs. This value is a tenth of the energy of the median energy value of a visible spectra photon; 4×10^{-19} J (Persinger, 2010). A neuron firing at 10Hz would produce a single photon to equate to 10^{-19} J, or vice-versa. If an endogenous process were to occur, a single photon can produce enough energy for a neuron to fire a single action potential in live human brains. Aggregates of cells depolarizing in the event of action potentials produce measurable emissions of photons within the visible spectra from living brain tissues (Dotta *et al.*, 2011).

The significance of the reported photon count lagged coherence between the cerebral hemispheres of living brains of humans may suggest that photonic communication or propagation of photons are occurring in living tissue, if the law of energy conservation is considered. The measurable emissions that occur during a human brain at rest from a previous

chapter demonstrates this phenomenon and shows similar findings from other research on photonic emissions of the human brain (Dotta & Persinger, 2011). Although not nervous tissue, the encoding of frequency-modulated sources of photic and magnetic energy onto cells displayed similar frequencies from photon emissions when measured from the same cells post-exposure. Cell photon emissions similarly resonated in response to externally applied energy sources which coincides with the work of Popp (1979) in the ability for biological systems to store photons, and further implies the storage of information. Neurons firing at specific frequencies by induction of surrounding neurons may allude to these results. If high frequency oscillations displayed in aggregates of neurons equivalent to ~10^7 neurons (Dotta & Persinger, 2012; Rouleau & Dotta, 2014) firing simultaneously were correlated to consciousness and cognition, and photon emissions are found to be a product (Dotta, Saroka & Persinger, 2012), then the spectral characteristics of the emissions may reveal specific sources of 'information' within the entirety of the system (brain). Likewise, the plasticity of the brain allows for the storage of photons within neurons that may be influenced by sources of photic and magnetic origins.

Conclusion

Photonic emissions of low intensities within the visible spectra are products of dynamic processes throughout differing levels of discourse. The amount of matter that may interact with, and emit energy is reflective of the space that it occupies. The photic energy exchanged between structured matter and their surroundings may be considered as a form cellular communication. There are both coherent time- and frequency-dependent domains. Photon information can be stored and emitted while maintaining relatively the same frequencies within biological systems.

References

Bianconi, E., Piovesan, A., Facchin, F., Beraudi, A., Casadei, R., Frabetti, F., Vitale, L., Pelleri, M. C., Tassani, S., Piva, F., Perez-Amodio, S., Strippoli, P., Canaider, S. (2013). An estimation of the number of cells in the human body. *Annals of Human Biology*, 40:6, 463-471.

Dotta, B.T., Buckner, C. A., Cameron, D., Lafrenie, R. F., Persinger, M. A. (2011). Biophoton emission from cell cultures: biochemical evidence for the plasma membrane as the primary source. *Gen. Physiol. Biophys*, 30:301-309.

Dotta, B. T., & Persinger, M. A. (2011). Increased Photon Emissions from the Right But Not the Left Hemisphere While Imagining White Light in the Dark: The Potential Connection Between Consciousness and Cerebral Light. *Journal of Consciousness Exploration & Research, 2*(10), 1463-1473.

Dotta, B. T., Persinger, M. A. (2012). "Doubling" of local photon emissions when two simultaneous spatially, separated, chemiluminescent reactions share the same magnetic field configurations. *J. Biol. Chem.*, 3:72-80.

Dotta, B.T., Saroka, K.S. & Persinger, M.A. (2012) Increased Photon Emission from the Head While Imagining Light in the Dark Is Correlated with Changes in Electroencephalographic Power: Support for Bókkon's Biophoton Hypothesis. *Neuroscience Letters*, 513, 151-154.

Lodish, H., Berk, A., Zipursky, S.L., et al. (2000). *Molecular Cell Biology*. 4th edition. New York: W. H. Freeman, Section 21.1, Overview of Neuron Structure and Function.

Pakkenberg, B., Pelvig, D., Marner, L., Bungaard, M. J., Gundersen, H. J. G., Nyengaard, J. R., Regeur, L. (2003). Aging and the human neocortex. *Experimental Gerontology,* 38, 95-99.

Persinger, M. A. (2010). 10^-20 Joules as a Neuromolecular Quantum in Medicinal Chemistry: An Alternative Approach to Myriad Molecular Pathways? *Current Medicinal Chemistry,* 17, 3094-3098.

Popp, F. A. 1979. Photon storage in biological systems. *Electromagnetic bioinformation*. Urban and Schwarzenberg: N.Y. 123-149.

Purves, D., Augustine, G.J., Fitzpatrick, D., et al. (2001). *Neuroscience*. 2nd edition. Sunderland (MA). Sinauer Associates. Chemical Synapses.

Rouleau, N., & Dotta, B. T. (2014). Electromagnetic fields as structure-function zeitgebers in biological systems: environmental orchestrations of morphogenesis and consciousness. *Frontiers in Integrative Neuroscience, 8*, 84.

Schrödinger, E. (1967). What is life?: The physical aspect of the living cell & Mind and matter. *Cambridge: University Press*.

Appendix – Published Works

Differential Spontaneous Photon Emissions from Cerebral Hemispheres of Fixed Human Brains: Asymmetric Coupling to Geomagnetic Activity and Potentials for Examining Post-Mortem Intrinsic Photon Information

Published in Neuroscience and Medicine, 2016

Authors: Justin N. Costa, Nicolas Rouleau, Michael A. Persinger

Contributions:

- Conceptualization: JC, NR, MP.
- Data curation: JC, NR.
- Formal analysis: JC, NR.
- Investigation: JC, NR, MP.
- Methodology: JC, NR.
- Project administration: JC, NR, MP.
- Resources: JC, NR, MP.
- Validation: JC, NR, MP.
- Visualization: JC, NR.
- Writing: JC, NR, MP.

Citation:

Costa, J.N., Rouleau, N. and Persinger, M.A. (2016) Differential Spontaneous Photon Emissions from Cerebral Hemispheres of Fixed Human Brains: Asymmetric Coupling to Geomagnetic Activity and Potentials for Examining Post-Mortem Intrinsic Photon Information. *Neuroscience & Medicine*, 7, 49-59. http://dx.doi.org/10.4236/nm.2016.72006

A Possible Flux Density Value of 10^{-12} W·m^{-2} for "Spontaneous" Photon Emissions in Fixed Human Brain Tissue: Was Spinoza Correct?

Published in Research in Neuroscience, 2016

Authors: Justin N. Costa, Michael A. Persinger

Contributions:

- Conceptualization: JC, MP.
- Data curation: JC.
- Formal analysis: JC, MP.
- Investigation: JC, MP.
- Methodology: JC, MP.
- Project administration: JC, MP.
- Resources: JC, MP.
- Validation: JC, MP.
- Visualization: JC.
- Writing: JC, MP.

Citation:

Justin N. Costa, Michael A. Persinger, A Possible Flux Density Value of 10^{-12} W·m^{-2} for "Spontaneous" Photon Emissions in Fixed Human Brain Tissue: Was Spinoza Correct?. *Research in Neuroscience* , Vol. 5 No. 1, 2016, pp. 10-14. doi: 10.5923/j.neuroscience.20160501.02.

Lagged Coherence of Photon Emissions and Spectral Power Densities between the Cerebral Hemispheres of Human Subjects during Rest Conditions: Phase Shift and Quantum Possibilities

Published in World Journal of Neuroscience, 2016

Authors: Justin N. Costa, Blake T. Dotta, Michael A. Persinger

Contributions:

- Conceptualization: JC, BD, MP.
- Data curation: JC, BD.
- Formal analysis: JC, BD.
- Investigation: JC, BD, MP.
- Methodology: JC, BD.
- Project administration: JC, BD, MP.
- Resources: JC, BD, MP.
- Validation: JC, BD, MP.
- Visualization: JC, BD.
- Writing: JC, BD, MP.

Citation:

Costa, J.N., Dotta, B.T. and Persinger, M.A. (2016) Lagged Coherence of Photon Emissions and Spectral Power Densities between the Cerebral Hemispheres of Human Subjects during Rest Conditions: Phase Shift and Quantum Possibilities. *World Journal of Neuroscience*, 6, 119-125. http://dx.doi.org/10.4236/wjns.2016.62015